

A Practical Guide to Estimating Conditional Marginal Effects: Modern Approaches ^{*}

Jiehan Liu
(Stanford)

Ziyi Liu
(Berkeley)

Yiqing Xu
(Stanford)

Abstract

This Element offers a practical guide to estimating conditional marginal effects—how treatment effects vary with a moderating variable—using modern statistical methods. Commonly used approaches, such as linear interaction models, often suffer from unclarified estimands, limited overlap, and restrictive functional forms. This guide begins by clearly defining the estimand and presenting the main identification results. It then reviews and improves upon existing solutions, such as the semiparametric kernel estimator, and introduces robust estimation strategies, including augmented inverse propensity score weighting with Lasso selection (AIPW-Lasso) and double machine learning (DML) with modern algorithms. Each method is evaluated through simulations and empirical examples, with practical recommendations tailored to sample size and research context. All tools are implemented in the accompanying `interflex` package for R.

Keywords: causal inference, conditional marginal effects, double machine learning

^{*}Jiehan Liu, PhD student, Department of Political Science, Stanford University. Email: jiehan1@stanford.edu. Ziyi Liu, PhD student, Haas School of Business, University of California, Berkeley. Email: zyliu2023@berkeley.edu. Yiqing Xu, Assistant Professor, Department of Political Science, Stanford University. Email: yiqingxu@stanford.edu. We are grateful to Justin Grimmer, Jens Hainmüller, and Jonathan Mummolo for helpful comments and suggestions. We thank the Series Editor, R. Michael Alvarez, for his guidance. We thank Ziyi Chen, Rivka Lipkowitz, Tianzhu Qin, Jinwen Wu, and Zehao Wang for excellent research assistance. Zehao and Tianzhu both contributed significantly to the implementation of the DML methods and the refinement of `interflex`. All errors are our own. We also thank the authors of the replicated studies for generously sharing their code and data.

Table 1: List of Acronyms and Their First Appearance

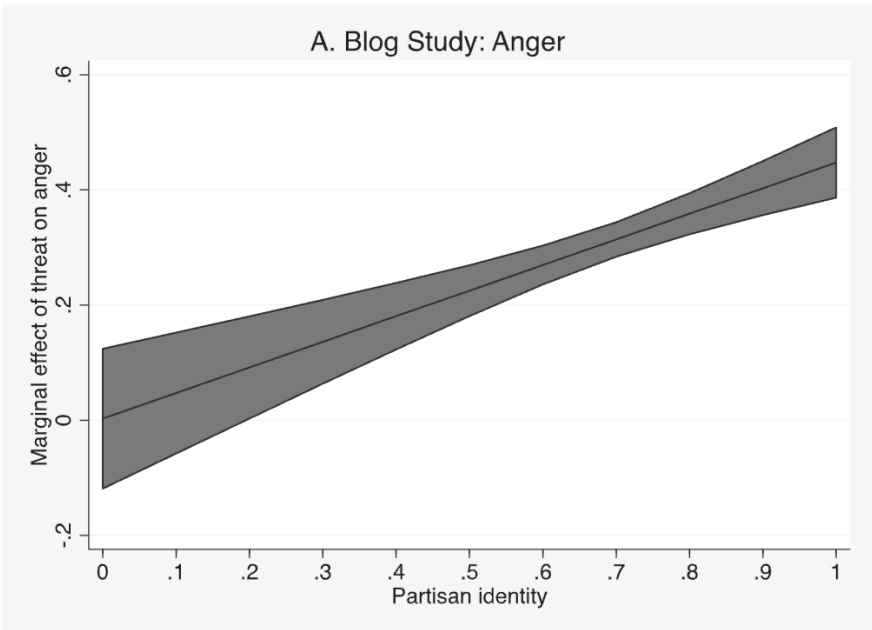
Acronym	Meaning	First Appearance
AIPW	Augmented Inverse Propensity Weighting	Ch1
ATE	Average Treatment Effect	Ch1
CATE	Conditional Average Treatment Effect	Ch1
CME	Conditional Marginal Effect	Ch1
DML	Double Machine Learning	Ch1
DGP	Data Generating Process	Ch1
SUTVA	Stable Unit Treatment Value Assumption	Ch1
IPW	Inverse Propensity Weighting	Ch1
LSCV	Least-Squares Cross-Validation	Ch2
MSPE	Mean-Squared Prediction Error	Ch2
OLS	Ordinary Least Squares	Ch2
SVCM	Smooth Varying Smooth Model	Ch2
PLRM	Partially Linear Regression Model	Ch3
PO-Lasso	Partialing-Out Lasso	Ch3
IRM	Interactive Regression Model	Ch4

Chapter 1. Introduction

Understanding conditional relationships is central to social science research. The impact of a treatment—such as an experimental intervention, a policy, or an institution—on social, political, and economic outcomes often varies systematically across subgroups or contexts. Researchers are particularly interested in how the effect of a treatment D on an outcome Y changes with the value of a covariate X , known as the moderator, which is unaffected by D .

Methods for analyzing conditional relationships have evolved over time. Traditionally, researchers have relied on linear interaction models to probe these relationships. [Brambor, Clark and Golder \(2006\)](#) (hereafter, BCG 2006) introduced best practices for estimating and interpreting such models, including the widely used “marginal effect plot” to visualize these relationships when the moderator X is continuous. Figure 1, reproduced from [Huddy, Mason and Aarøe \(2015\)](#), provides an example. The x-axis represents the moderator X (partisan identity), while the y-axis represents the effect of the treatment D (experimental partisan threat) on the outcome Y (anger). The gray ribbon indicates the 95% (pointwise) confidence intervals.

Figure 1: Adapted [Huddy, Mason and Aarøe \(2015\)](#), Figure 2A



Researchers typically draw several inferences from figures like this. First, they assess whether the causal effect of D on Y differs from zero by checking whether the horizontal zero line intersects the gray ribbon at a specific value of the moderator. Second, they identify regions where the gray ribbon lies entirely above or below zero (e.g., when partisan identity is > 0.2), interpreting these as conditions under which the theoretical effect is supported. Third, they examine whether the effect of D on Y changes monotonically with X , inferring whether the moderator amplifies or weakens the treatment effect, either causally or descriptively.

More recently, [Hainmueller, Mummolo and Xu \(2019\)](#) (hereafter, HMX 2019) highlighted the often-violated assumptions underlying these models, including the assumption of overlap and the reliance on linear interaction effects. To address these limitations, they introduced semiparametric kernel estimators, which relax functional form assumptions. Despite these advances, existing methods have several limitations. First, they are primarily motivated by an outcome-modeling perspective and often lack clear connections between estimation strategies and the underlying estimands of interest, leading to potential misinterpretation of estimated coefficients. Second, these approaches frequently rely on strong parametric assumptions. While the kernel estimator relaxes many of the functional form constraints of the linear estimator, it still imposes some structural constraints that may be violated in practice—for example, assuming that the higher order terms of the covariates, such as interactions, do not enter the outcome equation. Moreover, the overlap assumption is typically not critically evaluated. Third, existing methods have not systematically addressed important applications, such as those involving discrete outcomes.

This Element addresses these limitations through three key contributions. First, we provide precise definitions of the estimands of interest within the modern causal inference framework, clarifying the targets of inference and aligning estimation strategies—including parametric, semiparametric, and machine-learning methods—with theoretical objectives. Second, we leverage recent advances in double machine learning (DML) estimators to present a

flexible framework that accommodates a wide range of data-generating processes (DGPs) and use cases, including discrete and continuous treatments or outcomes, as well as potentially high-dimensional covariates, while ensuring valid inference for the targeted parameters. Finally, we offer practical recommendations for researchers based on evidence from simulations and empirical examples.

1.1 Define the Problem

We begin by defining our problem using the notations of the Neyman-Rubin potential outcomes framework (Neyman, 1923; Rubin, 1974), which provides the foundation for the rest of the Element. Consider a study with n units, indexed by $i = 1, 2, \dots, n$. These units are independently and identically distributed (i.i.d.) from a infinite population denoted by \mathcal{P} . To simplify the discussion of uncertainty measures, we assume the existence of a super-population. This assumption is also standard in the DML literature.

For each unit i , we observe the triplet (Y_i, D_i, V_i) , where Y_i denotes the outcome of interest, D_i is the treatment indicator, and V_i represents a set of covariates not causally affected by the treatment. The covariate vector $V_i \in \mathcal{V}$ comprises two components, $V_i = (X_i, Z_i)$: the moderator of interest $X_i \in \mathcal{X}$, which can be either discrete or continuous, and the remaining covariates $Z_i \in \mathcal{Z}$, which can be potentially high-dimensional. Within the scope of this Element, researchers are committed to studying the effect on D on Y conditional on X (and only X), meaning that they do not select variables for analysis after the data have been collected. We formalize the data structure and the sampling procedure as follows:

Assumption 1 *Random Sampling.*

$$\{(Y_i, D_i, V_i), i = 1, 2, \dots, n\} \text{ are i.i.d. sampled from the population } \mathcal{P}.$$

Next, let's invoke the stable unit treatment value assumption (SUTVA) to define the potential outcomes for unit i .

Assumption 2 *SUTVA*.

$$Y_i(d_1, d_2, \dots, d_n) = Y_i(d_i)$$

SUTVA state that unit i 's potential outcomes depend only on the treatment that unit receives, not on what others receive, and that each treatment has a single version (Imbens and Rubin, 2015; Rubin, 1986).

As a starting point, let us consider the case in which the treatment is binary, where $D_i = 1$ indicates that unit i receives the treatment condition, and $D_i = 0$ indicates the control condition. Under SUTVA and a binary treatment, unit i has exactly two potential outcomes, denoted by $\{Y_i(d_i) : d_i = 0, 1\}$. Therefore, we can link the observed outcome to the potential outcomes as follows:

$$Y_i = D_i Y_i(1) + (1 - D_i) Y_i(0). \tag{1}$$

Equation (1) is sometimes referred to as “consistency” in the causal inference literature; we avoid using this term to prevent confusion with the statistical concept of an estimator converging to the true value of a target parameter.

Conditional Marginal Effect With a binary treatment, unit i 's treatment effect is defined as $\tau_i = Y_i(1) - Y_i(0)$, and the average treatment effect (ATE) of the population as $\tau_{ATE} = \mathbb{E}[Y_i(1) - Y_i(0)]$, where the expectation is taken over the population \mathcal{P} . Building on the ATE, the *conditional average treatment effect* (CATE) captures the heterogeneous treatment effect given the value of covariates V_i .

$$\tau(v) = \mathbb{E}[Y_i(1) - Y_i(0) \mid V_i = v], \tag{2}$$

which can also be written as $\tau(x, z) = \mathbb{E}[Y_i(1) - Y_i(0) \mid X_i = x, Z_i = z]$. CATE measures the average treatment effect for specific groups defined by the value of V_i . In practice, estimating the CATE helps researchers better understand how the treatment effect varies across different population segments.

The main purpose of this Element is to examine how the treatment effect of D on Y changes given the value of X , a single moderator. Therefore, we introduce the *conditional marginal effect* (CME) as a special case of the CATE:

Definition 1 (CME w/ Binary Treatments)

$$\theta(x) = \mathbb{E}[Y_i(1) - Y_i(0) \mid X_i = x].$$

Note that $\theta(x)$ is essentially an aggregated version of $\tau(v)$, where we average out the effects of Z_i while keeping $X_i = x$. Formally, this means:

$$\theta(x) = \mathbb{E}[\tau(x, Z_i) \mid X_i = x] = \mathbb{E}[\tau(V_i) \mid X_i = x].$$

in which the expectation integrates out the influence of Z_i , focusing solely on the variation introduced by X_i , hence the term “marginal.”

Sometimes researchers are interested in comparing $\theta(x)$ at two (or more) different values of x . This estimand is referred to as *effect modification* in the statistics literature ([Bansak, 2020](#); [VanderWeele, 2009](#)):

$$\Delta\theta(x_1, x_2) = \theta(x_1) - \theta(x_2).$$

Importantly, effect modification is an associative estimand that describes treatment heterogeneity and should not be conflated with *causal moderation*, which refers to the causal effect of X on the effect of D on Y (such as in a factorial experiment). In this Element, we do not discuss causal moderation because the moderator X is usually not quasi-random or even manipulable.

A Toy Example To clarify the definition of $\theta(x)$, we provide a toy example consisting of eight units in [Table 2](#). Assume that these eight units represent the population of interest. In this example, $V_i = (X_i, Z_i)$ comprises two binary covariates, D_i is a binary treatment indicator, and $Y_i(1)$ and $Y_i(0)$ denote the potential outcomes under treatment and control, respectively. The observed outcome Y_i corresponds to the treatment actually received by

each unit. τ_i represents the individual treatment effect for unit i . We arrange the rows of the table according to the values of V_i . Our objective is to define the CATE and CME.

Table 2: Toy Example

i	X_i	Z_i	$Y_i(0)$	$Y_i(1)$	τ_i	D_i	Y_i	$\Pr(V_i = v)$
1	0	0	2	3	1	1	3	1/2
2	0	0	2	0	-2	0	2	1/2
3	0	1	3	7	4	1	7	1/2
4	0	1	5	3	-2	0	5	1/2
5	1	0	10	8	-2	1	8	2/3
6	1	0	4	1	-3	0	4	2/3
7	1	1	9	9	0	1	9	1/3
8	2	1	1	0	-1	0	1	1

Note: Numbers in shaded cells represent counterfactuals and are not observed in a real dataset.

Example 1 (CATE) Calculate $\tau(v)$ for $v = (0, 0)$:

$$\tau(v) = \mathbb{E}[Y_i(1) - Y_i(0) \mid V_i = (0, 0)] = \frac{1 + (-2)}{2} = -0.5$$

Example 2 (CME) Calculate $\theta(x)$ for $x = 0$:

$$v = (0, 0) : \quad \tau(v) = -0.5 \quad P(Z_i = 0 \mid X_i = 0) = \frac{2}{4} = 0.5$$

$$v = (0, 1) : \quad \tau(v) = 1 \quad P(Z_i = 1 \mid X_i = 0) = \frac{2}{4} = 0.5$$

$$\theta(0) = \tau(0, 0) \cdot P(Z_i = 0 \mid X_i = 0) + \tau(0, 1)P(Z_i = 1 \mid X_i = 0)$$

$$= (-0.5) \times 0.5 + (1) \times 0.5 = 0.25$$

Example 3 (Effect Modification) Calculate $\Delta\theta(x_1, x_2)$ for $x_1 = 0, x_2 = 2$:

$$\theta(0) = 0.25$$

$$\theta(2) = \tau((2, 1)) = -1$$

$$\Delta\theta(0, 2) = 0.25 - (-1) = 1.25$$

The fundamental problem of causal inference (Holland, 1986) states that for each unit, only one potential outcome can be observed at a time. For example, those numbers in shaded cells will never be observed. Therefore, given a sample, we cannot directly calculate the CATE or CME as demonstrated above. In the remainder of this Element, we will explore various estimation strategies that allow us to approximate these estimands under conditions of large sample sizes and when the necessary identifying assumptions are satisfied.

1.2 Identification

In this section, we focus on the identification and estimation of CME in the simplest scenario, where both the treatment D and the moderator X are discrete. While this setting is less common in the empirical literature, it provides a clear foundation for understanding the key concepts and results that will be applied throughout the Element.

We begin by presenting the identification results under two key assumptions: unconfoundedness and strict overlap. The goal of identification is to connect a statistical estimand, which can be estimated using observable data, to a meaningful causal estimand, such as the CME, which involves counterfactuals that are inherently unobservable. This connection is established through identifying assumptions. To simplify the discussion further, we assume that the treatment is binary.

Assumption 3 (Unconfoundedness)

$$\{Y_i(0), Y_i(1)\} \perp\!\!\!\perp D_i \mid V_i = v, \text{ for all } v \in \mathcal{V}.$$

The unconfoundedness assumption—also known as ignorability or selection on observables—is a key identifying assumption, though it is typically untestable. In randomized controlled trials, where the treatment assignment D_i is randomized, this assumption is satisfied because the potential outcomes, $\{Y_i(0), Y_i(1)\}$, are independent of the randomly assigned D_i . Furthermore, in an randomized controlled trial, the probability of receiving the treatment for each participant is known, ensuring that this assumption holds by design.

In observational studies, however, unconfoundedness assumes that treatment assignment D_i can be considered as good as randomized only after conditioning on a set of covariates $V_i = (X_i, Z_i)$, which capture all relevant confounders. This is equivalent to stating that within each cell defined by the vector v , the treatment is as-if randomly assigned. However, similar to a stratified randomized experiment, the probability of receiving the treatment may vary across cells. The key difference is that, in observational studies, researchers do not know what that probability is.

Assumption 4 (Strict overlap)

$$\exists \eta, \eta \leq \mathbb{P}(D_i = 1 \mid V_i = v) \leq 1 - \eta, \text{ with prob. } 1.$$

In addition to unconfoundedness, ensuring the identifiability of the estimand across all values of the covariates requires the overlap assumption, also known as positivity or common support assumption. This assumption states that every unit must have a non-zero probability of being assigned to each treatment condition, i.e., $0 < \mathbb{P}(D_i = 1 \mid V_i = v) < 1$. Intuitively, this means that within each cell defined by v , there are both treated and control units, provided the sample size is sufficiently large.

In Assumption 4, we require a slightly stronger condition than standard overlap, strict overlap. It says that the probabilities of treatment assignment given covariates, or propensity scores, must be uniformly bounded away from 0 and 1 by some positive constant η . Mechanically, this requirement avoids extreme values of propensity scores, thereby ensuring the identifiability of certain estimators, such as inverse propensity score weighting (IPW) and augmented inverse propensity score weighting (AIPW). It is also crucial for theoretical guarantees, including asymptotic normality of these estimators.

Now, we present two approaches for identifying the CME under unconfoundedness and strict overlap: (a) stratified difference-in-means and (b) IPW. When all covariates V_i are discrete, these two methods are numerically equivalent (Imbens and Rubin, 2015)—see also the proof for the CME case in the Appendix. However, discussing both methods in this

simple discrete setting is important, as they provide the foundation and intuition for more general cases.

Stratified difference-in-means. Denote $\mu^1(v) = \mathbb{E}[Y_i \mid D_i = 1, V_i = v]$ and $\mu^0(v) = \mathbb{E}[Y_i \mid D_i = 0, V_i = v]$, which represent the conditional mean outcomes under treatment and control conditions, respectively, given covariate values $V_i = (X_i, Z_i) = (x, z) = v$. The limit of the stratified difference-in-means estimator can be written as:

$$\begin{aligned}
& \Sigma_z\{\mu^1(v) - \mu^0(v) \cdot \Pr(Z_i = z \mid X_i = x)\} \\
&= \Sigma_z\{\tau(v) \cdot \Pr(Z_i = z \mid X_i = x)\} \quad (\text{unconfoundedness \& overlap}) \\
&= \Sigma_z\{(\mathbb{E}[Y_i(1) - Y_i(0) \mid X_i = x, Z_i = z]) \Pr(Z_i = z \mid X_i = x)\} \quad (\text{CATE definition}) \\
&= \mathbb{E}[Y_i(1) - Y_i(0) \mid X_i = x] \quad (\text{tower rule}) \\
&= \theta(x)
\end{aligned}$$

Under unconfoundedness and overlap, the stratified difference-in-means identifies the CME by taking a weighted average CATE across all strata defined by the values of v based on the conditional probability $\Pr(V_i = v \mid X = x) = \Pr(Z_i = z \mid X = x)$. The two conditional means, $\mu^1(v)$ and $\mu^0(v)$, are estimable by data given overlap and random sampling.

IPW. As an alternative, we can identify the CME by weighting each observation by the inverse of the propensity score, which represents the probability of receiving the treatment given covariates, i.e., $\pi(v) = \Pr(D_i = 1 \mid V_i = v)$. The derivation follows:

$$\begin{aligned}
& \mathbb{E}\left[\frac{D_i Y_i}{\pi(V_i)} - \frac{(1-D_i)Y_i}{1-\pi(V_i)} \mid X_i = x\right] = \mathbb{E}\left[\frac{D_i Y_i}{\pi(V_i)} \mid X_i = x\right] - \mathbb{E}\left[\frac{(1-D_i)Y_i}{1-\pi(V_i)} \mid X_i = x\right] \\
&= \mathbb{E}\left[\frac{D_i Y_i(1)}{\pi(V_i)} \mid X_i = x\right] - \mathbb{E}\left[\frac{(1-D_i)Y_i(0)}{1-\pi(V_i)} \mid X_i = x\right] \\
&= \mathbb{E}[Y_i(1) \mid X_i = x] - \mathbb{E}[Y_i(0) \mid X_i = x] \quad (\text{unconfoundedness \& overlap}) \\
&= \mathbb{E}[Y_i(1) - Y_i(0) \mid X_i = x] = \theta(x)
\end{aligned}$$

This expression recovers the same mean difference $\mathbb{E}[Y_i(1) - Y_i(0) \mid X_i = x]$ by appropriately weighting each observed Y_i with $X_i = x$, ensuring that the estimate accounts for differences in treatment assignment probabilities.

In terms of the variance of $\theta(x)$, since

$$\theta(x) = \sum_z P(Z_i = z \mid X_i = x) \cdot \tau(v)$$

the variance of $\theta(x)$ can be expressed as:

$$V(\theta(x)) = \sum_z [P(Z_i = z \mid X_i = x)]^2 V(\tau(v))$$

This expression accounts for the variability in $\tau(v)$ across different values of Z , weighted by the conditional probability of Z given X .

The discussion so far has focused on the simple scenario of binary treatments and discrete covariates. However, researchers are often interested in estimating and visualizing the CME when X is continuous. In fact, for the remainder of this book, we assume X is a continuous variable, treating the case of discrete X as a special case. While the intuition behind the identification results remains largely the same, the definition of the CME requires additional care when the treatment is continuous, as we discuss below.

1.3 Continuous Treatments

Following [Hirano and Imbens \(2004\)](#), we first adapt the potential outcomes framework to accommodate continuous treatments by considering D as an interval $\mathcal{D} = [d_0, d_1]$. This formulation allows us to explore the unit-level dose-response function. We assume that each unit i 's potential outcome function, $Y_i(d)$, is twice continuously differentiable with respect to d for all $d \in \mathcal{D}$, ensuring that the derivative $\frac{\partial Y_i(d)}{\partial d}$ exists and is well defined.

Moreover, we maintain [Assumption 1](#) (random sampling) and [Assumption 2](#) (SUTVA). To link the observed outcome with the potential outcomes, we assume $Y_i = Y_i(D_i)$. For each unit i , given a vector of covariates Z_i and the moderator X_i , we define the CME as follows:

Definition 2 (CME with Continuous Treatments)

$$\theta(x) = \mathbb{E} \left[\frac{\partial Y_i(d)}{\partial d} \mid X_i = x \right].$$

This represents the expectation of the partial derivative of the potential outcome with respect to the treatment value, conditional on $X_i = x$. It averages over the entire population \mathcal{P} and accounts for the distributions of Z and D . As before, we also need unconfoundedness and overlap assumptions to identify the CME.

Assumption 5 (Unconfoundedness for continuous D)

$$Y_i(d) \perp\!\!\!\perp D_i \mid V_i = v, \quad \text{for all } d \in \mathcal{D} \text{ and } v \in \mathcal{V}$$

Assumption 6 (Strict overlap for continuous D)

$$f_{D|V}(d \mid v) > 0, \quad \text{for all } d \in \mathcal{D} \text{ and } v \in \mathcal{V}$$

In the continuous treatment case, identifying the CME requires additional assumptions on functional form, which we will discuss in the subsequent chapters along with estimation strategies.

1.4 Approach and Organization

Now that we have clarified the primary estimand, the CME, and the key identification assumptions, the goal of this Element is to discuss identification results, estimation strategies, and inferential methods suitable for various empirical scenarios. These methods progressively relax functional form restrictions but require larger datasets. We will illustrate these approaches using empirical examples from political science.

Throughout this Element, we will primarily focus on *unconfoundedness* (or selection-on-observables) as the main identification strategy for estimating the effect of D on Y , which is particularly well-suited for cross-sectional data. We make this choice because most panel data methods commonly used in the social sciences rely on fundamentally different

identifying assumptions, such as parallel trends, and their formal treatment using the DML approach falls outside the scope of this Element. Nonetheless, we can accommodate panel data either by first differencing the outcome or by partialling out the fixed effects using the Frisch–Waugh–Lovell (FWL) theorem.

This Element is organized as follows:

Chapter 2 reviews classic approaches to estimating the CME. We start with the widely used parametric linear interaction model. While this approach is versatile and easy to implement, it often suffers from issues such as lack of overlap and an inability to capture nonlinear CME, as pointed out by HMX (2019). To address these challenges, we first emphasize a design phase to improve overlap. We then review alternative methods proposed by HMX (2019), including the binning estimator as a diagnostic tool and the semiparametric kernel estimator, which relaxes the functional form assumption. We illustrate these challenges and solutions using several empirical examples. While the kernel estimator offers greater flexibility, it remains an outcome modeling approach that does not account for the treatment assignment process.

Chapter 3 introduces IPW and AIPW estimators for estimating the CME when X is continuous, addressing limitations of traditional outcome modeling approaches. IPW estimates the CME by weighting outcomes using the inverse of the estimated propensity score, while AIPW combines outcome and propensity models to achieve double robustness. We detail how to construct signals from data using outcome modeling, IPW, and AIPW approaches, which serve as key building blocks for the DML methods developed in Chapter 4. To relax functional form assumptions, we incorporate basis expansions, Lasso regularization, and post-selection estimation, which we refer to as AIPW-Lasso. We extend this approach to continuous treatments using partially linear regression and a partialling-out strategy, constructing “denoised” variables before applying kernel or spline regression. We evaluate the performance of these estimators through simulated and empirical applications, demonstrating the advantages of each component in improving robustness, flexibility, and

accuracy.

In Chapter 4, we formally introduce the DML framework, which extends AIPW to accommodate high-dimensional or nonlinear nuisance functions using machine learning methods. While AIPW leverages signals that satisfy Neyman orthogonality and achieves robustness against model misspecification, DML ensures \sqrt{n} -rate consistency even when nuisance functions are estimated with flexible machine learning models. The chapter outlines three key components of DML: (i) Neyman orthogonality, which ensures that small errors in estimating nuisance functions do not introduce first-order bias; (ii) high-quality machine learning methods, such as random forests and neural networks, which approximate nuisance functions while controlling regularization bias; and (iii) sample splitting and cross-fitting, which mitigate overfitting by estimating nuisance functions and treatment effects on separate data folds.

We then apply DML to estimating CME under both binary and continuous treatments. For binary treatments, the estimator builds on the interactive regression model and uses an AIPW-style Neyman orthogonal score to estimate the CATE, which is then projected onto the moderator X to obtain the CME. For continuous treatments, DML adopts a partially linear regression, using a residual-on-residual approach to partial out the influence of covariates before estimating the CME. The chapter concludes with empirical applications, demonstrating DML in both binary and continuous treatment settings. Comparisons with kernel estimators highlight DML’s advantages in capturing complex relationships while maintaining valid inference. Chapter 4 also addresses an important use case where the outcome variable Y is discrete. We demonstrate that double nonlinearity—nonlinearity in the outcome and nonlinearity in the CME—can be better addressed using DML methods than parametric approaches.

An important unanswered question is under what conditions the DML approach outperforms the kernel estimator or AIPW-Lasso in common research settings. To explore this, Chapter 5 presents a series of Monte Carlo simulations. Our results show that even under

fairly complex DGPs, AIPW-Lasso (with basis expansion and regularization) generally outperforms DML estimators in small to medium-sized datasets. DML performs better when the sample size is sufficiently large (e.g., at least 5,000 observations). These findings highlight a fundamental trade-off between model flexibility and the ability to handle smaller samples. Simply put, DML offers greater flexibility but requires larger datasets to perform well, while AIPW-Lasso provides a desirable middle ground in most practical applications.

In Chapter 6, the final chapter, we summarize our findings and provide practical recommendations for researchers, drawing on the insights gained throughout the Element. All the methods discussed in this Element can be implemented using the `interflex` package in R.

1.5 Summary

Understanding conditional relationships is a common objective in social science research. Researchers are often interested in how the effect of a treatment D on an outcome Y depends on a moderating variable X . While the methodological literature has made significant progress in this area, current approaches face several challenges, including a lack of clarity regarding the intended estimand, misinterpretation of estimation results, insufficient overlap in real-world data, rigid functional form assumptions, and difficulties in handling complex scenarios such as discrete outcomes. This Element introduces a simple but general framework that addresses these challenges while ensuring statistical validity.

Our key estimand is the conditional marginal effect (CME). When the treatment is binary, it is defined as

$$\theta(x) = \mathbb{E}[Y_i(1) - Y_i(0) \mid X_i = x],$$

which represents the CATE marginalized over all covariates except X . When the treatment is continuous, it is defined as

$$\theta(x) = \mathbb{E} \left[\frac{\partial Y_i(d)}{\partial d} \mid X_i = x \right],$$

which is the partial derivative of the potential outcome function with respect to the treatment

value, marginalized over all covariates except X and the observed treatment levels. In addition, researchers may be interested in effect modification,

$$\Delta\theta(x_1, x_2) = \theta(x_1) - \theta(x_2),$$

which quantifies the difference in treatment effects between two values of the moderator, x_1 and x_2 . This provides a descriptive (rather than causal) measure of the extent to which treatment effects are heterogeneous.

In cross-sectional settings, the unconfoundedness and overlap assumptions are crucial for identifying the CME. When the treatment or covariates, including the moderator, contain continuous variables, additional functional form or smoothness assumptions are needed for causal identification. In the following chapters, we present a progression of methods for identifying and estimating these quantities, starting with the traditional linear interaction model and gradually moving toward more flexible approaches that accommodate more complex DGPs.

Chapter 2. The Classic Approaches

In this chapter, we discuss classic approaches to estimating and visualizing the CME. We begin with the linear interaction model, which remains widely used in social science research. We introduce the variance estimator for the CME based on this model, which forms the basis for hypothesis testing. We also address the issue of multiple comparisons and explain how uniform confidence intervals can be constructed using a bootstrap procedure to mitigate this concern.

Next, we examine two key challenges in applying the linear interaction model: violations of the overlap assumption (or lack of common support) and model misspecification (such as omitted interactions and nonlinearity). We discuss simple diagnostic tools and strategies to detect and address these issues.

Finally, to relax functional form assumptions, we explore the kernel estimator proposed by HMX (2019) and introduce several improvements, including a fully interacted specification and an adaptive kernel. Throughout this chapter, we emphasize the importance of clearly defining the estimand and explicitly stating identifying and modeling assumptions.

2.1 Linear Interaction Model

In the previous chapter, we considered the CME with a binary treatment $D \in \{0, 1\}$, a discrete moderator X , and additional discrete covariates Z . The empirical estimand of the CME at a particular value $X_i = x$ was defined as:

$$\mathbb{E}_z\{\mathbb{E}[Y_i \mid D_i = 1, X_i = x, Z_i = z]\} - \mathbb{E}_z\{\mathbb{E}[Y_i \mid D_i = 0, X_i = x, Z_i = z]\},$$

where $\mathbb{E}[Y_i \mid D_i = d, X_i = x, Z_i = z]$, $d = \{0, 1\}$ is a conditional expectation function that could take an arbitrary form. As discussed previously, when D is binary and the covariates are discrete and limited in number, it is feasible to estimate conditional expectations non-parametrically. However, as the number of covariates increases or continuous variables are

introduced, nonparametric estimation becomes impractical. To address this, we can impose modeling assumptions that restrict the functional form of $\mathbb{E}[Y_i \mid D_i, V_i]$, simplifying both estimation and interpretation.

The linear interaction model is the most commonly used approach in political science for studying marginal effects. We formally incorporate this widely used specification as a functional form assumption:

Assumption 7 (Linear interaction model, or the linear estimator)

$$Y_i = \beta_0 + \beta_1 D_i + \beta_2 X_i + \beta_3 (D_i \cdot X_i) + Z_i \beta_4 + \epsilon_i$$

where ϵ_i represents an idiosyncratic error.

Given Assumption 7, the unconfoundedness assumption implies:

$$\{\beta_0 + \beta_1 d + \beta_2 X_i + \beta_3 (d \cdot X_i) + Z_i \beta_4 + \epsilon_i\} \perp\!\!\!\perp D_i \mid X_i, Z_i$$

which further implies that $\epsilon_i \perp\!\!\!\perp D_i \mid X_i, Z_i$. This leads to the zero-conditional-mean assumption: $\mathbb{E}[\epsilon_i \mid D_i, X_i, Z_i] = 0$. Therefore, if the model is correctly specified, the coefficients in the linear interaction model can be consistently estimated using Ordinary Least Squares (OLS) under unconfoundedness.

Given unconfoundedness, Assumption 7 (the linear interaction model) implies the following conditional expectation function:

$$\mathbb{E}[Y_i \mid D_i, X_i, Z_i] = \beta_0 + \beta_1 D_i + \beta_2 X_i + \beta_3 (D_i \cdot X_i) + Z_i \beta_4 \tag{3}$$

The binary treatment case. When D_i is binary, Equation (3) is equivalent to the following conditional expectations:

$$\mathbb{E}[Y_i \mid D_i = 0, X_i, Z_i] = \beta_0 + \beta_2 X_i + Z_i \beta_4$$

$$\mathbb{E}[Y_i \mid D_i = 1, X_i, Z_i] = (\beta_0 + \beta_1) + (\beta_2 + \beta_3) X_i + Z_i \beta_4$$

These equations imply linear relationships between X and the expected outcome, as well as between Z and the expected outcome. In addition, the coefficients for Z are constant across

treatment values, and there are no interactions between X and Z .

Given Equation (3), the CME can be written as:

$$\begin{aligned}\theta(x) &= \mathbb{E}_z[\beta_0 + \beta_1 + \beta_2x + \beta_3 \cdot x + Z_i\beta_4] - \mathbb{E}_z[\beta_0 + \beta_2x + Z_i\beta_4] \\ &= (\beta_0 + \beta_1 + \beta_2x + \beta_3 \cdot x + \beta_4\mathbb{E}_z[Z_i]) - (\beta_0 + \beta_2x + \mathbb{E}_z[Z_i]\beta_4) \\ &= \beta_1 + \beta_3x\end{aligned}$$

which is a linear combination of β_1 and β_3 . Therefore, $\hat{\theta}(x) = \hat{\beta}_1 + \hat{\beta}_3x$. This logic can be easily extended to discrete D_i .

The continuous treatment case. When D_i is continuous, the CME is the expectation of the partial derivative of the outcome with respect to D_i , conditioned on the moderator and covariates:

$$\theta(x) = \mathbb{E} \left[\frac{\partial Y_i}{\partial D_i} \mid X_i = x \right]$$

Given the linear interaction model and unconfoundedness, the CME becomes:

$$\theta(x) = \beta_1 + \beta_3x$$

which is the same as in the binary treatment case. Unconfoundedness is crucial because it ensures $\epsilon_i \perp\!\!\!\perp D_i \mid X_i, Z_i$.

Inference & Hypothesis Testing The above results suggest that, under the linear interaction model, the CME is a simple, linear function of x . For statistical inference, 95% *pointwise confidence intervals* are commonly used in empirical research. By pointwise 95% confidence interval, we mean that at each specific value of x , there is a 95% probability that the interval constructed will contain the true CME for that particular x . These intervals are calculated independently for each value of x , without considering the joint coverage probability across multiple values of x .

We can use one of the following two approaches to construct the pointwise confidence intervals, both implemented in `interflex`: (i) analytical asymptotic variance based on nor-

mal approximation or (iii) bootstrapping, which involves repeatedly resampling the data and re-estimating $\hat{\theta}(x)$. Analytically, the variance of $\hat{\theta}(x)$ can be estimated as follows:

$$\widehat{\text{Var}}(\hat{\theta}(x)) = \widehat{\text{Var}}(\hat{\beta}_1) + x^2 \widehat{\text{Var}}(\hat{\beta}_3) + 2x \widehat{\text{Cov}}(\hat{\beta}_1 \hat{\beta}_3).$$

in which $\widehat{\text{Var}}(\hat{\beta}_1)$, $\widehat{\text{Var}}(\hat{\beta}_3)$ and $\widehat{\text{Cov}}(\hat{\beta}_1 \hat{\beta}_3)$ are often obtained using the Eicker-Huber-White robust estimator and cluster-robust estimator (if a group structure exists).

In their seminal work, BCG (2006) recommend visualizing the CME, which they refer to as the marginal effects, using a plot where x is placed on the x-axis and $\hat{\theta}(x)$, derived from the linear interaction model, is displayed on the y-axis. See Figure 1 in Chapter 1 for example. The plot also includes the 95% pointwise confidence interval to provide a visual representation of the uncertainty associated with the estimates. We provide the details of the example and R code to replicate this figure below.

Example 4 *Huddy, Mason and Aarøe (2015) explores the effect of the expressive model of partisanship. Drawing on four survey studies, the authors argue that partisan identity drives campaign participation and strong emotional responses to ongoing campaign events. We replicate Figure 2A in the original paper, which suggests that strongly identified partisans are more likely to exhibit stronger emotional reactions—such as anger when threatened with electoral loss—compared to those with weaker partisan identities. The variables of interest include:*

- *Outcome: level of anger (continuous, $\in [0, 1]$)*
- *Treatment: electoral loss threat or electoral win reassurance (binary, $\in \{0, 1\}$)*
- *Moderator: strength of partisan identity (continuous, $\in [0, 1]$)*

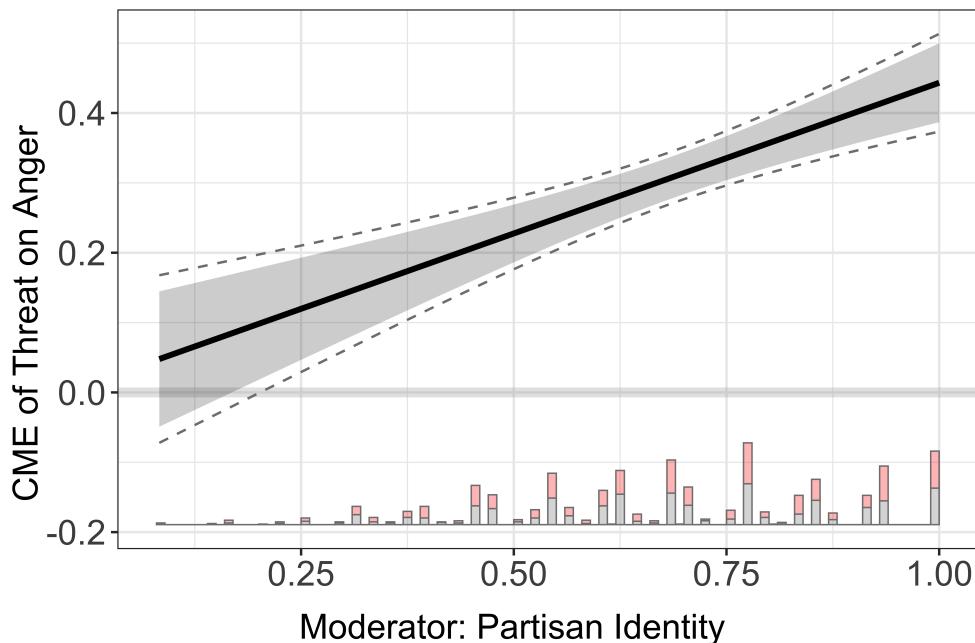
```
1 # R code excerpt
2 library(interflex)
3
4 Y="totangry" # Anger
```

```

5 D="threat" # Threat
6 X="pidentity" # Partisan Identity
7 Z <- c("issuestr2", "issuestr2_threat", "knowledge" , "educ" , "male" , "
      age10" )
8
9 ## linear interaction model
10 out.linear <- interflex(estimator =
11 "linear", data = df,
12   Y = Y, D = D, X = X, Z = Z,
13   vartype = "bootstrap", na.rm = TRUE)
14
15 # plot the CME
16 plot(out.linear)

```

Figure 2: Replicating Huddy, Mason and Aarøe (2015) Figure 2A



Notes: The black line represents the CME estimates based on the linear interaction model. The shaded area represent 95% pointwise confidence intervals. The dashed lines represent 95% uniform confidence intervals. The histograms at the bottom of the figure depict the distributions of X across treatment (pink) and control (gray) groups.

As mentioned in Chapter 1, researchers are often interested in testing three types of

hypotheses:

- $H_{0a} : \theta(x) = 0$ given a specific x . Researchers ask whether, at this particular value of x , the CME is statistically distinguishable from zero.
- $H_{0b} : \Delta\theta(x_1, x_2) = 0$ or $\Delta\theta(x_1, x_2) > 0$ given specific values of x_1 and x_2 . Researchers compare two CMEs and determine whether they are statistically distinguishable or whether one CME is larger than the other.
- $H_{0c} : \theta(x) = 0$ (or $\theta(x) \geq 0$), $x \in \mathcal{X}$, a pre-specified set. Researchers investigate whether the CME across a set or region of x values is jointly statistically distinguishable from zero or jointly larger or smaller than zero.

To test H_{0a} , we can perform a t -test using $\hat{\theta}(x)$ and $\widehat{\text{Var}}(\hat{\theta}(x))$. This is equivalent to visually inspecting whether the pointwise confidence interval in the marginal effect plot intersects the horizontal zero line. For instance, in Figure 2, at $x = 0.5$, the pointwise confidence interval does not overlap with zero. This allows us to reject the null hypothesis that $\theta(0.5) = 0$ at the 5% significance level.

To test H_{0b} , we first estimate $\Delta\theta(x_1, x_2)$ using the following approach:

$$\begin{aligned}\widehat{\Delta\theta}(x_1, x_2) &= \hat{\theta}(x_1) - \hat{\theta}(x_2) \\ &= (\hat{\beta}_1 + \hat{\beta}_3 x_1) - (\hat{\beta}_1 + \hat{\beta}_3 x_2) \\ &= \hat{\beta}_3(x_1 - x_2).\end{aligned}$$

The variance of this estimate is given by: $\widehat{\text{Var}}(\widehat{\Delta\theta}(x_1, x_2)) = \widehat{\text{Var}}(\hat{\beta}_3)(x_1 - x_2)^2$. Because $(x_1 - x_2)$ is a constant, testing H_{0b} is equivalent to testing whether $\beta_3 = 0$. Indeed, researchers often interpret the statistical significance of $\hat{\beta}_3$, the coefficient of the interaction term, as evidence for heterogeneous treatment effects.

To test H_{0c} , we need to construct uniform confidence intervals. Before doing so, we first discuss the issue of multiple comparisons.

Multiple Comparisons Esarey and Sumner (2018) highlight a multiple comparisons issue associated with CME plots. They argue that BCG (2016)’s suggestion to use a visual test—examining whether the (pointwise) confidence interval includes zero at a given value of the moderator X to conclude that the treatment D and outcome Y are statistically related at that value—is overly optimistic. This approach does not account for the multiple comparisons problem, which arises when making inferences across a range of moderator values, leading to inflated Type I error (or uncontrolled false positive rates).

In the context of the linear interaction model, using an example with a binary moderator, Esarey and Sumner (2018) point out that the visual test is equivalent to conducting hypothesis testing twice, once in each subsample defined by X , with each test carrying its own probability of a false positive. This issue becomes even more pronounced when the treatment D or the moderator X is continuous, as the number of comparisons increases significantly, further compounding the likelihood of false positives. Esarey and Sumner (2018) recommend applying procedures that control the overall false discovery rate or familywise error rate, such as the sequential test procedure by Benjamini and Hochberg (1995) or the joint F -test proposed by Franzese and Kam (2009).

In the `interflex` package, we address the multiple comparisons issue in estimating CME by incorporating *uniform confidence intervals*, also known as simultaneous confidence intervals. These intervals ensure a specified overall coverage level across all estimates, controlling the family-wise error rate and addressing the multiple comparisons problem. They are implemented using the sup- t band approach introduced by Montiel Olea and Plagborg-Møller (2017) using bootstrapping, which is a simulation-based method that involves repeatedly resampling the data with replacement to estimate the sampling distribution of an estimator. The procedure takes the following three steps:

1. For each parameter at evaluation point x_0 , empirical quantiles are computed from the bootstrap estimates: $Q_{j,\zeta}(x_0)$ and $Q_{j,1-\zeta}(x_0)$ for the ζ -th and $(1 - \zeta)$ -th quantiles respectively, across all bootstrap replicates B , where j indexes the parameters

$\mu, \alpha, \eta, \beta, \gamma$.

2. The largest ζ is determined such that the coverage across all parameters for all x_0 points satisfies the collective confidence level:¹

$$\zeta = \sup \left\{ \zeta \in \left[\frac{\alpha}{2k}, \frac{\alpha}{2} \right] \left| \frac{1}{B} \sum_{b=1}^B \mathbf{1} \left(\hat{\theta}_b \in \prod_{j=1}^k [Q_{j,\zeta}, Q_{j,1-\zeta}] \right) \geq 1 - \alpha \right. \right\}$$

3. The uniform confidence intervals for each parameter at each x_0 are constructed using these quantiles, resulting in confidence bands $C_{j,x_0} = [Q_{j,\zeta^*}(x_0), Q_{j,1-\zeta^*}(x_0)]$ for each j .

This method ensures that the confidence intervals are uniformly adjusted across all parameters. In other words, if none of points $x \in \mathcal{X}$ on the zero horizontal line is covered by the uniform confidence intervals, the joint null hypothesis $H_{0c} : \theta(x) = 0, x \in \mathcal{X}$ is rejected with a probability of less than 5%.

In Figure 2, the dotted lines represent the uniform confidence intervals, while the shaded area depicts the pointwise confidence intervals. The uniform confidence intervals are consistently wider, reflecting a more conservative approach to interval estimation that adjusts for multiple comparisons across the moderator's range. We observe that the lower bounds of the uniform confidence intervals cross the horizontal zero line around $x = 0.25$, suggesting that for values of the moderator X greater than 0.25, the effect of the treatment becomes statistically distinguishable from zero at the 5% level, indicating a significant treatment effect. Therefore, a visual test using the uniform confidence intervals provides a practical method for performing hypothesis testing for H_{0c} .

Using the linear interaction model to estimate the CME presents several challenges, primarily lack of common support and model misspecification, as discussed in HMX (2019). In the remainder of this chapter, we illustrate these challenges with examples and propose several solutions to address them.

¹The lower bound of $\zeta, \frac{\alpha}{2k}$, corresponds to the quantiles with the Bonferroni correction, while the upper bound, $\frac{\alpha}{2}$, corresponds to the quantile of the pointwise confidence interval.

2.2 Lack of Common Support

HMX (2019) highlight that the overlap assumption is often violated in applications, particularly in observational studies, a problem commonly referred to as a “lack of common support.” Researchers using the linear interaction model typically report the CME by substituting x values into the conditional marginal effect formula, $\hat{\theta}(x) = \hat{\beta}_1 + \hat{\beta}_3x$, without checking for overlap. This occurs because regression produces estimates regardless of whether the overlap assumption holds.

When X is continuous, the overlap assumption requires two conditions: (1) a sufficient number of observations with values of the moderator X close to x_0 , and (2) sufficient variation in the treatment D at or around x_0 for similar values of Z . For example, if all data points near $X = x_0$ belong to the treatment group ($D = 1$), overlap is violated. If either of these conditions is not met, CME estimates must rely on extrapolation or interpolation based on the assumed functional form, extending the model to regions with little or no data. In such cases, the CME estimates become highly model-dependent and unreliable. We provide such an example below.

Example 5 *Chapman (2009) examines the effect of international organization, specifically the authorizations granted by the U.N. Security Council, on public opinion of U.S. foreign policy. The authors use the size of rallies, which measures the short-term change in presidential approval ratings surrounding military disputes, as a proxy for support for foreign policy. We replicate the Figure 2 of the original paper, which suggests the effect of U.N. authorizations is conditional on similarity of preferences between the U.S and the U.N. Security Council: the public is more likely to favor policies that are explicitly approved by relatively conservative institutions, i.e., institutions with more heterogeneous preferences. The variables of interest include:*

- *Outcome: size of rallies supporting the authorization (continuous, $\in [-16, 33]$)*
- *Treatment: granting of a U.N. authorization (binary, $\in \{0, 1\}$)*

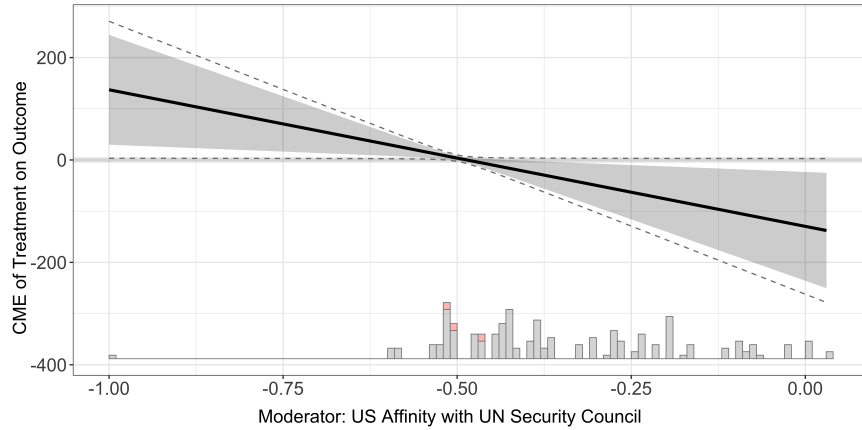
- Moderator: preference distance between the U.S. and the Security Council (continuous, $\in [-1, 0]$)

```

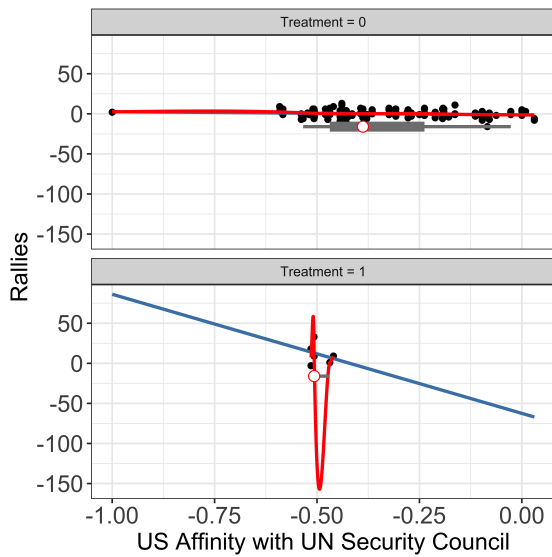
1 # R code excerpt
2
3 library(interflex)
4
5 Y="rally" # size of rallies
6 D="unauth" # U.N. authorization
7 X="S" # US affinity with UN Security Council
8 Z=c("priorpop", "bipart", "statemnt", "nextelec", "nytcov", "buscon", "revorg", "
    wardumk", "majopp", "allies", "war", "SCappeal", "regorgact", "ordsever", "
    hostlvl")
9
10 ## linear estimator with uniform CI
11 out.linear<-interflex(estimator = "linear",
12     Y=Y,D=D,X=X,Z=Z, data=d,
13     vartype = "bootstrap", na.rm = TRUE)
14 plot(out.linear)
15
16 ## diagnostic plot
17 out.raw <- interflex(estimator = "raw", data = d,Y=Y,D=D,X=X, na.rm = TRUE
18     )
19 plot(out.raw)
20
21 ## propensity score computation
22 V<-append(Z, X)
23 covariate_matrix <- d[V]
24 covariate_matrix[] <- lapply(covariate_matrix, function(x) as.numeric(as.
25     character(x)))
26 covariate_matrix<-as.matrix(covariate_matrix)
27
28 cf<-causal_forest(covariate_matrix, d$rally, d$unauth)

```

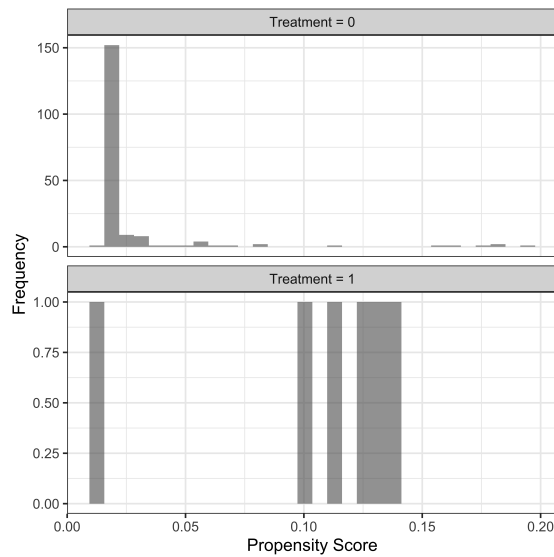
Figure 3: Replicating Chapman (2009) Figure 2



(a) CME plot



(b) Outcome by treatment condition



(c) Propensity score

Notes: Treatment measures UN authorization, outcome is the size of rallies, measuring the short-term change in presidential approval ratings surrounding military disputes. (a) The CME plot. The black line represents the CME estimates based on a linear interaction model. The shaded area represents pointwise confidence intervals, while the dotted line indicates uniform confidence interval, both of which are calculated via bootstrap. (b) Raw outcome plot by treatment condition; (c) Propensity score, estimated with `grf` package, by treatment condition.

Figure 3(a) presents the CME plot based on the linear interaction model. The author interprets the positive estimated CME when the moderator is smaller than -0.5 as evidence

that the positive effect of U.N. authorizations on U.S. public opinion is conditional the U.S. policy position is far from those of the countries serving on the Security Council.

However, this finding appears to be entirely driven by extrapolation, and the lack of common support is easy to detect using simple plots. HMX (2019) recommend (i) adding a histogram at the bottom of the CME plot and (ii) using a diagnostic plot, such as Figure 3(b), that displays the raw data by treatment condition. When the treatment is binary, we also recommend plotting the propensity score, a standard approach for assessing overlap (Heckman, LaLonde and Smith, 1999; Imbens and Xu, 2024).

Indeed, the histogram in Figure 3(b) reveals that there are almost no observations when the moderator is below -0.7 . Even more concerning is the lack of treated units (with U.N. authorization), which are concentrated in a narrow range around -0.5 . This indicates a severe lack of overlap in the regions where the author interprets the effect as positive. In fact, as shown in Figure 3(a), the downward slope of the CME estimates is almost entirely driven by six treated units through extrapolation. The propensity score plot in Figure 3(c) further confirms this issue, showing insufficient common support in these regions.

Design Phase to Improve Overlap Later in this chapter and in the next two chapters, we introduce methods that relax Assumption 7. To address concerns about lack of overlap, we recommend incorporating a *design phase* prior to any outcome analysis. This approach, proposed by Imbens and Rubin (2015, Chapter 15), reflects a growing consensus in the causal inference literature that study design should precede analysis, even in non-experimental settings.

In observational studies, the design phase refers to a preparatory stage in which researchers structure or preprocess the data *before* analyzing outcomes. The goal is to approximate the conditions of a randomized controlled trial using only information on covariates and treatment assignment—without referencing the outcome variable. In other words, the design phase should be used to construct a balanced sample or subsamples of treated and

control units that are comparable in their covariate distributions, ensuring that “within this selected subsample, inferences are most robust and credible” (Imbens and Rubin, 2015). The design phase directly addresses the lack of overlap by identifying—and, if necessary, removing—observations in regions of the covariate space where treated and control units do not sufficiently overlap. This prevents researchers from extrapolating treatment effects to areas unsupported by the data. Even when overlap is present, the design phase helps improve covariate balance and reduce potential confounding.

To conduct a design phase in practice, we encourage researchers to apply matching, trimming, and/or reweighting methods. Crucially, outcome data should not be used during this phase, and hypothesis testing should be avoided to reduce the risk of p -hacking and preserve the validity of subsequent analyses.

It is important to note, however, that the design phase does not resolve all identification or estimation challenges. First, it does not make an unlikely unconfoundedness assumption suddenly valid. Second, it does not address issues related to nonlinearity or heterogeneity in the CME. Even after achieving covariate balance, the relationship between treatment and outcome may still vary with the moderator or other covariates in complex ways. These challenges are addressed during the estimation phase using flexible modeling strategies

To illustrate the value of design-based preprocessing, we reference studies such as Noble (2024), which show how these methods can effectively standardize treatment groups and improve the reliability of causal inference.

Example 6 *Noble (2024) examines how Members of Congress in the United States leverage the president’s symbolic power. The study argues that legislators—particularly those from the out-party—strategically reference the president to nationalize debates, shape constituent opinions, increase in-party approval, and reduce incentives for compromise. The analysis draws on a dataset of nearly two million floor speeches from 1973 to 2016. Here, we replicate the top panel of Figure 2 from the original paper, which shows that out-party legislators reference the president more frequently—and that this difference narrows as constituency*

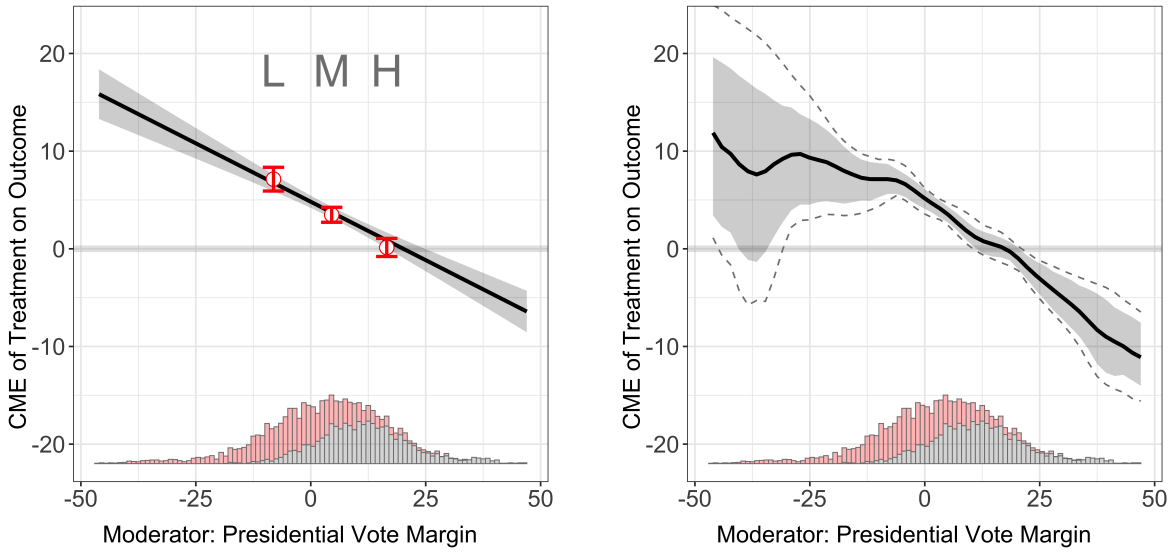
support for the president increases. The variables of interest are:

- *Outcome: Frequency of presidential references in Congressional speeches (continuous, $\in [0, 258]$)*
- *Treatment: Out-partisanship of lawmakers (binary, $\in \{0, 1\}$).*
- *Moderator: District past presidential vote margin (continuous, $\in [-46.06, 46.99]$).*

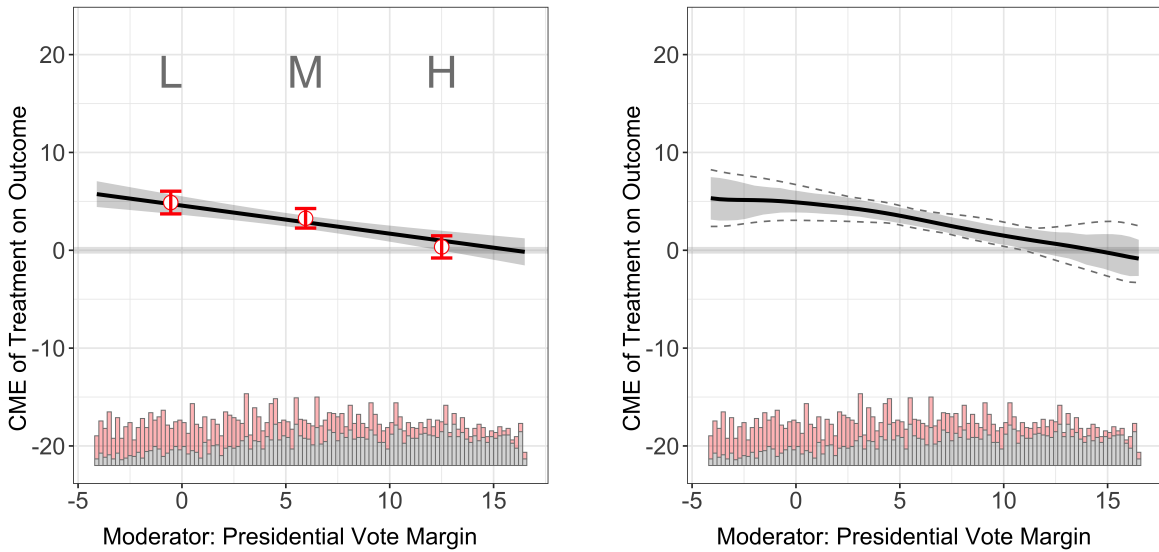
Using a large observational dataset, lack of overlap arises naturally due to partisan sorting in congressional districts: districts that overwhelmingly support the president tend to elect fewer out-party legislators, leading to imbalance across covariates—particularly the moderator. Figure 4(a) shows CME estimates based on the linear estimator (left panel), overlaid with binning estimates, and the kernel estimator (right panel). At the bottom of each panel, we plot histograms of the moderator by treatment condition. The plots reveal limited common support at the extremes of the moderator (when $X \notin [-10, 20]$). Despite this, the linear estimator still produces estimates in these regions, which are not credible as they rely heavily on extrapolation. In contrast, the kernel estimator reflects this lack of support through very wide confidence intervals. It is worth noting that the author is clearly aware of this issue and presents CME estimates over the range $x \in [-4, 16]$, using the linear estimator, although the estimation is based on the full sample.

To ensure reasonable overlap, we trimmed the data based on the central 95% quantile range of the moderator X . After trimming, both estimators exhibit more stable and nearly linear patterns, as shown in Figure 4(a). The narrower confidence intervals and smoother trends reflect improved covariate balance between treated and control units in the trimmed sample. The resulting estimates support the original finding: as a constituency becomes more supportive of the president, the gap between out-party and in-party lawmakers in referencing the president in congressional speeches narrows. This example shows that data trimming during the design phase improves the credibility of the estimates and may even help justify simpler models.

Figure 4: Replicating Noble (2024) Figure 2



(a) Full sample



(b) Trimmed sample

Notes: Treatment D is the out-partisanship of lawmakers, outcome Y . In each figure, the black dashed line represents the CME estimates; the red points (and bars) represent the binning estimates (and 90% pointwise confidence intervals); the shaded area and dotted lines represent 95% pointwise and uniform confidence intervals, respectively.

2.3 Misspecification

The linear interaction model makes rigid parametric assumption and can lead to misleading conclusions when misspecified. Below, we discuss two key scenarios where this occurs: (1) missing interaction terms between X and Z and (2) a nonlinear CME.

Missing Interaction Terms Blackwell and Olson (2022) highlight that the linear interaction model (as specified in Assumption 7) may omit potential interactions between the moderator X and other covariates Z , which are likely to be correlated in observational studies where neither D nor X is randomized. They refer to this specification as the single-interaction model, contrasting it with the fully-moderated model, where X_i is interacted with all covariates:

$$Y_i = \beta_0 + \beta_1 D_i + \beta_2 X_i + \beta_3 (D_i \cdot X_i) + Z_i \beta_4 + \beta_5 (X_i \cdot Z_i) + \epsilon_i.$$

The linear interaction model produces inconsistent estimates when (a) the treatment–moderator interaction is predictive of omitted interactions and (b) the omitted interactions significantly influence the outcome (Beiser-McGrath and Beiser-McGrath, 2020). This issue arises, for example, when the heterogeneous effect of D on Y depends not only on X but also on Z , yet Z is included only as a level term.

To address this issue, Blackwell and Olson (2022) recommend using a fully moderated model combined with a post-double-selection (PDS) procedure, originally introduced by Belloni, Chernozhukov and Hansen (2014). This method involves three steps: (i) applying Lasso to select interactions between X_i and Z_i that predict both Y and D ; (ii) taking the union of the selected variables from each model; and (iii) running a post-Lasso regression using this union to estimate the causal effect. The key advantage of PDS-Lasso is that it mitigates regularization bias by using Lasso only for variable selection, while relying on unpenalized OLS in the final step. This preserves interpretability and guards against omitted variable bias without distorting parameter estimates.

The kernel estimator introduced in the next section is fully moderated and thus immune to this criticism, provided the number of additional covariates is limited.

In Chapter 3, we introduce Lasso-based methods that are similar in spirit but differ in two key ways. First, they incorporate more flexible basis expansions of X and Z , to accommodate higher-order terms and interactions among covariates. Second, for binary treatments, we propose an AIPW estimator, and for continuous treatments, we use a partialling-out approach—both of which go beyond the post-Lasso regression strategy described here.

Nonlinear CME As discussed earlier, while the linear interaction model allows the effect of D on Y to vary with X , it imposes the restriction that $\theta(x) = \beta_1 + \beta_3 x$. When D is continuous, this implies that the effect of D on Y changes with X at a constant rate, determined by β_3 . However, in many empirical settings, this assumption is unrealistic, as treatment effects are rarely strictly linear in a covariate and may not even be monotonic. HMX (2019) highlight this limitation and emphasize that violating this assumption can lead to misinterpretation of the CME.

Binning estimator as a diagnostic tool. To diagnose potential nonlinearity in the CME, HMX (2019) propose the binning estimator, which partitions the range of the continuous moderator X into intervals and estimates the CME at an evaluation point within each interval. For simplicity, consider dividing X into three bins using cutoff points $\delta_{1/3}$ and $\delta_{2/3}$, representing the first and second terciles of the X distribution. Define three dummy variables:

$$G_{1,i} = \begin{cases} 1 & X_i < \delta_{1/3} \\ 0 & \text{otherwise} \end{cases}, \quad G_{2,i} = \begin{cases} 1 & \delta_{1/3} \leq X_i < \delta_{2/3} \\ 0 & \text{otherwise} \end{cases}, \quad G_{3,i} = \begin{cases} 1 & X_i \geq \delta_{2/3} \\ 0 & \text{otherwise.} \end{cases}$$

Within each bin, we select an evaluation point x_j (such as the median of X values in that bin) and model the outcome Y as a piecewise linear function of X , interacting with the

treatment D . We then estimate the following model using OLS:

$$Y_i = \sum_{j=1}^3 [\mu_j + \alpha_j W_i + \eta_j (X_i - x_j) + \beta_j (X - x_j) D_i] \cdot G_{j,i} + Z_i \gamma + \epsilon_i,$$

where $\mu_j, \alpha_j, \eta_j, \beta_j$ are unknown parameters to be estimated, Z represents additional covariates, and ϵ is an error term with $\mathbb{E}[\epsilon_i | X_i = x, W_i, Z_i] = 0$. The key insight is that at the chosen evaluation points x_j , the CME simplifies to $\theta(x_j) = \alpha_j$ since $(X - x_j) = 0$ at these points.

By allowing α_j to vary across bins, the binning estimator accommodates flexible CME patterns across different segments of the moderator. Unlike the linear interaction model, which imposes a single global linear relationship on the CME, this piecewise approach relaxes the linearity assumption on the CME and can capture more nuanced patterns. At the same time, the binning estimator remains easier to implement than fully nonparametric or semiparametric methods, as it relies on standard regression techniques and well-established inference methods. Standard errors for $\theta(x_j)$ are readily obtained from the regression output, eliminating the need for additional estimation steps or complex inference procedures. We illustrate the issue of nonlinear CME and the effectiveness of the binning estimator using the following example, which is also featured in HMX (2019).

Example 7 *Clark and Golder (2006) studies the topic in the number of parties in a polity. The authors examines the effect of temporal proximity of presidential elections, because presidential elections, as the most important election in a polity, are most likely to have the strongest effect when held concurrently with legislative elections. The directions of this “coat-tails effect” is moderated by the number of presidential election candidates: temporal proximity of presidential elections decrease the number of parties participating in the elections, if number of presidential candidates is small, because parties that are not competitive in presidential races are at a disadvantage. We replicate Figure 2 in the original paper, the variables of interest are:*

- *Outcome: number of parties compete in an election (continuous)*

- *Treatment: temporal proximity of presidential elections (continuous, $\in [0, 1]$)*
- *Moderator Variable: number of presidential candidates. (continuous)*

```

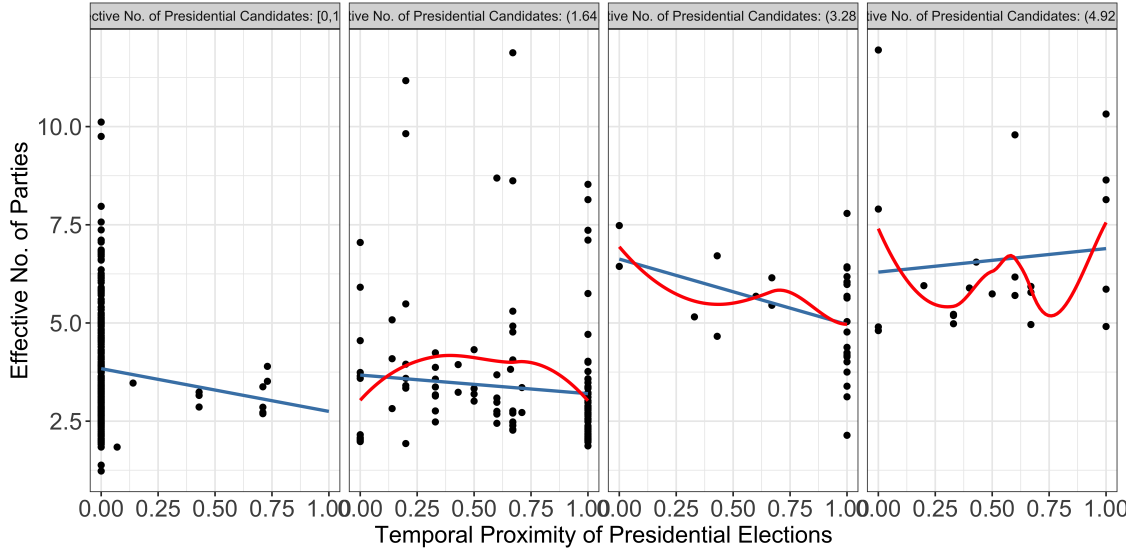
1 # R code excerpt
2
3 library(interflex)
4
5 Y="enep1" #Effective number of electoral parties
6 D="proximity1" #Temporal proximity of presidential elections
7 X="enpres" #Number of presidential candidates"
8 Z=c("uppertier" ,"logmag" , "uppertier_neg" ,"eneg", "logmag_neg")
9
10 ## diagnostic plot
11 cuts_raw<-c(0,1.64,3.28,4.92)
12 out.raw <- interflex(estimator = "raw", data = d,
13   Y=Y,D=D,X=X, na.rm = TRUE,
14   ncols = 4, cutoffs = cuts_raw)
15 plot(out.raw)
16
17 ## binning estimator with uniform CI
18 cuts_bin<-c(0,0.1,3,4,7)
19 out.binning<-interflex(estimator = "binning",data = d,
20   Y=Y,D=D,X=X,Z=Z, data=d,
21   vartype ="bootstrap", nbins = 4, cutoffs = cuts_bin)
22 plot(out.binning)

```

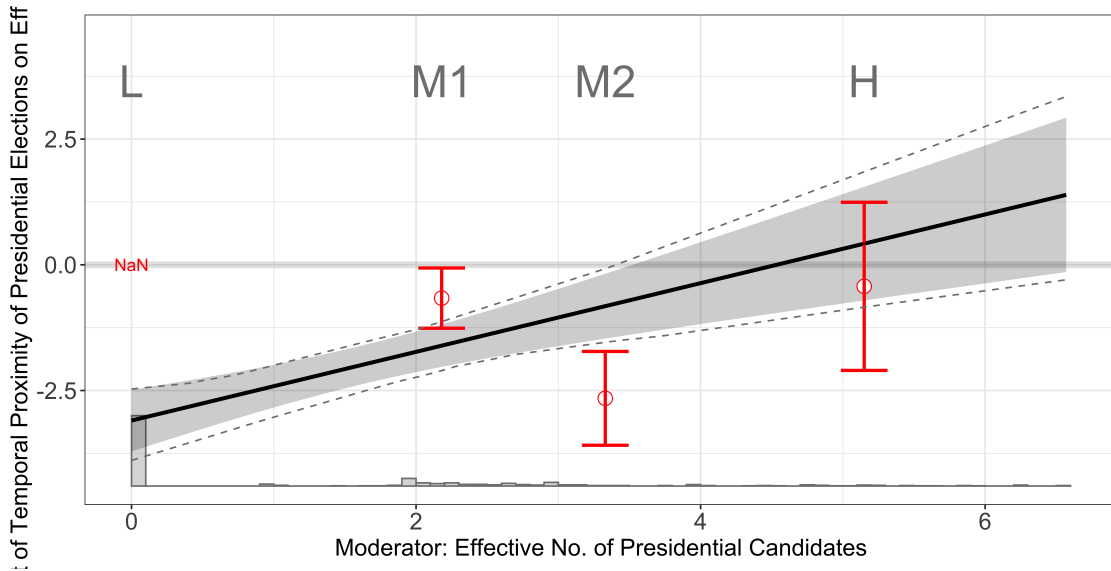
Because a significant portion of the observations in the sample (59%) have $X = 0$, as shown in Figure 5(a), we discretize X into four bins: $\{0\}$, $(0, 3]$, $(3, 4]$, and $(4, 6.57]$. The last three bins contain approximately equal numbers of observations. Figure 5(a) also reveals that the bivariate relationship between D and Y does not appear to increase with the moderator.

Figure 5(b) compares the CME estimates from the linear interaction model and the binning estimator. Contrary to the study's claim of a positive interaction based on the linear

Figure 5: Replicating Clark and Golder (2006) Figure 2



(a) Raw outcome plot by moderator values



(b) CME plot

Notes: Treatment D is presidential elections, outcome Y is the effective number of electoral parties. (a) Plot of the raw outcome data in each bin of the moderator. (b) The CME estimates based on the linear interaction model (black line) and the binning estimator (red hollow circles). The gray ribbon and red bars show the 95% pointwise confidence intervals, respectively. The dashed lines represent 95% uniform confidence intervals of the linear interaction model.

interaction model, the binning estimator indicates highly nonlinear effects. Specifically, the effect is negative and small in the second bin ($X \in (0, 3]$), turns negative and statistically

significant in the third bin ($X \in (3, 4]$), and then approaches zero in the last bin ($X \in (4, 6.57]$). This pattern suggests that the linear interaction model is misspecified.

Moreover, the treatment has no variation in the first bin ($X = 0$), making the treatment effect non-identifiable at $x = 0$ due to a lack of common support. This further highlights the limitations of the linear interaction model in this case. Additionally, the uniform confidence interval for the second bin (M1) covers zero, meaning that we cannot reject the null hypothesis that $\theta(x) < 0$ for all $x \leq 3$ at the 5% level, contradicting what the linear interaction model might have suggested.

While we typically do not assume that the CME changes with X in a piecewise manner, this example demonstrates that the binning estimator is an easy-to-implement and powerful diagnostic tool for detecting potential nonlinearity in the CME. To achieve greater flexibility in modeling the functional form of the CME, we turn to more advanced methods, such as the kernel estimator, which we will discuss later in this chapter, and AIPW and DML estimators, which we will explore in the next two chapters.

2.4 The Kernel Estimator

While parametric methods rely on strong and often unrealistic functional form assumptions, and nonparametric models avoid such assumptions but suffer from the “curse of dimensionality,” semiparametric methods offer a middle ground. They relax functional form restrictions by allowing some components of the model to be flexible while maintaining parametric structure in others. HMX (2019) propose a semiparametric kernel estimator based on smooth varying-coefficient models (SVCM) (Hastie, 2017) to estimate the CME. In the remainder of the Element, we refer to this method as the kernel estimator. We introduce two improvements: (i) allowing the coefficient on Z to vary with X , making the model fully moderated, and (ii) incorporating an adaptive kernel to improve estimation accuracy across different regions of the data distribution.

Assumption 8 *Smooth varying-coefficient model , SVCM*

$$Y_i = f(X_i) + g(X_i)D_i + Z_i\gamma(X_i) + \epsilon_i$$

in which $f(\cdot), g(\cdot)$ and $\gamma(\cdot)$ are smooth functions.

SVCM assumes that Y is a function of D , X , and Z , while their impact on Y is modeled as an unspecified smooth function of X . At each evaluation point x_0 , each of them is approximated by a centered, linear regression:

$$f(X)|_{X-x_0|<\epsilon} = \mu(x_0) + \eta(x_0)(X - x_0)$$

$$g(X)|_{X-x_0|<\epsilon} = \alpha(x_0) + \beta(x_0)(X - x_0)$$

$$\gamma(X)|_{X-x_0|<\epsilon} = \rho(x_0) + \delta(x_0)(X - x_0)$$

HMX (2019) assume a slightly more restrictive form of SVCM: $Y_i = f(X_i) + g(X_i)D_i + Z_i\gamma + \epsilon_i$, where γ does not vary with X . Assumption 8 represents a fully moderated version of their model.

As before, unconfoundedness implies $\mathbb{E}[\epsilon_i|X_i, D_i, Z_i] = 0$. Given Assumption 8, the CME becomes:

$$\theta(x) = \mathbb{E}_Z [f(x) + g(x) + Z'\gamma(x)] - \mathbb{E}_Z [f(x) + Z\gamma(x)] = g(x).$$

when D is binary. CME for a continuous D similarly yields:

$$\theta(x) = \mathbb{E}_Z \left[\frac{\partial(f(x) + g(x)W + Z'\gamma(x))}{\partial D} \right] = g(x).$$

Therefore, our goal is to obtain valid inference for $g(x)$. In SVCM, the intercept $f(x)$, treatment effect $g(x)$, and control coefficients $\gamma(x)$ are all flexible functions of the moderator X , allowing for nonlinear CME.

HMX (2019) propose a kernel (smoothing) estimator for the CME within SVCM. For each x_0 in the support of X , $\hat{f}(x_0)$, $\hat{g}(x_0)$, and $\hat{\gamma}(x_0)$ are estimated by minimizing the following weighted least-squares objective function. The kernel estimator incorporates all observed data points, assigning greater weight to those closer to x_0 .

HXM (2019) propose a kernel smoothing estimator for the CME with SVCMM. For each given x_0 in the support of X , $\hat{f}(x_0)$, $\hat{g}(x_0)$, and $\hat{\gamma}(x_0)$ are estimated by minimizing the following weighted least-squares objective function. With our two improvements, the kernel estimator that considers the influence of potentially all data points with greater emphasis on points closer to x_0 can be written as:

$$\left(\hat{\mu}(x_0), \hat{\alpha}(x_0), \hat{\eta}(x_0), \hat{\beta}(x_0), \hat{\rho}(x_0), \hat{\delta}(x_0)\right) = \arg \min_{\tilde{\mu}, \tilde{\alpha}, \tilde{\eta}, \tilde{\beta}, \tilde{\rho}, \tilde{\delta}} L(\tilde{\mu}, \tilde{\alpha}, \tilde{\eta}, \tilde{\beta}, \tilde{\rho}, \tilde{\delta})$$

in which:

$$L = \sum_{i=1}^N \left\{ \left[Y_i - \tilde{\mu} - \tilde{\alpha}D_i - \tilde{\eta}(X_i - x_0) - \tilde{\beta}D_i(X_i - x_0) - \tilde{\rho}Z_i - \tilde{\delta}Z_i(X_i - x_0) \right]^2 K \left(\frac{|X_i - x_0|}{h(x_0)} \right) \right\}$$

Kernel smoothing averages data points using a kernel function, with weights determined by proximity to the estimation point. The kernel function, $K(\cdot)$, assigns higher weights to observations closer to the target point x_0 . With the above kernel estimator, $\hat{f}(x_0) = \hat{\mu}(x_0)$ and $\hat{g}(x_0) = \hat{\alpha}(x_0)$. Smoothing is performed using a Gaussian kernel $K(\cdot)$, while the parameter of the bandwidth function $h(x_0)$ is selected via least-squares cross-validation.

Adaptive Kernel Classical bandwidth selection methods perform well only when the underlying density is approximately normal. They become problematic for long-tailed or multimodal distributions. A fixed-bandwidth kernel estimator performs well near the mode, where data density is high, but oversmooths in the tails, where observations are sparse, leading to biased estimates. To mitigate this issue, adaptive kernel density estimation adjusts the bandwidth for each data point, allowing for finer resolution in sparse regions while maintaining stability in denser areas.

With an adaptive kernel, the bandwidth h is no longer constant but varies with the location x , denoted as $h(x)$, allowing for more flexible smoothing across different regions of the data distribution:

$$h(x) = h \times \left(1 + \log \left(\frac{\rho_{max}}{\rho(x)} \right) \right)$$

where h is the base bandwidth, ρ_{max} is the maximum kernel density estimate across all

x_i , and $\rho(x)$ represents the local density at x_0 , determined by the kernel density at the nearest data point or minimum distance. The goal of this approach is to make $h(x)$ inversely proportional to the local data density. In regions with sparse data, the bandwidth increases, allowing for broader smoothing across X values, while in denser regions, the bandwidth decreases, enabling more localized smoothing and preserving finer details in the estimation. The base bandwidth h is selected using least-squares cross-validation, which minimizes the cross-validation score computed via 10-fold cross-validation. In this approach, the dataset is randomly partitioned into 10 folds. For each fold k , the kernel regression estimate $\hat{m}_h^{(-k)}(x_i)$ is computed by fitting the model on the remaining nine folds, and the prediction error is measured on the held-out fold. The overall cross-validation score is then given by

$$CV(h) = \frac{1}{N} \sum_{k=1}^{10} \sum_{i \in I_k} \left[Y_i - \hat{m}_h^{(-k)}(x_i) \right]^2,$$

where I_k denotes the set of indices in the k -th fold. This procedure selects the bandwidth that minimizes the mean-squared prediction error, effectively balancing bias and variance in the estimation.

A common issue in semiparametric regression is boundary bias, where estimates near the edges of the data range tend to be less accurate due to fewer observations. As recommended by [Fan, Heckman and Wand \(1995\)](#), [HMX \(2019\)](#) address this problem by incorporating two additional terms, $\eta(X - x_0)$ and $\beta D(X - x_0)$, which capture the first partial derivative of Y with respect to X at each x_0 . With a fully moderated version, $\delta Z(X - x_0)$ is also included for each covariate Z . These terms adjust for the local slope of the response surface, helping to reduce bias at the boundaries of the support of X , where data are sparse and estimation uncertainty is higher.

Inference Once we obtain the CME estimates through kernel-weighted least squares, the next step is to estimate the standard errors of the estimated parameters. This can be done using two approaches: (i) analytically, via the delta method, and (ii) empirically, using bootstrapping.

We can estimate pointwise variance analytically using the delta method, which approximates the variance of a function of an estimator through a first-order Taylor expansion. The delta method assumes that the estimator θ is approximately normally distributed, particularly in large samples, allowing the function $g(\theta)$ to be similarly approximated.

In our context, where $\theta = (\mu, \alpha, \eta, \beta, \rho, \delta)$, the function $g(x)$ is given by $g(\theta) = (\hat{\alpha}(x_0), \hat{\beta}(x_0))$. The variance of $g(\theta)$ is then approximated as:

$$\text{Var}(g(\theta)) \approx \nabla g(\theta)^T \cdot \text{Cov}(\theta) \cdot \nabla g(\theta)$$

where $\nabla g(\theta)$ is the gradient of g with respect to θ , and $\text{Cov}(\theta)$ is the covariance matrix of the estimator θ . The confidence interval for θ is calculated as:

$$CI : \hat{\theta} \pm z \times SE(\hat{\theta})$$

where z is the critical value from the t -distribution for a 95% confidence interval, and $SE(\hat{\theta})$ is the standard error of the estimate.

An alternative approach is bootstrapping. Given a dataset S with n observations, we generate B bootstrap samples S_1, S_2, \dots, S_B by sampling with replacement from S . For each bootstrap sample S_b , we compute the kernel estimates $\hat{\theta}_b = (\hat{\mu}_b, \hat{\alpha}_b, \hat{\eta}_b, \hat{\beta}_b, \hat{\rho}_b, \hat{\delta}_b)$, and the standard deviation of these estimates approximates the standard error:

$$SE(\hat{\theta}) \approx \sqrt{\frac{1}{B-1} \sum_{b=1}^B (\hat{\theta}_b - \bar{\theta}_B)^2}$$

where $\bar{\theta}_B$ is the mean of the bootstrap estimates.

Because bootstrapping requires many resampling iterations, it can be computationally intensive, especially for large datasets or complex models. To improve efficiency, the `interflex` package implements parallel computing for analytical standard error estimation. The bootstrapping process is distributed across multiple cores, with each core handling a subset of bootstrap iterations independently, significantly reducing computation time. Let θ_{ij} denote the estimate of parameter θ from the j -th bootstrap sample on the i -th core. The final

estimate and variance are computed as:

$$\hat{\theta} = \frac{1}{n} \sum_{i=1}^C \sum_{j=1}^B \hat{\theta}_{ij}, \quad \text{Var}(\hat{\theta}) = \frac{1}{n-1} \sum_{i=1}^C \sum_{j=1}^B (\hat{\theta}_{ij} - \hat{\theta})^2$$

Furthermore, we extend the bootstrap approach to construct uniform confidence intervals, similar to those used with the linear interaction model. Again, we implement the bootstrap-based sup- t band method, ensuring valid inference across the entire range of X .

We apply the kernel estimator to Examples 4 and 7. The CME estimates from both examples are shown in Figure 6. Using data from Huddy, Mason and Aarøe (2015), the kernel estimator yields CME estimates that are nearly identical to those from the linear interaction model, suggesting that Assumption 7 is reasonable in this setting.

```

1 # R code excerpt
2
3 library(interflex)
4 ### Huddy et. al 2015
5 Y="totangry" #Angre
6 D="threat" #Threat
7 X="pidentity" #Partisan Identity
8 Z<-c("issuestr2", "pidstr2", "knowledge", "educ", "male", "age10" )
9
10 out.kernel1 <- interflex(estimator = "kernel",
11                          Y=Y,D=D,X=X,data=d,
12                          vartype = "bootstrap", ## uniform CI
13                          full.moderate = TRUE,
14                          na.rm = TRUE)
15 plot(out.kernel1)
16
17 ### Clark and Golder 2006
18 Y="enep1" #Effective number of electoral parties
19 D="proximity1" #Temporal proximity of presidential elections
20 X="enpres" #Number of presidential candidates"

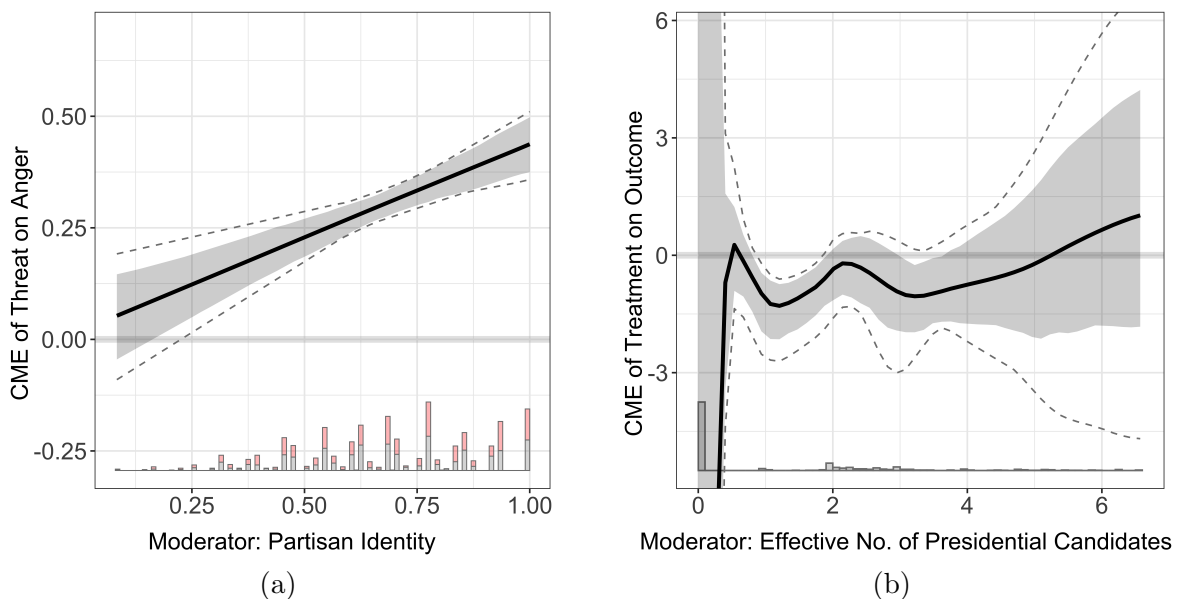
```

```

21 Z=c("uppertier" ,"logmag" ,"uppertier_neg" ,"eneg" ,"logmag_neg")
22
23 out.kernel2 <- interflex(estimator = "kernel",
24                          Y=Y,D=D,X=X,data=d,
25                          vartype = "bootstrap", ## uniform CI
26                          full.moderate = TRUE, na.rm = TRUE)
27 plot(out.kernel2)

```

Figure 6: Applying the Kernel Estimator



Notes: The above figures replicate Figure 2A from [Huddy, Mason and Aarøe \(2015\)](#) (a) and Figure 2 from [Clark and Golder \(2006\)](#) (b). In figure (b), treatment is presidential elections, outcome is the effective number of electoral parties. (a) Plot of the raw outcome data in each bin of the moderator. In each figure, the black dashed line represents the CME estimates based on the kernel estimator; shaded area and dotted lines represent pointwise and uniform confidence intervals, respectively, via nonparametric bootstrapping.

In contrast, using data from [Clark and Golder \(2006\)](#), the CME estimates differ substantially from those based on the linear interaction model. The first thing we notice is the absence of variation in the treatment variable when the moderator value is zero, indicating that the treatment effect is unidentifiable at this point due to lack of common support. This is not captured by the linear interaction model, but with kernel estimator, the confidence intervals blow up as the moderator approaches zero, given that there is no variation in the

treatment variable at this point.

The kernel estimator also picks up on nonlinearity in the CME masked by the linear interaction model. Contrary to the anticipated positive interaction suggested by the study, the CME estimates are insignificant when X is close to 0, shifts to a negative and statistically significant as the moderator ranges from approximately $[0.5, 2]$, and then reverts nearly to indistinguishable from zero when X is bigger than 0.

It is worth noting that in both examples, the patterns revealed by the kernel estimator are broadly consistent with the findings from the binning estimator, which we recommend as a diagnostic tool.

2.5 Summary

This chapter examines classic methods for estimating and visualizing the CME. We begin with the widely used linear interaction model, discussing its variance estimator and hypothesis testing procedures. To address the issue of multiple comparisons, we introduce uniform confidence intervals constructed via bootstrapping.

Next, we highlight two key challenges associated with the linear interaction model: lack of common support and model misspecification. We propose diagnostic tools, such as raw data plots and a binning estimator, to detect these issues and discuss strategies to mitigate them, including a design phase to improve overlap in observational studies.

Finally, we introduce a semiparametric kernel estimator to relax the functional form assumptions of linear interaction models. Building on HMX (2019), we propose two key improvements: a fully moderated specification and an adaptive kernel for more accurate estimation across different data regions. We also implement uniform confidence intervals for the kernel estimator to ensure valid inference.

Below, we summarize the challenges associated with the linear interaction model, along with diagnostic methods and potential solutions.

- **Challenge:** Multiple comparisons

- **Solution:** Uniform confidence interval
- **Challenge:** Lack of common support
 - **Diagnostics:** Raw outcome plot, Propensity score plot
 - **Solution:** Design phase
- **Challenge:** Rigid functional form
 - **Diagnostics:** Raw outcome plot, Binning estimator
 - **Solution:** Fully moderated model, kernel estimator, AIPW and extensions (Chapter 3), double machine learning (Chapter 4)

Chapter 3. AIPW and Extensions

So far, our analysis has primarily focused on modeling the conditional expectation function of the outcome $\mathbb{E}[Y \mid D, X, Z]$. For example, the linear interaction model posits that

$$\mathbb{E}[Y \mid D, X, Z] = \beta_0 + \beta_1 D + \beta_2 X + \beta_3(D \cdot X) + \beta_4' Z,$$

while a semi-parametric kernel estimator assumes

$$\mathbb{E}[Y \mid D, X, Z] = f(X) + g(X) D + Z' \gamma(X).$$

However, these models have limitations. First, they do not take into account the treatment assignment process. In the binary-treatment setting, for instance, one might consider modeling the propensity score $\mathbb{E}[D \mid X, Z] = \Pr[D = 1 \mid X, Z]$ to improve robustness when estimating the CME. Second, while we allow for nonlinearity in X , we have largely overlooked potential nonlinearities and high-dimensional interactions among the other covariates Z . Although the kernel estimator allows the relationship between Z and Y to be nonlinear, it does not accommodate higher-order interactions among the covariates.

In this chapter, we address these limitations using the AIPW approach and its extensions. We first focus on the scenario where D is binary. We review the IPW estimator discussed in Chapter 1—now with a continuous moderator—and introduce the AIPW framework. The IPW estimator estimates the CME using the propensity score without specifying an outcome model, while the AIPW estimator integrates both the outcome model and the propensity score model, making it a *doubly robust* estimator, meaning that it is consistent as long as at least one of the two models is correctly specified. When the treatment D is continuous, we can estimate the CME using an approach analogous to AIPW. Specifically, we first partial out the covariates from both the outcome and treatment models, producing “denoised” versions of Y and D . The CME is then estimated based on the relationship between these adjusted variables.

3.1 Why AIPW Works

We first discuss the theoretical properties of AIPW in the binary treatment case. In Chapter 1, we define the conditional mean outcome by treatment condition $\mu^d(v) = \mathbb{E}[Y_i \mid D_i = d, V_i = v]$, $d = 0, 1$ and the propensity score, $\pi(v) = \Pr(D_i = 1 \mid V_i = v)$. We have shown that, when D is binary and all covariates in V are discrete, under unconfoundedness and overlap assumptions, the stratified difference-in-means can identify the CME:

$$\sum_v \{(\mu^1(v) - \mu^0(v)) \cdot \Pr(V = v \mid X = x)\} = \theta(x),$$

which naturally extends to cases where Z includes continuous variables by replacing the sum with an integral:

$$\int (\mu^1(v) - \mu^0(v)) \cdot f_{V|X}(v \mid x) dv = \theta(x),$$

where $f_{V|X}(v \mid x)$ denotes the conditional density of V given $X = x$. We can therefore use expectation notation to cover both cases:

$$\mathbb{E}[\mu^1(V_i) - \mu^0(V_i) \mid X_i = x] = \theta(x). \quad (4)$$

Moreover, in Chapter 1, we also prove that the IPW estimator can identify the CME:

$$\mathbb{E} \left[\frac{D_i \cdot Y_i}{\pi(V_i)} - \frac{(1 - D_i) \cdot Y_i}{1 - \pi(V_i)} \mid X_i = x \right] = \theta(x). \quad (5)$$

Both expectations are taken over the conditional density of V given X .

Note that the IPW estimator can be highly sensitive to extreme weights, particularly when the estimated propensity score $\pi(V_i)$ is close to 0 or 1. A common technique to mitigate this issue is trimming, which excludes units whose estimated propensity scores fall outside a predefined range $[\alpha, 1 - \alpha]$, where α is a chosen threshold ([Crump, Hotz, Imbens and Mitnik, 2006](#)). By truncating extreme weights, trimming reduces variance and improves the precision of estimates. However, doing so alters the target parameter, as it excludes units with extreme propensity scores. In the remainder of this chapter, we fix α to 10^{-2} in implementations.

Building on the strengths of both outcome modeling and IPW, [Robins, Rotnitzky and Zhao \(1994\)](#) introduced the AIPW estimator, which combines the outcome model and the propensity score model to improve robustness and efficiency in estimating the CME. The AIPW estimator for the CME can be constructed in the following way:

$$\begin{aligned} & \mathbb{E} [\mu^1(V_i) - \mu^0(V_i) \mid X_i = x] + \\ & \mathbb{E} \left[\frac{D_i}{\pi(V_i)} (Y_i - \mu^1(V_i)) - \frac{1 - D_i}{1 - \pi(V_i)} (Y_i - \mu^0(V_i)) \mid X_i = x \right] = \theta(x). \end{aligned} \quad (6)$$

The proof in the appendix shows that the equality holds (i.e., AIPW is consistent) when either the outcome models, $\mu^1(V_i)$ and $\mu^0(V_i)$, or the propensity score model, $\pi(V_i)$, is correctly specified, but not necessarily both. This property is known as double robustness.

In large samples, beyond its double robustness property, the AIPW estimator typically exhibits lower variance than IPW when both the outcome and propensity score models are correctly specified. [Robins, Rotnitzky and Zhao \(1994\)](#) show that AIPW achieves the smallest asymptotic variance within the class of inverse probability-weighted estimators. However, when only the outcome models are correctly specified, the AIPW estimator remains consistent but can exhibit higher variance compared to a purely outcome-based model.

In finite samples, AIPW does not necessarily outperform the outcome model or the IPW estimator. [Li, Thomas and Li \(2019\)](#) demonstrate through simulations that the finite-sample performance of AIPW depends heavily on the degree of overlap in propensity scores. When overlap is poor, particularly without trimming extreme propensity scores, the AIPW estimator often performs worse than an outcome-based estimator.

Signals. Now we introduce the concept of *signals*, which refer to transformations of the data that are relevant for target parameter estimation, as commonly used in the double

robustness literature. Define signals based on outcome-modeling, IPW, and AIPW as:

$$\begin{aligned}\Lambda_i^{(\text{outcome})} &= \mu^1(V_i) - \mu^0(V_i); \\ \Lambda_i^{(\text{ipw})} &= \frac{D_i}{\pi(V_i)} Y_i - \frac{1 - D_i}{1 - \pi(V_i)} Y_i; \\ \Lambda_i^{(\text{aipw})} &= \mu^1(V_i) - \mu^0(V_i) + \frac{D_i}{\pi(V_i)} (Y_i - \mu^1(V_i)) - \frac{1 - D_i}{1 - \pi(V_i)} (Y_i - \mu_0(V_i)).\end{aligned}$$

Therefore, Each of Equations (4)–(6) implies an identification result for a specific type of signals:

$$\text{Equation (4)} \Rightarrow \mathbb{E}[\Lambda_i^{(\text{outcome})} \mid X_i = x] = \theta(x),$$

$$\text{Equation (5)} \Rightarrow \mathbb{E}[\Lambda_i^{(\text{ipw})} \mid X_i = x] = \theta(x),$$

$$\text{Equation (6)} \Rightarrow \mathbb{E}[\Lambda_i^{(\text{aipw})} \mid X_i = x] = \theta(x).$$

In other words, taking the conditional expectation of any of the outcome, IPW, or AIPW signals given $X_i = x$, under their respective modeling assumptions, identifies the CME.

3.2 Estimation Strategies

Implementing the AIPW estimator for the CME takes three steps (Semenova and Chernozhukov, 2021). First, we estimate the propensity score, $\Pr[D = 1 \mid X, Z]$, and the conditional means based on outcome models, $\mathbb{E}[Y \mid D = 0, X, Z]$ and $\mathbb{E}[Y \mid D = 1, X, Z]$. Later, we will refer to these terms as *nuisance parameters*, as they are not of direct interest but are essential for obtaining an unbiased estimate of the CME.

Next, we construct adjusted outcome signals using the fitted propensity score and/or residuals from the outcome models. Specifically, we weight the residualized outcomes by the inverse of the estimated propensity score, creating a pseudo-population where the residuals from treated and control outcomes are balanced with respect to Z . In the IPW estimator, this residualizing step using the outcome models is omitted, as it relies solely on the propensity score for adjustment.

Finally, we estimate the CME with respect to X using the constructed signals. When X

is discrete, the CME is obtained by averaging the adjusted signals within each subgroup of X . When X is continuous, we can regress the adjusted signal on a flexible representation of X , such as a B-spline basis expansion, to obtain a smooth estimate of the CME. Alternatively, we can use semiparametric kernel regression techniques, as introduced in Chapter 2, to estimate this relationship.

Constructing Signals We begin by discussing how to construct signals from data using outcome modeling, IPW, and AIPW. Once the signals are obtained, we can estimate the CME by fitting them to a flexible function of X , denoted $\hat{f}(X)$, which we will examine in detail later.

Signals from outcome modeling. With the outcome modeling approach, we fit two separate linear regression for data with $D_i = 1$ and $D_i = 0$. Specifically, we regress Y_i on $(1 V_i)$ *separately* within each treatment group, yielding the following estimates:

$$\hat{\mu}^0(V_i) = \hat{\beta}_0^0 + V_i \hat{\beta}_V^0, \quad \hat{\mu}^1(V_i) = \hat{\beta}_0^1 + V_i \hat{\beta}_V^1,$$

where $(\hat{\beta}_0^0, \hat{\beta}_V^0)$ and $(\hat{\beta}_0^1, \hat{\beta}_V^1)$ are the OLS coefficients obtained from these two regressions. For each observation i , we then construct the signals from the outcome model:

$$\hat{\Lambda}_i^{(\text{outcome})} = \hat{\mu}^1(V_i) - \hat{\mu}^0(V_i) = (\hat{\beta}_0^1 - \hat{\beta}_0^0) + V_i(\hat{\beta}_V^1 - \hat{\beta}_V^0),$$

which represents the predicted treatment effect for observation i .

IPW signals. For the IPW estimator, we first fit a propensity score model using a logistic regression of D on V . For each observation i , the estimated propensity score is

$$\hat{\pi}(V_i) = \hat{\text{Pr}}(D_i = 1 \mid V_i) = \frac{\exp(\hat{\gamma}_0 + V_i \hat{\gamma}_V)}{1 + \exp(\hat{\gamma}_0 + V_i \hat{\gamma}_V)}.$$

where $(\hat{\gamma}_0, \hat{\gamma}_V)$ are coefficients from the logistic regression.

For each observation i , we then construct the IPW signals, which are the IPW-adjusted

outcomes:

$$\hat{\Lambda}_i^{(\text{ipw})} = \frac{D_i}{\hat{\pi}(V_i)} Y_i - \frac{1 - D_i}{1 - \hat{\pi}(V_i)} Y_i.$$

This adjustment reweights the treated and control outcomes by $\frac{1}{\hat{\pi}(V_i)}$ and $\frac{-1}{(1-\hat{\pi}(V_i))}$, respectively:

$$\hat{\Lambda}_i^{(\text{ipw})} = \frac{Y_i}{\hat{\pi}(V_i)} \quad \text{if } D_i = 1, \quad \text{and} \quad \hat{\Lambda}_i^{(\text{ipw})} = \frac{-Y_i}{1 - \hat{\pi}(V_i)} \quad \text{if } D_i = 0.$$

This reweighting creates a pseudo-population where covariates V_i are (asymptotically) balanced between treated and control groups via the propensity score, ensuring that a simple difference in means in this pseudo-population can recover the treatment effect. Specifically, among treated units, those with smaller estimated propensity scores receive more weight, while among control units, those with higher propensity scores receive more weight. This adjustment corrects for selection bias induced by V by aligning the covariate distributions across treatment groups.

AIPW signals. The AIPW estimator combines elements of both outcome modeling and IPW. We first fit two linear regression models $\hat{\mu}_1(V_i)$ and $\hat{\mu}_0(V_i)$, as well as the propensity score model $\hat{p}(V_i)$. We then construct the signal as follows:

$$\hat{\Lambda}_i^{(\text{aipw})} = \hat{\mu}_1(V_i) - \hat{\mu}_0(V_i) + \frac{D_i}{\hat{\pi}(V_i)} (Y_i - \hat{\mu}_1(V_i)) - \frac{1 - D_i}{1 - \hat{\pi}(V_i)} (Y_i - \hat{\mu}_0(V_i)).$$

Note that

$$\begin{aligned} \hat{\Lambda}_i^{(\text{aipw})} &= \hat{\mu}_1(V_i) - \hat{\mu}_0(V_i) + \frac{1}{\hat{\pi}(V_i)} (Y_i - \hat{\mu}_1(V_i)) && \text{if } D_i = 1, \\ \hat{\Lambda}_i^{(\text{aipw})} &= \hat{\mu}_1(V_i) - \hat{\mu}_0(V_i) - \frac{1}{1 - \hat{\pi}(V_i)} (Y_i - \hat{\mu}_0(V_i)) && \text{if } D_i = 0. \end{aligned}$$

For both treated and control units, the first term, $\hat{\mu}_1(V_i) - \hat{\mu}_0(V_i)$, represents the predicted treatment effect for unit i based on the outcome model. The second term, $\frac{1}{\hat{\pi}(V_i)} (Y_i - \hat{\mu}_1(V_i))$ for treated units and $\frac{1}{1-\hat{\pi}(V_i)} (Y_i - \hat{\mu}_0(V_i))$ for control units, adjusts for discrepancies between observed outcomes and their model-based predictions by reweighting *residuals from the outcome model*. Similar to the IPW estimator, treated units with smaller estimated propensity

scores receive more weight, while control units with larger estimated propensity scores are weighted more heavily. However, instead of reweighting the raw outcome Y_i , AIPW reweights the residuals, $(Y_i - \hat{\mu}_D(V_i))$, which helps reduce sensitivity to misspecifications in the outcome model.

Next, we use a simulated example to illustrate the advantages of IPW and AIPW over a purely outcome-modeling approach. In this example, the CME is nonlinear, but the researcher misspecifies the outcome model as a linear interaction model. Fortunately, she correctly specifies the propensity score model. This scenario highlights the limitations of relying solely on outcome modeling, particularly when using rigid parametric models. Later, we introduce basis expansions to relax parametric assumptions and enhance estimation flexibility.

Example 8 (A Simulated Sample with a Misspecified Outcome Model) *The sample consists of 1,000 observations, with a moderator X_i uniformly distributed on $[-2, 2]$ and two covariates Z_{i1} and Z_{i2} uniformly distributed on $[0, 1]$. Let $V_i = [X_i, Z_{i1}, Z_{i2}]$ be the set of all confounders. Treatment is assigned as a binary variable with probability*

$$\Pr(D_i = 1) = \frac{\exp(0.5X_i + 0.5Z_{i1})}{1 + \exp(0.5X_i + 0.5Z_{i1})}.$$

The outcome Y is generated via

$$Y_i = 1 + X_i + D_i - X_i^2 D_i + Z_{i1} + \epsilon_i,$$

where $\epsilon_i \sim \mathcal{N}(0, 1)$. Unconfoundedness holds: $D_i \perp\!\!\!\perp Y_i(0), Y_i(1) \mid V_i$. The CME is nonlinear in x , i.e., $\theta(x) = 1 - x^2$. Covariate Z_{i2} is redundant since it does not directly affect D_i or Y_i .

However, the researcher correctly specifies the propensity score model but misspecifies the outcome model as:

$$Y_i = 1 + X_i + D_i + Z_{i1} + \epsilon_i,$$

Figure 7(a) plots the raw outcome Y_i against the moderator X_i , using deep blue for

treated units ($D_i = 1$) and shallow blue for control units ($D_i = 0$). In both groups, the relationships between X_i and Y_i are nonlinear.

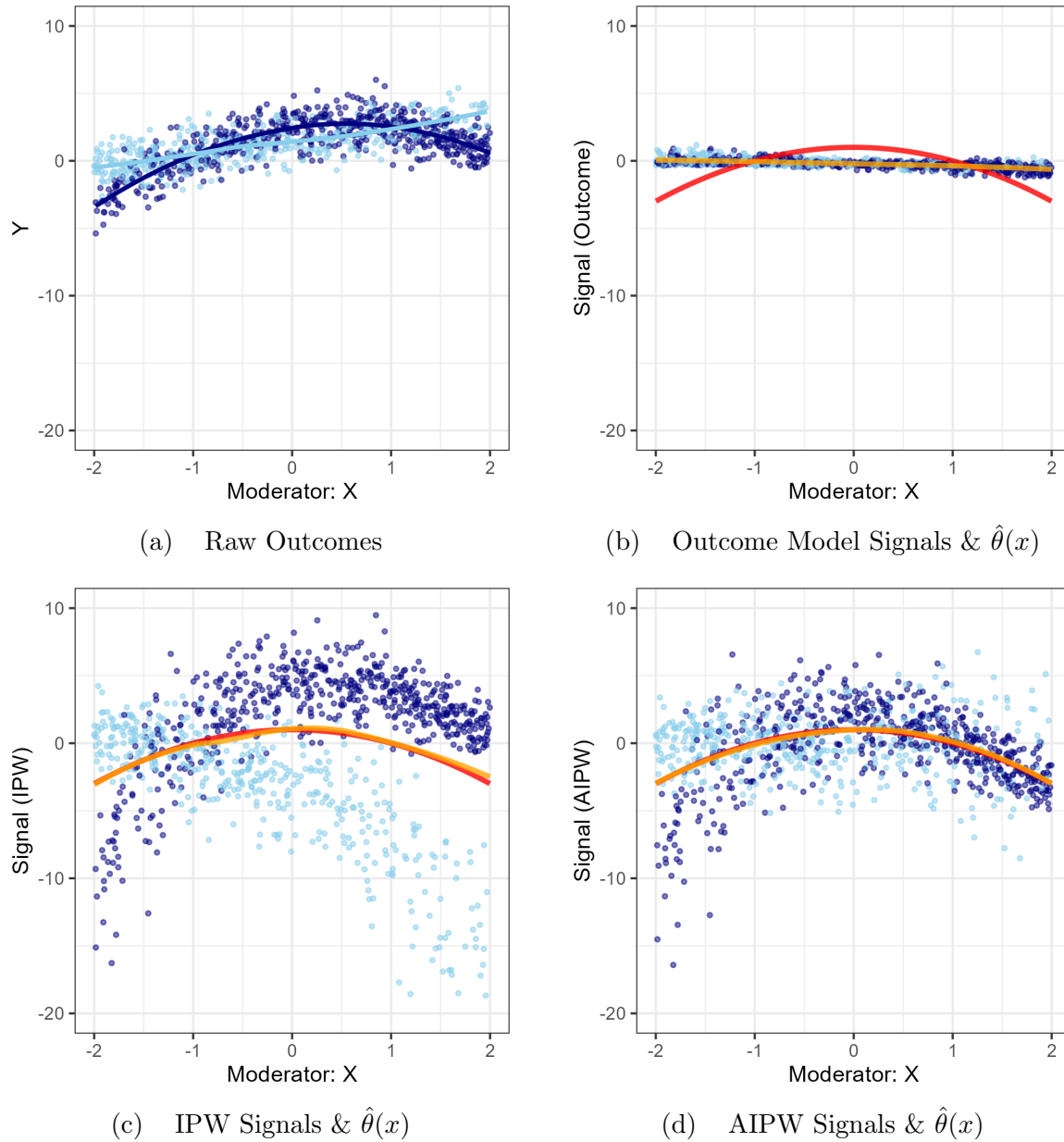
Figure 7(b) plots the signals from the outcome model, $\hat{\Lambda}_i^{(\text{outcome})}$. Because the model is misspecified, the signals—representing predicted treatment effects—are linear in X . After we apply a smoother (a B-spline regression), these signals lead to misleading CME estimates (orange line), which are also linear in X .

Figure 7(c) plots the signals from the IPW estimator, $\hat{\Lambda}_i^{(\text{ipw})}$. Compared to the corresponding raw outcome values, treated observations (deep blue) with small X values are relatively upweighted (i.e., their absolute values are magnified), as are control observations (light blue) with large X values. This occurs because D (and the estimated propensity score) is positively correlated with X . Since the propensity score model is correctly specified, this adjustment mitigates selection bias and helps reveal the true CME after smoothing.

In Figure 7(d), we plot the AIPW signals, $\hat{\Lambda}_i^{(\text{aipw})}$. They behave similarly to the IPW signals and successfully recover the true CME after smoothing even when the outcome model is misspecified, illustrating the doubly robust property. Notably, their spread is much smaller than that of IPW because the misspecified outcome model still retains some predictive power over the outcome. Moreover, they exhibit fewer extreme values, particularly for control units, compared to the IPW signals.

Smoothing So far, we have glossed over the smoothing step, which reduces the signals to the one-dimensional CME along X ; now, we formally discuss it. Once we obtain the signals $\hat{\Lambda}_i$ from outcome modeling, IPW, or AIPW, the final step is to approximate the CME by fitting a flexible function $f(X)$ that represents the conditional mean of these signals given X . When the moderator X is discrete, this reduces to simply averaging the signals within each group defined by X . For a continuous moderator, we consider two approaches for estimating $f(X)$: one using kernel regressions, which parallel the kernel estimator discussed in Chapter 2, and another using B-spline regressions.

Figure 7: Constructed Signals



Note: In (a), the dark blue and light blue dots represent outcome values from the treatment and control groups, respectively; the dark blue and light blue lines represent the LOESS fits for the two groups. In (b)-(d), the dark blue and light blue dots represent outcome values or signals from the treatment and control groups, respectively; the red line represents the true CME while the orange line represents the CME estimates based the signals after smoothing.

Kernel Regression One can employ local polynomial smoothing regression, also known as LOESS regression or kernel regression. For each evaluation point x_0 , LOESS constructs

a locally weighted regression of $\hat{\Lambda}$ on X within a neighborhood around x_0 . Users can specify a `span` parameter, α , which determines the size of this local neighborhood as a fraction of the overall range of X . Let

$$D_i(x_0; \alpha) = K\left(\frac{|X_i - x_0|}{\alpha \text{range}(X)}\right),$$

where $K(\cdot)$ is a kernel function (often the tricube kernel in standard LOESS). One then solves a weighted least squares problem:

$$(\hat{\beta}_0(x_0), \hat{\beta}_1(x_0)) = \underset{\beta_0, \beta_1}{\operatorname{argmin}} \sum_{i=1}^n \left[\hat{\Lambda}_i - \beta_0 - \beta_1(X_i - x_0) \right]^2 D_i(x_0; \alpha),$$

where $\hat{\Lambda}_i$ represents the signals. The coefficient β_0 represents the local intercept at x_0 , while β_1 captures the local slope in the neighborhood of x_0 . Therefore, the fitted function at x_0 is

$$\hat{f}(x_0) = \hat{\beta}_0(x_0).$$

This approach ensures that data points closer to x_0 receive higher weight, while those farther away have less influence. If a higher-order polynomial fit is desired (e.g., quadratic), one includes additional terms such as $\beta_2(X_i - x_0)^2$, $\beta_3(X_i - x_0)^3$, etc., with the kernel weights $D_i(x_0; \alpha)$ remaining unchanged.

To select an optimal α , we employ K -fold cross-validation. For each candidate α in a predefined grid, we compute the mean-squared error (MSE) over the folds:

$$\text{MSE}(\alpha) = \frac{1}{K} \sum_{k=1}^K \frac{1}{n_k} \sum_{i \in \text{Fold}_k} \left(\hat{\Lambda}_i - \hat{f}_{-k}(X_i; \alpha) \right)^2,$$

where \hat{f}_{-k} denotes the LOESS fit *excluding* observations in the k -th fold, and n_k is the number of observations in that fold. We then choose

$$\alpha^* = \underset{\alpha}{\operatorname{argmin}} \text{MSE}(\alpha),$$

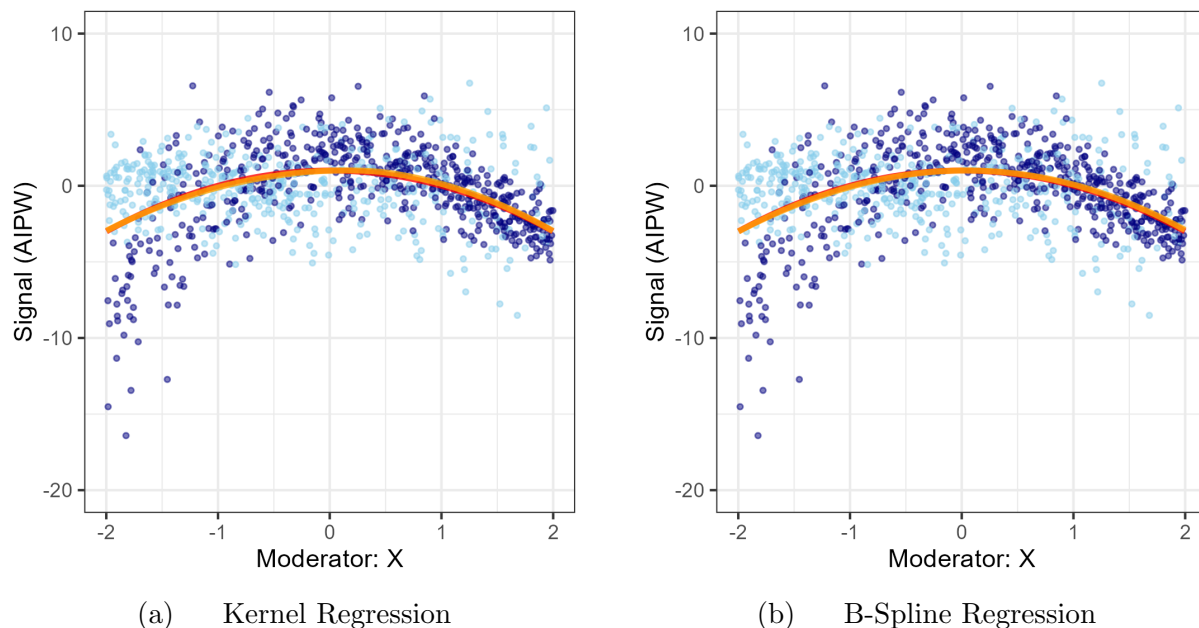
and refit LOESS on the entire dataset using α^* . Predicting over the same evaluation grid yields the final estimate $\hat{f}(x)$, which in turn provides the CME at each x .

B-Spline Regression. A B-spline is a piecewise polynomial function that ensures smoothness at the junctions of polynomial segments (the *knots*). In our setting, for the signals $\hat{\Lambda}_i$, we can fit a linear model of the form

$$\hat{\Lambda}_i = \beta_0 + \sum_{j=1}^K \beta_j B_j(X_i) + \epsilon_i,$$

where $B_j(\cdot)$ is the j -th B-spline basis function of chosen degree (`spline_degree`) and dimension (`spline_df`). By selecting an adequate number of knots and a suitable polynomial degree, the B-spline expansions $\{B_j(X)\}_{j=1}^K$ capture nonlinearities in the signal as a function of X . After estimating the parameters $\{\beta_j\}$ via least squares, we predict $\hat{f}(x)$ over an evaluation grid to obtain $\theta(x)$. Formally, $\hat{f}(x) = \hat{\beta}_0 + \sum_{j=1}^K \hat{\beta}_j B_j(x)$.

Figure 8: Kernel vs. B-Spline Regressions for Smoothing



Note: Dark blue and light blue dots represent AIPW signals for the treatment and control groups respectively. The red line represents the true CME while the orange line represents the estimated CME.

Both kernel and B-spline regressions are flexible modeling strategies for capturing nonlinear relationships, but they differ in how smoothness is regulated and how tuning parameters (knot configuration vs. α -span) are selected. B-spline regressions employ a polynomial basis with continuity constraints at knot boundaries, whereas kernel regressions adaptively weight

data within localized neighborhoods to achieve smooth fits. In either case, the estimated function $\hat{f}(x)$ captures the shape of $\hat{\Lambda}$ as a function of X , delivering pointwise CME estimates across the range of the moderator. Figure 8 compares these two approaches (orange lines) in practice, showing that they, in general, produce similar fits when applied to $\hat{\Lambda}_i^{(\text{aipw})}$. In all subsequent CME estimations in this chapter, we continue to use kernel regression to obtain the CME from the constructed signals.

3.3 Basis Expansion and Variable Selection

One way to increase the flexibility of the outcome and propensity score models is to expand the set of regressors $V = (X, Z)$ beyond their raw forms. Specifically, each covariate—whether the moderator X or an additional covariate $Z_j \in Z$ —can be replaced with a set of basis functions that capture nonlinearities, while interactions among them can also be incorporated. Common approaches include polynomial expansions (e.g., second-degree or higher) and B-spline expansions, which partition the support of a variable into segments while enforcing smoothness across boundaries. By enriching the model space, the estimated relationships can better adapt to complex patterns that might otherwise be inadequately captured by purely linear terms.

Concretely, suppose we have $V \in \mathbb{R}^{(1+p)}$, in which p is the dimension of covariates. For each variable L in V , including X , we can generate a set of transformed variables $\{\phi_k(L)\}$, where each function represents a polynomial or B-spline basis expansion. Interaction terms can be constructed by multiplying these expansions for X with those for Z , allowing the model to capture effect modification across covariates. We denote the full set of expansions $\psi(V)$.

Once expanded, these regressors can be incorporated into both the outcome model $\mathbb{E}[Y \mid D, X, Z]$ and the propensity score model $\mathbb{E}[D \mid X, Z]$. In the outcome model, basis expansions enable more flexible relationships between X , Z , and Y . If the true relationship is nonlinear, involves threshold effects, or exhibits heterogeneous slopes across different regions of X or Z ,

the expanded basis helps capture these complexities. In the propensity score model, these expansions allow the probability of treatment to vary nonlinearly with the covariates. With a sufficiently rich expansion—and appropriate regularization, such as Lasso—these flexible specifications can reduce bias by better approximating the unknown DGP.

We illustrate the benefit of basis expansions using another simulated example. We apply the outcome-modeling approach, the IPW approach, and the AIPW approach, and show results for each with and without basis expansion.

Example 9 (A simulated example with complex nonlinear relationships.) *We simulate $V = (X_i, Z_{i1}, Z_{i2}, Z_{i3})$ with $X_i \sim \text{Unif}[-2, 2]$ and each $Z_j \sim \text{Unif}[0, 1], j = 1, 2, 3$. The treatment is generated by*

$$D_i \sim \text{Bernoulli}\left(\text{logit}^{-1}(-1 + 0.5Z_{i1} + |X_i| - X \cdot Z_{i2} + Z_{i3}^2)\right),$$

and the outcome is generated by

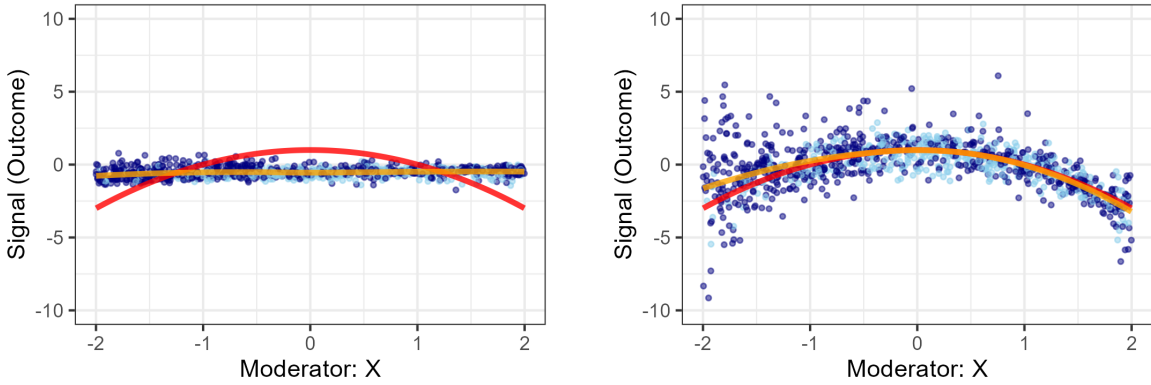
$$Y_i = 1 + X_i + D_i - D_i X_i^2 + Z_{i1}^2 + \sin(Z_{i2}) + 0.5Z_{i1} \exp(Z_{i3}) + \varepsilon_i,$$

where $\varepsilon_i \sim \mathcal{N}(0, 1)$. Under this DGP, the true CME is $\theta(x) = 1 - x^2$. Unconfoundedness holds: $D_i \perp\!\!\!\perp Y_i(0), Y_i(1) \mid V_i$, but the researcher is unaware of the functional form of either the propensity score model or the outcome model.

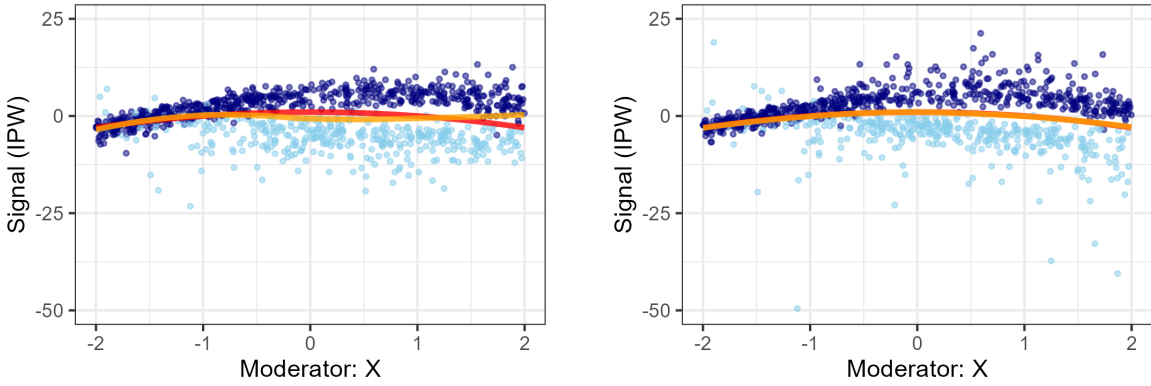
Figure 9 shows the results. The left panel in each subfigure presents the signals and CME estimates without basis expansion, and the right panel includes basis expansions on both X and Z . The left panels in Figure 9 demonstrate that (i) the linear outcome model fails to capture the nonlinearity; (ii) the IPW estimator also misses the true shape and occasionally produces large outliers in the estimated signals; and (iii) the AIPW estimator performs somewhat better even with a linear outcome model, likely because the two models compensate for each other’s deficiencies.

The right panels of Figure 9 show that both the outcome and AIPW estimators capture the inverse-U shape of the CME, $\theta(x) = 1 - x^2$, more accurately and outperform their

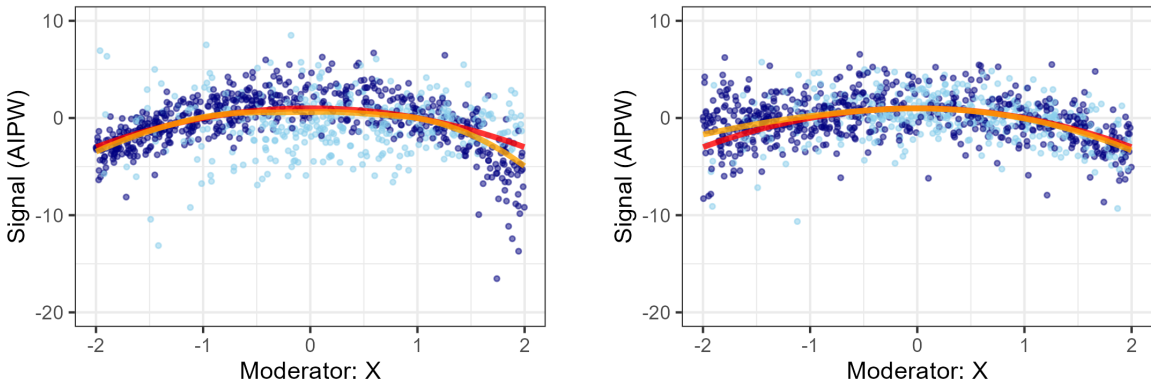
Figure 9: Without and With Basis Expansion



(a) Outcome Modeling: w/o and w basis expansion



(b) IPW: w/o and w basis expansion



(c) AIPW: w/o and w basis expansion

Note: Dark blue and light blue dots represent signals for the treatment and control groups respectively. The red line represents the true CME while the orange line represents the estimated CME. In each subfigure, the left and right panels show results without and with basis expansion, respectively.

counterparts without basis expansions. However, the IPW estimator remains sensitive to propensity scores near 0 or 1, which result in large inverse weights and unstable estimates. In contrast, the AIPW signals are far more stable and concentrated within a narrow band, yielding more precise CME estimates.

Although basis expansions can enhance model flexibility, they also introduce more parameters to estimate, potentially leading to larger variance and a greater risk of overfitting, particularly when the number of covariates is large. Next, we will show that regularized methods, such as Lasso, are essential for managing this high-dimensional setting and ensuring stable, reliable inference.

Variable Selection When the number of covariates or expanded basis functions is large, conventional OLS or logistic regression may overfit and yield unstable estimates. To address this limitation, one can apply Lasso to achieve both regularization and variable selection. Lasso imposes an ℓ_1 -penalty on the regression coefficients, shrinking many of them toward zero and effectively selecting a sparse subset of relevant predictors. In its canonical form for a linear model with response $\{y_i\}_{i=1}^n$ and predictors $\{x_i\}_{i=1}^n \in \mathbb{R}^p$, the Lasso estimate $\hat{\beta}_\lambda$ is defined as

$$\hat{\beta}_\lambda = \arg \min_{\beta \in \mathbb{R}^p} \left\{ \frac{1}{n} \sum_{i=1}^n (y_i - x_i^\top \beta)^2 + \lambda \sum_{j=1}^p |\beta_j| \right\}.$$

The ℓ_1 penalty shrinks many coefficients to zero, and the tradeoff between sparsity and goodness of fit is governed by the penalty parameter $\lambda \geq 0$. A straightforward application of Lasso in this context is to estimate *separate* Lasso regressions for each outcome model (one for the treated and one for the control subsample) and for the propensity score model. Let

$$I_1 = \{i : D_i = 1\} \quad \text{and} \quad I_0 = \{i : D_i = 0\},$$

and, with some abuse of notation, let $\{X_i\}$ denote the vector of predictors—including basis expansions and their interactions—for observation i . Then one solves:

$$\begin{aligned}\hat{\beta}_{1,\lambda_1} &= \arg \min_{\beta_1} \left\{ \frac{1}{|I_1|} \sum_{i \in I_1} (Y_i - X_i^\top \beta_1)^2 + \lambda_1 \|\beta_1\|_1 \right\} \implies \hat{\mu}^1(V_i) = X_i^\top \hat{\beta}_{1,\lambda_1}, \\ \hat{\beta}_{0,\lambda_0} &= \arg \min_{\beta_0} \left\{ \frac{1}{|I_0|} \sum_{i \in I_0} (Y_i - X_i^\top \beta_0)^2 + \lambda_0 \|\beta_0\|_1 \right\} \implies \hat{\mu}^0(V_i) = X_i^\top \hat{\beta}_{0,\lambda_0}.\end{aligned}$$

and, using all n observations for the propensity score,

$$\begin{aligned}\hat{\gamma}_{\lambda_p} &= \arg \min_{\gamma} \left\{ -\frac{1}{n} \sum_{i=1}^n [D_i X_i^\top \gamma - \log(1 + \exp(X_i^\top \gamma))] + \lambda_p \|\gamma\|_1 \right\} \\ \implies \hat{\pi}(V_i) &= \frac{1}{1 + e^{-X_i^\top \hat{\gamma}_{\lambda_p}}}.\end{aligned}$$

Here, λ_1 , λ_0 , and λ_p are penalty parameters for each model that can be selected via cross-validation. The estimated coefficients are then used to construct the outcome or propensity score models and, subsequently, to build various signals as discussed previously.

Post-Selection Lasso. A well-known issue with Lasso is that the standard errors of its coefficients are not readily available, and their inference remains an open question. Because Lasso produces sparse solutions, one can define the model selected by Lasso as the set of predictors with nonzero coefficients:

$$\hat{\mathcal{A}}_1 = \{j : \hat{\beta}_{1,\lambda_1,j} \neq 0\}, \quad \hat{\mathcal{A}}_0 = \{j : \hat{\beta}_{0,\lambda_0,j} \neq 0\}, \quad \hat{\mathcal{A}}_p = \{j : \hat{\gamma}_{\lambda_p,j} \neq 0\}.$$

Post-selection coefficients are obtained by refitting the model using the appropriate *unpenalized* estimator—OLS for linear models and logistic regression for logit models—on the variables selected by Lasso. Specifically, the post-selection coefficients for β_{1,λ_1} , denoted $\tilde{\beta}_{1,\lambda_1}$, are estimated by running a standard OLS regression on the treated units using only the predictors in $\hat{\mathcal{A}}_1$; similarly, one obtains $\tilde{\beta}_{0,\lambda_0}$ and $\tilde{\gamma}_{\lambda_p}$. The various signals are then constructed based on these refined estimates.

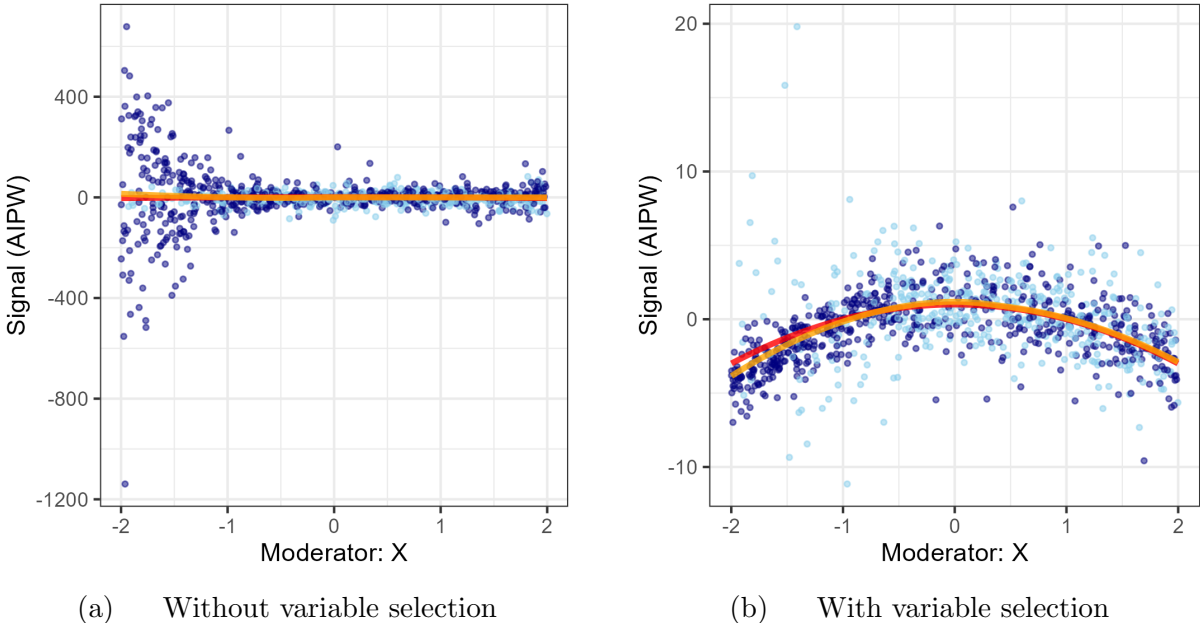
Belloni, Chen, Chernozhukov and Hansen (2012) and Belloni and Chernozhukov (2013) provide results showing that predictions based on post-selection coefficients perform at least

as well as those based on penalized coefficients. Under the conditions that guarantee valid predictions by Lasso, the post-selection coefficients often yield slightly improved performance, and in other cases, they perform comparably.

Example 10 (Many covariates and complex nonlinear relationships.) *We simulate a sample of 1,000 units with $V_i = (X_i, Z_{i1}, Z_{i2}, \dots, Z_{i,10})$ with $X_i \sim \text{Unif}[-2, 2]$ and each $Z_j \sim \text{Unif}[0, 1], j = 1, 2, \dots, 10$. The treatment and outcome are generated in the same way as in Example 9, meaning that covariates $Z_{i4}, \dots, Z_{i,10}$ are redundant. The true CME is $\theta(x) = 1 - x^2$. Unconfoundedness holds: $D_i \perp\!\!\!\perp Y_i(0), Y_i(1) \mid V_i$.*

Figure 10 presents the AIPW signals and CME estimates without and with Lasso selection. Because the additional variables $Z_{i4}, \dots, Z_{i,10}$ are included despite having little influence on the treatment or outcome, identifying the relevant covariates becomes nontrivial. Figure 10 illustrates how Lasso improves estimation by selecting a sparse, informative subset of predictors, leading to drastically more stable signals and more accurate CME estimates.

Figure 10: AIPW with Basis Expansion: w/o and w/ Variable Selection



Note: Dark blue and light blue dots represent AIPW signals for the treatment and control groups respectively. The red line represents the true CME while the orange line represents the estimated CME.

In summary, the outcome-modeling, IPW, and AIPW estimators for the CME follow a common three-step procedure: (1) model the outcome and/or the propensity score; (2) construct signals; and (3) smooth the signals over the moderator X . IPW relies solely on propensity scores to balance treated and control units—an approach that is simple but can suffer from high variance when scores are near 0 or 1. AIPW combines both models and offers double robustness: as long as either the outcome or propensity model is correctly specified, the CME estimates remain consistent. Across all methods, reliable inference depends on thoughtful model specification, regularization (e.g., post-selection Lasso), and sufficient overlap in covariate distributions. In the remainder of the Element, we refer to the AIPW estimator with basis expansion and post-Lasso selection as *AIPW-Lasso*, and refer to the post-Lasso estimators based on outcome signals and IPW signals as *outcome-Lasso* and *IPW-Lasso*, respectively. We summarize the AIPW-Lasso procedure in Algorithm 1.

Algorithm 1 AIPW-Lasso

- 1: **Inputs:**
 - 2: Data: $\{(X_i, Z_i, D_i, Y_i)\}$ for $i = 1, \dots, n$
 - 3: $D_i \in \{0, 1\}$ is a binary treatment
 - 4: $V_i := (X_i, Z_i)$ are covaraites, of which X_i is the moderator
 - 5: Y_i is the outcome
 - 6: Choice of basis functions and smoothing method
 - 7: **Outputs:**
 - 8: Estimated function $\hat{\theta}(x) = \mathbb{E}[Y_i(1) - Y_i(0)|X_i = x]$
 - 9: **1) Estimate the outcome models**
 - 10: * For $\{i : D_i = 1\}$, run Lasso regression with basis expansion, selecting covaraites $\hat{\mathcal{A}}_1$
 - 11: * For $\{i : D_i = 1\}$, run post-Lasso OLS regression with $\hat{\mathcal{A}}_1$, obtaining $\hat{\mu}^1(V_i)$ for each i
 - 12: * For $\{i : D_i = 0\}$, run Lasso regression with basis expansion, selecting covaraites $\hat{\mathcal{A}}_0$
 - 13: * For $\{i : D_i = 0\}$, run post-Lasso OLS regression with $\hat{\mathcal{A}}_0$, obtaining $\hat{\mu}^0(V_i)$ for each i
 - 14: **2) Estimate the propensity score model**
 - 15: * Run logit Lasso regression with basis expansion, selecting covaraites $\hat{\mathcal{A}}_p$
 - 16: * Fit the propensity model with $\hat{\mathcal{A}}_p$, obtaining $\hat{\pi}(V_i)$ for each i :
 - 17: **3) Compute AIPW signals**
 - 18: $\hat{\Lambda}_i(\hat{\mu}, \hat{\pi}) = \hat{\mu}^1(V_i) - \hat{\mu}^0(V_i) + \frac{D_i}{\hat{\pi}(V_i)}(Y_i - \hat{\mu}^1(V_i)) - \frac{1-D_i}{1-\hat{\pi}(V_i)}(Y_i - \hat{\mu}^0(V_i))$
 - 19: **4) Project AIPW signals onto X to obtain $\hat{\theta}(x)$**
 - 20: Regress $\hat{\Lambda}_i$ on X_i , using the kernel or B-spline regression $\Rightarrow \hat{\theta}(x)$.
 - 21: **Return:**
 - 22: The function $\hat{\theta}(x) =$ estimated CME as a function of x .
-

3.4 Inference

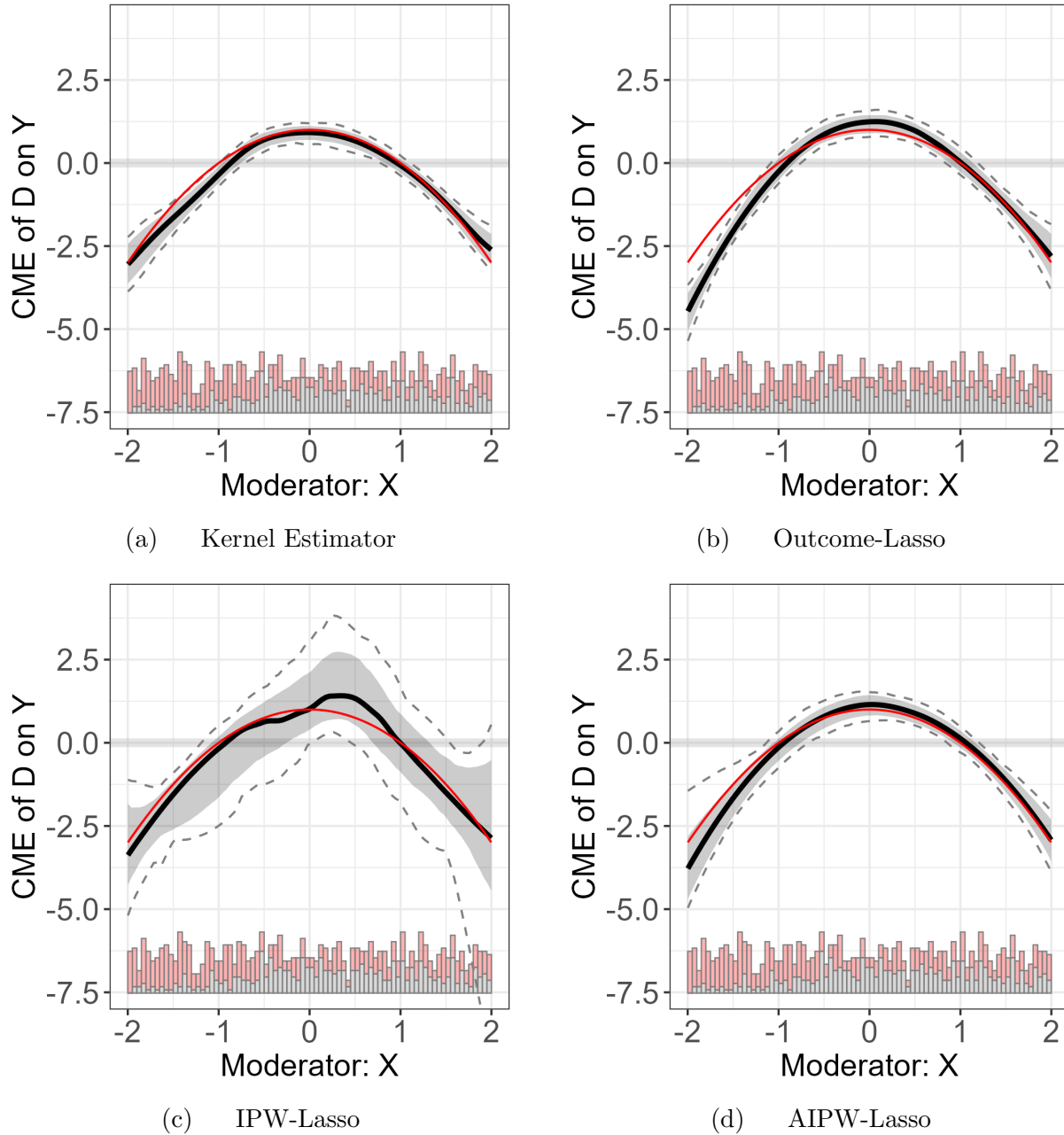
Constructing confidence intervals analytically for the CME is challenging due to the multi-step nature of the estimation procedure. Our aim is to capture uncertainty arising from two main sources: (1) the estimation of the outcome and propensity score models, which includes the uncertainty from Lasso-based variable selection; and (2) the smoothing step that derives the CME from the resulting signals. We do not account for uncertainty from tuning or model selection decisions—such as the choice of knots in the B-spline expansion, the selection of the Lasso penalty parameter λ , or the choice of the span parameter in kernel regression.

To approximate the sampling distribution of the CME estimates, $\hat{\theta}(x)$, we implement a nonparametric bootstrap procedure that replicates the full estimation pipeline. In each bootstrap iteration, we resample the data with replacement and re-run the Lasso variable selection step—using the same fixed penalty parameter as in the original estimation—to identify the active covariates. We then refit the outcome and propensity score models using OLS and logistic regression on the selected covariates. The CME is subsequently estimated via kernel regression, using the span parameter fixed at its original cross-validated value. The B-spline expansion (including knot placement and polynomial degree) is also held fixed across bootstrap iterations.

Pointwise confidence intervals for $\theta(x)$ at each evaluation point x can be constructed using either a percentile-based method or a normal approximation based on the empirical bootstrap variance. Similarly, uniform confidence intervals—ensuring simultaneous coverage across the entire range of x —can be constructed following the approaches outlined in previous chapters.

In Figure 11, we display the estimated CME along with their pointwise and uniform confidence intervals on the simulated data from **Example 3**, using the kernel estimator introduced in Chapter 2, the outcome modeling approach (using post-Lasso regression), the IPW-Lasso estimator, the AIPW-Lasso estimator. The outcome modeling approach yields

Figure 11: Estimated CME with Simulated Data: Kernel vs Post-Lasso Methods



Note: In each figure, the red line represents the true CME; the black line represents the estimated CME. The shaded area and the dashed lines represent the 95% point-wise and uniform confidence intervals, respectively. The histograms at the bottom of the figure depict the distributions of X across treatment (pink) and control (gray) groups.

an estimated CME that deviates slightly from the true CME when X is relatively small. The IPW estimator produces noisier estimates and wider confidence intervals. The AIPW

estimator provides an estimated CME that more closely aligns with the truth than other post-Lasso estimators. Interestingly, the kernel estimator performs fairly well, too.

Finally, we apply four methods, including the kernel estimator, outcome-Lasso, IPW-Lasso, and AIPW-Lasso, to the data from **Example 6**. The last three methods employ basis expansion and post-selection-Lasso regression. The code snippet below demonstrates how to implement all three procedures using the `interflex` package:

```
1 D <- "opp"
2 Y <- "pres_ref"
3 X <- "pres_vote_margin"
4 Z <- c("prev_vote", "majority", "leadership", "seniority", "tot_speech")
5 d <- d[which(d[,X] <= 16.5 & d[,X] >= -4.1),]
6
7 ## Use AIPW Signals
8
9 est.aipw <- interflex(estimator = 'aipw', signal = 'aipw',
10                      data = d, nboots = 2000,
11                      Y = Y, D = D, X = X, Z = Z,
12                      treat.type = "discrete",
13                      reduce.dimension = 'kernel',
14                      na.rm = TRUE)
15
16 ## Use IPW Signals
17
18 est.ipw <- interflex(estimator = 'aipw', signal = 'ipw',
19                     data = d, nboots = 2000,
20                     Y = Y, D = D, X = X, Z = Z,
21                     treat.type = "discrete",
22                     reduce.dimension = 'kernel',
23                     na.rm = TRUE)
24
25 ## Use Outcome Modeling Signals
```

```

26
27 est.outcome<-interflex(estimator='aipw',signal = 'outcome',
28                         data = d, nboots = 2000,
29                         Y=Y,D=D,X=X, Z = Z,
30                         treat.type = "discrete",
31                         reduce.dimension = 'kernel',
32                         na.rm = TRUE)

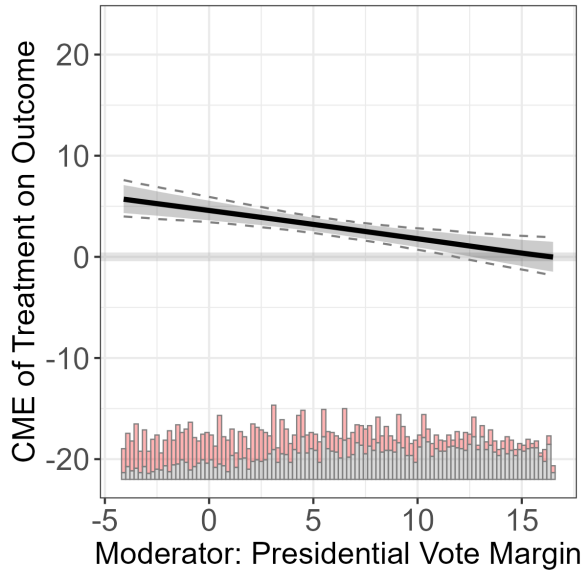
```

In Figure 12, we display the estimated CME along with their pointwise and uniform confidence intervals. The gray band represents the pointwise confidence intervals, while the dashed lines indicate the uniform confidence intervals that ensure simultaneous coverage across all values of x . The uniform intervals are wider because they capture the uncertainty of the entire estimated curve rather than at individual points. Overall, the figure demonstrates that the main conclusion from Noble (2024) remains robust across various estimators. The kernel estimator selects a large bandwidth via cross-validation, resulting in a nearly linear estimated CME. The outcome modeling approach also shows a decreasing CME, although the rate of decrease is smaller than that estimated by the kernel method. The IPW estimator exhibits a clear decreasing pattern but comes with noisy estimates and wide confidence intervals. Finally, the AIPW estimator produces narrower confidence intervals than the outcome modeling approach and generally shows a decreasing trend; however, when the local vote margin is not lopsided (i.e., $-5 \leq X \leq 5$), the estimated CME does not appear strictly monotonic.

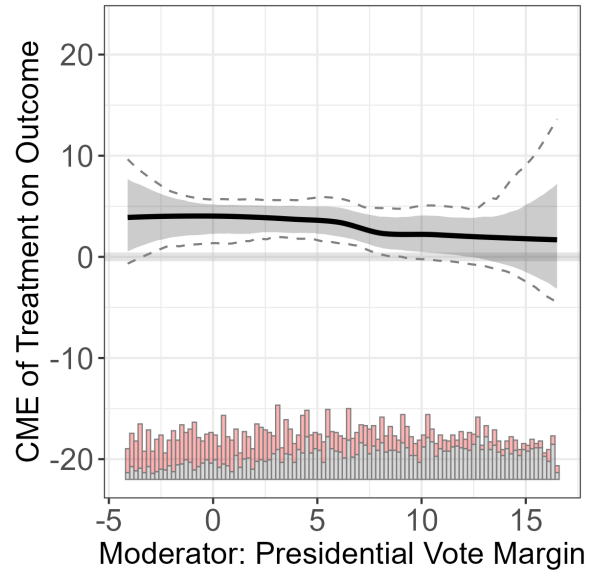
3.5 Continuous Treatment

Having discussed the AIPW approach in the binary-treatment setting, we now introduce a framework suitable for *continuous* treatments. Our goal remains to estimate the CME, i.e., $\theta(x) = \mathbb{E}\left[\frac{\partial Y}{\partial D} \mid X = x\right]$, which captures how D affects Y at each value of X , marginalizing other variables such as Z . Unlike the binary case, there is no propensity score to estimate. Instead, we adopt a partially linear regression model (PLRM), first introduced by Robinson

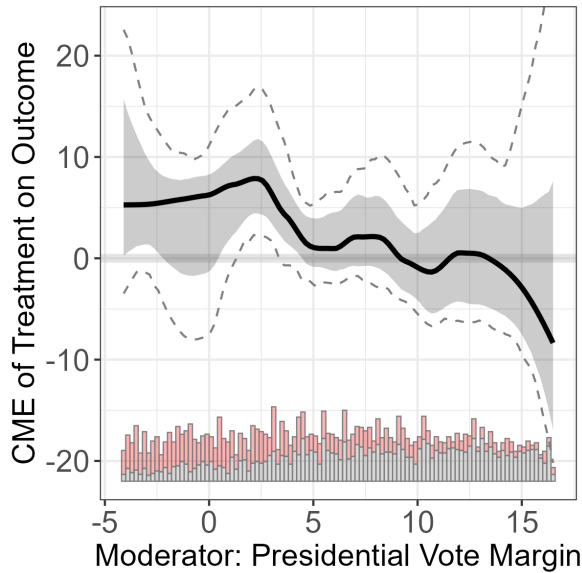
Figure 12: Replicating Noble (2024) Figure 2: Kernel vs Post-Lasso-Methods



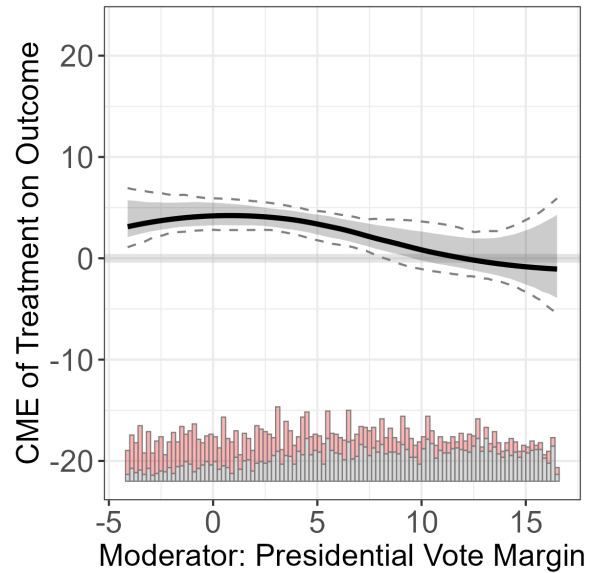
(a) Kernel Estimator



(b) Outcome-Lasso



(c) IPW-Lasso



(d) AIPW-Lasso

Note: The treatment is out-partisanship of lawmakers, the outcome is frequency of presidential references in Congressional speeches. In each figure, the black line represents the estimated CME. The shaded area and the dashed lines represent the point-wise and uniform confidence intervals, respectively. The histograms at the bottom of the figure depict the distributions of X across treatment (pink) and control (gray) groups.

(1988).

Assumption 9 (Partially linear regression model, PLRM)

$$Y_i = \theta(X_i)D_i + \mu(V_i) + \zeta_i,$$

$$D_i = \pi(V_i) + \varepsilon_i, \quad \mathbb{E}(\varepsilon_i | V_i) = 0.$$

Unconfoundedness (Assumption 3) implies $\mathbb{E}(\zeta_i | D_i, V_i) = 0$. To elucidate the identification strategy, note that one can write

$$\mathbb{E}[Y_i | V_i] = \underbrace{\mathbb{E}[\theta(X_i) D_i | V_i]}_{=\theta(X_i)\mathbb{E}[D_i|V_i]} + \underbrace{\mathbb{E}[\mu(V_i) | V_i]}_{=\mu(V_i)} + \underbrace{\mathbb{E}[\zeta_i | V_i]}_{=0}.$$

$\mathbb{E}[\zeta_i | V_i] = 0$ by unconfoundedness. Here, $\theta(X_i)$ captures the effect of D_i on Y_i , while $\mu(V_i)$ absorbs other nonlinear effects of V_i . Similarly, because

$$\mathbb{E}[D_i | V_i] = \mathbb{E}[\pi(V_i) | V_i] + \mathbb{E}[\varepsilon_i | V_i] = \pi(V_i),$$

substituting these expressions yields

$$\tilde{Y}_i \equiv Y_i - \mathbb{E}[Y_i | V_i] = \theta(X_i) \{D_i - \mathbb{E}[D_i | V_i]\} + \zeta_i,$$

or equivalently,

$$\tilde{Y}_i = \theta(X_i) \tilde{D}_i + \zeta_i,$$

where we define $\tilde{Y}_i = Y_i - \mathbb{E}[Y_i | V_i]$ and $\tilde{D}_i = D_i - \mathbb{E}[D_i | V_i]$. In this decomposition, \tilde{Y}_i and \tilde{D}_i represent the residualized outcome and treatment after removing the effects of all covariates in V_i (including X_i and Z_i). [Chernozhukov, Hansen and Spindler \(2015\)](#) gives an introduction to this “partialling out” procedure.

In practice, we can estimate $\mathbb{E}[Y | V_i]$ and $\mathbb{E}[D_i | V_i]$ using flexible methods—such as basis expansions combined with post-selection Lasso—to “denoise” Y_i and D_i , yielding \tilde{Y}_i and \tilde{D}_i . We then estimate the CME by regressing \tilde{Y}_i on \tilde{D}_i , relying on the key property that ζ_i remains orthogonal to \tilde{D}_i (i.e., $\mathbb{E}[\zeta_i | \tilde{D}_i] = 0$). This orthogonality follows because $\mathbb{E}[\zeta_i | D_i, V_i] = 0$ and $\tilde{D}_i = D - \mathbb{E}[D_i | V_i]$ is a function of (D_i, V_i) . Formally, $\mathbb{E}[\zeta_i | \tilde{D}] = \mathbb{E}[\mathbb{E}[\zeta_i | D_i, V_i] | \tilde{D}_i] = 0$.

For implementation, one approach is to fit the following B-spline regression:

$$\hat{\theta}(X_i) = \arg \min_{\theta(X_i) \in \Theta_{\text{bs}}} \mathbb{E} \left[(\tilde{Y}_i - \theta(X_i) \tilde{D}_i)^2 \right],$$

where $\theta(X_i)$ is approximated by a set of basis functions $\phi(X_i)$, so that $\theta(X_i) \approx \beta^T \phi(X_i)$. Once the coefficients β are estimated, the CME can be constructed as $\hat{\beta}^T \phi(X_i)$. Alternatively, one can use the kernel estimator introduced in Chapter 2:

$$\tilde{Y}_i = \phi(X_i) + \theta(X_i) \tilde{D}_i + \zeta_i, \quad \mathbb{E}[\zeta_i | X_i, \tilde{D}_i] = 0,$$

in which

$$\phi(X_i)_{|X_i - x_0| < \epsilon} = \mu(x_0) + \eta(x_0)(X_i - x_0),$$

$$\theta(X_i)_{|X_i - x_0| < \epsilon} = \alpha(x_0) + \beta(x_0)(X_i - x_0),$$

$$\left(\hat{\mu}(x_0), \hat{\alpha}(x_0), \hat{\eta}(x_0), \hat{\beta}(x_0) \right) = \arg \min_{\tilde{\mu}, \tilde{\alpha}, \tilde{\eta}, \tilde{\beta}} L(\tilde{\mu}, \tilde{\alpha}, \tilde{\eta}, \tilde{\beta}),$$

$$L = \sum_{i=1}^N \left[\tilde{Y}_i - \tilde{\mu} - \tilde{\alpha} \tilde{D}_i - \tilde{\eta}(X_i - x_0) - \tilde{\beta} \tilde{D}_i (X_i - x_0) \right]^2 K \left(\frac{X_i - x_0}{h(x_0)} \right).$$

Researchers can select the bandwidth function $h(x_0)$ via cross-validation, fit the local linear model, and compute the estimated CME at each evaluation point x_0 . We summarize this procedure in Algorithm 2, which is modified based on [Chernozhukov, Hansen and Spindler \(2015\)](#).

We provide a simulated example below.

Example 11 (Complex DGP with a Continuous Treatment) *We simulate a sample of 1000 observations. The moderator $X_i \sim \text{Unif}[-2, 2]$. Four additional covariates $\{Z_{i1}, Z_{i2}, Z_{i3}, Z_{i4}\}$ are sampled from $\mathcal{N}(0, 1)$, though in this setup only Z_{i1} and Z_{i2} feature prominently. The continuous treatment D_i is generated as*

$$D_i = 0.5Z_{i1} + X_i^2 + \nu_i.$$

where $\nu_i \sim \mathcal{N}(0, 1)$. The outcome Y_i depends on X_i , D_i , and their interactions (including

Algorithm 2 PO-Lasso

- 1: **Inputs:**
 - 2: Data: $\{(X_i, Z_i, D_i, Y_i)\}$ for $i = 1, \dots, n$
 - 3: D_i is a continuous treatment
 - 4: $V_i := (X_i, Z_i)$ are covariates, in which X_i is the moderator
 - 5: Y_i is the outcome
 - 6: Choice of basis functions and smoothing method
 - 7: **Outputs:**
 - 8: Estimated function $\hat{\theta}(x) = \mathbb{E}\left[\frac{\partial Y}{\partial D} \mid X_i = x\right]$
 - 9: **1) Partial out covariates from the outcome**
 - 10: * Run a Lasso regression of Y_i on $\psi(V_i)$, selecting covariates $\tilde{\psi}_y(V_i)$
 - 11: * Regress Y_i on $\tilde{\psi}_y(V_i)$, obtaining residuals \tilde{Y}_i for all i
 - 12: **2) Partial out covariates from the treatment**
 - 13: * Run a Lasso regression of D_i on $\psi(V_i)$, selecting covariates $\tilde{\psi}_d(V_i)$
 - 14: * Regress D_i on $\tilde{\psi}_d(V_i)$, obtaining residuals \tilde{D}_i for all i
 - 15: **3) Estimate varying coefficients using residuals**
 - 16: Regress \tilde{Y}_i on \tilde{D}_i using the kernel or B-spline regression $\Rightarrow \hat{\theta}(x)$.
 - 17: **Return:**
 - 18: The function $\hat{\theta}(x) =$ estimated CME as a function of x .
-

an exponential term in Z_{i1} and a thresholded contribution from Z_{i2}):

$$Y_i = 1 + 1.5X_i + D_i - D_iX_i^2 + 2X_i \exp(1 + Z_{i1}) + 2\mathbf{1}\{Z_{i2} > 0\}Z_2 + \epsilon_i.$$

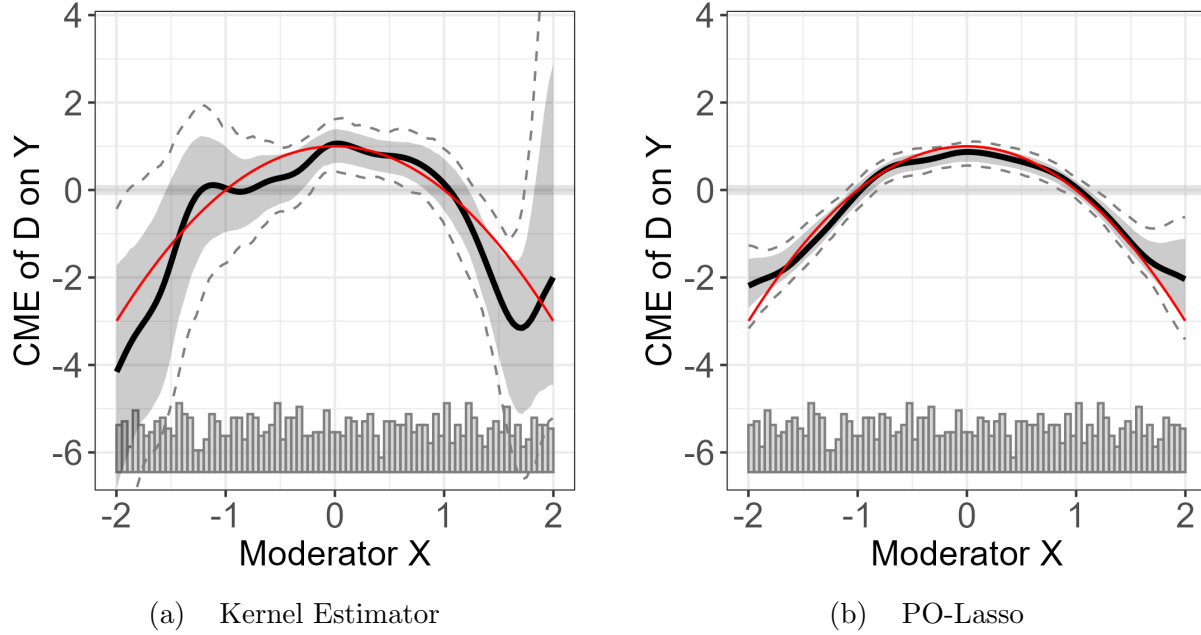
with $\epsilon_i \sim \mathcal{N}(0, 1)$. This formulation introduces considerable nonlinearity and cross-terms involving (X_i, D_i, Z_1) , creating a realistic challenge for estimation.

In Figure 13, we compare the two strategies using data from **Example 11**. In panel (a), we apply the kernel estimator discussed in Chapter 2. Because it cannot effectively accommodate the strong nonlinearity in Z_i , the resulting black curve diverges from the true effect (red), especially in the tails of X_i . In contrast, panel (b) shows the result from PO-Lasso using kernel regression for smoothing. Here, the black curve closely aligns with the true effect (red) across most of the domain. This illustrates how partialling out can correct for distortions caused by nonlinearities and covariate interactions in the DGP, yielding a substantially more accurate estimate of the CME.

Finally, we illustrate PO-Lasso using an empirical example from political science.

Example 12 *Adiguzel, Cansunar and Corekcioglu (2023)* examines the impact of incumbent's public health provision on electoral outcomes. The authors use a reform in Turkey

Figure 13: CME Estimates for Example 4: Continuous Treatment



Note: In each figure, the red line represents the true CME; the black line represents the estimated CME. The shaded area and the dashed lines represent the 95% point-wise and uniform confidence intervals, respectively. The histograms at the bottom of the figure depict the distributions of X .

that significantly altered the geographic distribution of health clinics. Here, we replicate Figure 4A in the study. The authors find that reduced congestion levels significantly increased the AKP's vote share, especially in poorer communities which exhibited a more substantial response to the improvements in health care access. The variables of interest are:

- *Outcome:* Change in the vote share for the incumbent AKP party (continuous, $\in [-33.9, 39.5]$)
- *Treatment:* Change in congestion (continuous, $\in [-28.8, 20.8]$); congestion is measured by the number of patients per doctor at the nearest clinic, with lower congestion indicating improved service quality
- *Moderator:* Logarithm of median property value (continuous, $\in [-0.2, 7.7]$)

We apply the kernel estimator from Chapter 2 and the PO-Lasso estimator. The code snippet below demonstrates how to implement the PO-Lasso estimator using the `interflex`

package. We trim the data to exclude moderator values where the distribution is sparse.

```
1 D <- "Dpop1000_asm_dr_3"
2 Y <- "Dakp_3"
3 X <- "lograyic09"
4 Z <- c('Duniversity_3', 'Dodr_3', 'Dydr_3', 'Dpopulation_3', 'Dhospital_
      pri_3', 'Dhospital_pub_3')
5
6 df<-df %>%
7   dplyr::filter(lograyic09 <=7) %>%
8   dplyr::filter(lograyic09 >=3)
9
10 est.aipw<-interflex(estimator='aipw',
11                    data = df, nboots = 2000,
12                    Y=Y,D=D,X=X, Z = Z,
13                    na.rm = TRUE)
```

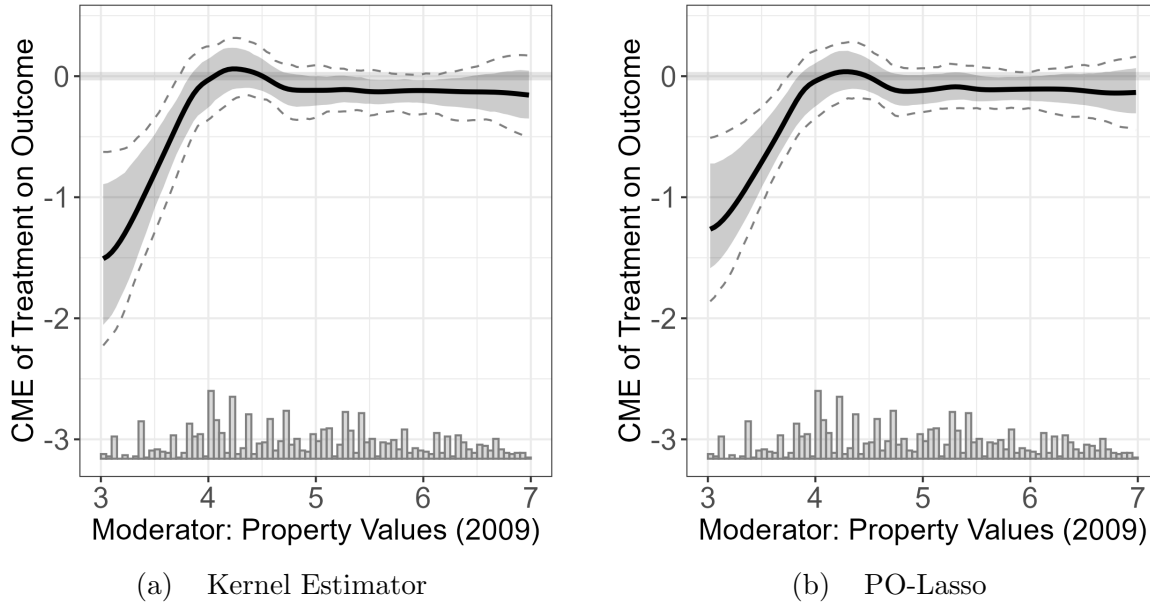
In Figure 14, we display the estimated CME along with their 95% pointwise and uniform confidence intervals. The gray band represents pointwise intervals, while the dashed lines indicate uniform intervals that ensure simultaneous coverage across all values of x . Both the kernel estimator and PO-Lasso yield broadly consistent findings: poorer neighborhoods with $X < 4$ respond more strongly to improvements in health care, while the effect is essentially nonexistent in other areas. Although the main argument in Adiguzel, Cansunar and Corekcioglu (2023) remains supported, the more flexible estimators reveal a more nuanced pattern than the original linear model.

3.6 Summary

This chapter introduces the AIPW-Lasso and PO-Lasso estimators. We begin by discussion the limitations of existing approaches, such as neglecting the treatment assignment mechanism and potential nonlinearities or interactions in covariates.

To address these issues, we first review the outcome-modeling and IPW approaches in

Figure 14: Replicating Adiguzel, Cansunar and Corekcioglu (2023) Figure 4A



Note: The treatment is the change in congestion level, the outcome is the change in the vote share for the incumbent AKP party. In each figure, the black line represents the estimated CME. The shaded area and the dashed lines represent the 95% point-wise and uniform confidence intervals, respectively. The histograms at the bottom of the figure depict the distributions of the moderator.

the continuous moderator setting. The main limitation of IPW is its sensitivity to extreme weights and specification of the propensity score model. We then introduce the AIPW estimator, which integrates outcome modeling with propensity score weighting. This combination offers the double robustness property—consistency provided at least one of these two models is correctly specified. By residualizing outcomes with respect to both treatment and covariates, AIPW reduces bias and variance compared to IPW alone. We illustrate these properties using simulated data, showing that AIPW signals, compared to those from outcome modeling or IPW alone, yield more accurate CME estimates even under model misspecification.

Next, we emphasize improving model flexibility through basis expansions and discuss regularization via Lasso to manage high-dimensional covariates. Using simulated and empirical examples, we demonstrate that basis expansion and variable selection through Lasso significantly improve the accuracy and stability of CME estimates. We call this method

AIPW-Lasso. We also discuss implementing inference for CMEs using a bootstrap procedure that accounts for estimation uncertainty.

Finally, we extend the AIPW framework to continuous treatments through partial linear regression models (PLRM). This extension involves “partialing out” Lasso-selected covariates from the treatment and outcome, leading to more reliable CME estimation with complex DGPs. We therefore refer to this method as PO-Lasso.

Chapter 4. Double Machine Learning

In previous chapters, we introduced IPW and AIPW methods for estimating the CME. With AIPW, we emphasized the idea of combining both outcome and treatment models to obtain a doubly robust estimator that remains valid under moderate misspecification of either model. In this chapter, we formally introduce the concept of *Neyman orthogonality* and show that the AIPW signals satisfy this condition. Neyman orthogonality is a central property underlying recent advances in doubly robust estimation and high-dimensional inference. Intuitively, it ensures that small modeling errors in the nuisance functions do not introduce first-order bias in the final causal effect estimate, such as the CME.

In this Element, we focus on the CME $\theta(x)$ as the primary causal estimand. It is a function-valued, low-dimensional quantity, representing the effect of the treatment along a single moderator. A key component in estimating the CME is accurately estimating the nuisance parameters as functions of covariates, $\eta_0(v)$, which may be high-dimensional. These nuisance components—such as the propensity score $\Pr(D_i = 1 \mid V_i)$, the outcome model $\mathbb{E}[Y_i \mid D_i, V_i]$, or variance functions—can exhibit complexities that exceed the capacity of parametric or semiparametric models to capture accurately. Although approaches like IPW, AIPW, and post-Lasso expansions handle moderate nonlinearity or moderate-dimensional covariates, they may struggle with truly high-dimensional or strongly nonlinear data.

Flexible machine learning methods address this challenge by approximating complex relationships in η without strong assumptions on functional form. Techniques such as Lasso, random forests (RF), neural networks (NN), histogram gradient boosting (HGB), and hybrid or ensemble approaches offer considerable flexibility but achieve slower convergence rates. Intuitively, flexible models require stronger regularization to control complexity and avoid overfitting, thereby introducing regularization bias. While regularization reduces variance and practically balances the bias–variance trade-off, it systematically biases the estimated nuisance functions. Naively “plugging in” these biased ML estimates $\hat{\eta}$ into the

estimation formula for $\theta(x)$ risks losing the \sqrt{n} consistency required for asymptotic normality and valid hypothesis testing—consistency otherwise assured by orthogonality (Chernozhukov, Chetverikov, Demirer, Duflo, Hansen, Newey and Robins, 2018; Semenova and Chernozhukov, 2021).

Double machine learning (DML), also known as “double/debiased-machine learning” or “orthogonalized machine learning”, builds on precisely the idea of Neyman orthogonality, generalizing the AIPW framework to accommodate high-dimensional or complex nuisance functions η with machine learning method, while retaining valid \sqrt{n} -rate consistency. The DML framework mitigates the bias introduced by flexible machine learning estimation of nuisance functions, through two key strategies: orthogonalization, which corrects for regularization bias, and cross-fitting, which corrects for overfitting bias. In modern high-dimensional inference, the DML framework was first developed by Chernozhukov et al. (2018) for estimating fixed-dimensional parameter. Semenova and Chernozhukov (2021) extent it by allowing the target parameter to be a function, which is an infinite-dimensional parameter.

In its canonical form, DML operates through a two-stage procedure, designed primarily for scalar causal parameters such as the ATE. In the first stage, one uses machine learning method with cross-fitting to estimate the nuisance functions. In the second stage, one constructs a Neyman-orthogonal score from nuisance estimates and solves the corresponding moment condition to obtain the target parameter, enjoying \sqrt{n} -rate convergence and asymptotic normality under mild assumptions. However, if the estimand is a function rather than a scalar, such as the CME $\theta(x)$, an additional smoothing step is required. Equivalent to the smoothing step we have introduced in previous chapter, after building the orthogonal signal in the usual way, one projects the signal onto a set of basis functions that scales with the sample size for dimension reduction (Semenova and Chernozhukov, 2021). Thus, while the core DML machinery - orthogonality and cross-fitting - handles the nuisance estimation and removes first-order bias, we employ a final smoothing step to “collapse out” the remaining covariates Z and recover CME as a function of $X = x$.

The remainder of the chapter unfolds as follows: first, we introduce the key components of the general DML framework, allowing $\theta_0 \in \Theta$ to be either a finite-dimensional vector or an element of an infinite-dimensional function space. Next, we examine causal models of CME under various scenarios, including the interactive regression model (IRM) for binary treatments and the partially linear regression model (PLRM) for continuous treatments. We then elaborate on constructing Neyman-orthogonal score functions, employing cross-fitting procedures, and implementing smoothing techniques within these causal models. We illustrate how to implement these estimators with empirical examples from political science.

4.1 Key Ingredients of DML

The general DML framework includes three key ingredients: (i) Neyman orthogonality, (ii) high-quality machine learning methods, and (iii) sample-splitting and cross-fitting strategies. We show the properties of DML estimator holds for both fixed dimensional parameter and infinite-dimensional parameter, as long as the structural function is smooth and the basis is sufficiently rich.

Table 3: Key Ingredients of DML

Component	Purpose
Neyman orthogonal score	Ensures that the estimation of the parameter of interest θ_0 is robust against biases from estimation of nuisance parameters $\hat{\eta}$.
High-quality machine learning method	Ensures the estimated nuisance parameter, $\hat{\eta}$, converges to the true parameter, η , at a sufficiently fast rate, specifically $o_P(n^{-1/4-\delta})$ for some $\delta \geq 0$.
Sample splitting and cross-fitting	Utilizes sample splitting to mitigate overfitting bias by independently estimating η and θ_0 using different data subsets.

Neyman Orthogonality In the previous chapter, we saw that AIPW constructs an estimator for the CME that remains consistent if either the outcome model or the propensity model is correctly specified. This double robustness arises primarily from Neyman orthogonality: the AIPW signals are constructed so that small errors in nuisance functions induce

only second-order biases, preventing first-order bias in the CME estimate. Recall that, in the binary-treatment setting, the AIPW signals takes the form:

$$\Lambda_i = \mu^1(V_i) - \mu^0(V_i) + \frac{D_i}{\pi(V_i)}(Y_i - \mu^1(V_i)) - \frac{1 - D_i}{1 - \pi(V_i)}(Y_i - \mu^0(V_i)), \quad (7)$$

where $\mu^d(V_i)$ estimates the outcome model $\mathbb{E}[Y_i | D_i = d, V_i]$ and $\pi(V_i)$ estimates the propensity score model $\Pr(D_i = 1 | V_i)$. The key property is that if $\hat{\mu}^d(\cdot)$ and $\hat{\pi}(\cdot)$ are slightly misspecified around their true values, the first-order bias in the final estimation for signal $\mathbb{E}[\Lambda_i]$ still cancels out. This insensitivity to small modeling errors reflects Neyman orthogonality. We say that AIPW signals Λ_i are Neyman orthogonal because they satisfy the following condition:

$$\left. \frac{\partial}{\partial \eta} \left(\mathbb{E}[\Lambda_i(\eta)] \right) \right|_{\eta=\eta_0} = 0,$$

where η_0 denotes the true nuisance functions $(\mu_0^0, \mu_0^1, \pi_0)$. This derivative is taken with respect to local perturbations of η_0 . We provide proofs in the Appendix showing that the partial derivative with respect to the nuisance functions is zero, meaning that small errors in estimating η do not affect the target parameter θ to the first order. In the AIPW formula, Neyman orthogonality underlies the double robustness property: even if one nuisance function is misspecified, the main parameter θ remains consistently estimated.

DML builds on the idea of Neyman orthogonality. When estimating the target function θ in the presence of high-dimensional nuisance functions η_0 , a key concern is the potential influence of regularization bias in η_0 on the estimation of $\theta(x)$. Neyman orthogonality, introduced in [Neyman \(1959\)](#) and [Neyman \(1979\)](#), offers a structured approach to reduce the sensitivity of the final estimator to certain classes of errors in the nuisance function estimates. We begin with a generic score $\psi(W_i, \theta(\cdot), \eta)$, where $W_i = (Y_i, D_i, X_i, Z_i)$ represents data, to specify a population moment condition:

$$\mathbb{E}[\psi(W_i; \theta_0, \eta_0)] = 0,$$

Neyman orthogonality requires the score function to satisfy the following condition:

Definition 3 (Neyman orthogonality)

$$\left. \frac{\partial}{\partial \eta} \mathbb{E}[\psi(W_i; \theta_0, \eta)] \right|_{\eta=\eta_0} = 0$$

In other words, infinitesimal changes in η around η_0 do not alter the main moment condition to first order. This is exactly what we observed in the classic AIPW formula: each component involving μ_1 , μ_0 , and e is constructed so that small estimation errors cancel out. The score function is linear in the parameter of interest as well.

In practice, constructing the score function begins with a naive moment function that would correctly identify θ_0 if η_0 were known exactly. This function is then adjusted—or “debiased”—to satisfy the orthogonality condition. We will show this process in more detail in the context of CME estimation with binary and continuous treatments in the following subsections.

High-quality Machine Learning Method The double robustness property of the DML approach ensures resilience to mild errors in $\hat{\eta}_0$. The key requirement is that the estimated nuisance parameter $\hat{\eta}$ converges to the true parameter η_0 at a sufficiently fast rate, specifically $o_P(n^{-1/4-\delta})$ for some $\delta \geq 0$. This condition can be satisfied when η_0 is effectively approximated using methods such as decision trees or advanced neural network architectures (Chernozhukov et al., 2018). The `interflex` package implements three machine learning approaches: NN, RF, and HGB.

It is important to note that no single machine learning algorithm performs best across all scenarios. Therefore, no algorithm strictly dominates in all applications; performance varies widely depending on factors such as the specific task and the dimensionality of the dataset. In Table 4, we outline some broadly accepted pros and cons of each machine learning method.

Table 4: Comparison of Machine Learning Techniques

Method	Pros	Cons
NN	<ul style="list-style-type: none"> • Excel in processing large, complex datasets, particularly those involving unstructured forms such as images, text, and audio. • Use multiple layers to capture intricate patterns and dependencies within data, facilitating high levels of data abstraction and understanding. 	<ul style="list-style-type: none"> • NN have many hyperparameters that require careful tuning to achieve optimal performance. • NN usually require much more data than traditional machine learning algorithms, which is less suitable for applications with limited data availability
RF	<ul style="list-style-type: none"> • Proven efficacy in classification tasks, leveraging multiple decision trees to improve accuracy and control overfitting. • Generally robust against overfitting in comparison to other models like decision trees, especially with more trees in the forest. 	<ul style="list-style-type: none"> • When data are sparse, the random selection of features and bootstrapped samples might not provide enough variability for effective node splitting. • RF does not perform well with data that involves interconnected relationships or sequences, such as graph-based or time series data. It also performs relatively worse when the relationships are linear or smooth.

Method	Pros	Cons
HGB	<ul style="list-style-type: none"> • Particularly strong in scenarios involving imbalanced datasets, where it can effectively adjust to focus on rare events. • Capable of managing missing data and outliers. • More susceptible to overfitting compared to ensemble methods like RF, particularly when the number of trees is large. 	<ul style="list-style-type: none"> • Tends to focus excessively on correcting outliers, which can lead to models that are overly specialized to the training data and may not generalize well. • Due to sequential tree building, HGB is computationally expensive

Sample Splitting and Cross-Fitting Sample splitting serves as crucial techniques alongside the use of orthogonal score functions and machine learning methods for estimating nuisance components. Overfitting bias can arise when the nuisance parameters are estimated on the same sample used to estimate the parameter of interest θ . Sample splitting helps mitigate this bias by ensuring independence between the data used to estimate the nuisance functions (η_0 , training data) and the data used to estimate the causal parameter (θ_0 , holdout data).

Cross-fitting, as an efficient form of data splitting, maximizes the use of available data by alternating the roles of training and holdout sets in a cross-validated framework and combining the estimates from multiple splits to improve efficiency. The process can be outlined as follows:

1. Randomly partition the dataset into K folds, $(I_k)_{k=1}^K$, where each fold I_k contains $n = N/K$ observations and $I_k^c = \{1, \dots, N\} \setminus I_k$ denotes the complement set used for training.

2. For each fold k , estimate the nuisance parameters $\hat{\eta}_{0,k}$ using the data in I_k^c .
3. Compute the estimator $\hat{\theta}_0$ using the empirical expectation over observations in I_k and average the results across all K folds.

The cross-fitting procedure leverages the full dataset while enhancing the robustness of the estimation process by reducing dependence on any single data partition. It is important to note that this procedure focuses solely on fitting the nuisance components; it does not include hyperparameter tuning or other model refinement techniques, which remain essential in predictive modeling.

The three key ingredients, namely Neyman orthogonality, the high-quality machine learning method, and sample-splitting and cross-fitting strategy, when effectively integrated, lead to the robust properties of the canonical DML estimator.

Theorem 4.1 (Properties of the DML) *Suppose that (1) the Neyman-orthogonal score is constructed for the parameter of interest θ , and (2) the nuisance functions are estimated with fast enough rate $o_P(n^{-1/4-\delta})$ with cross fitting. In addition, suppose that $\delta_n \geq n^{-1/2}$ for all $n \geq 1$. Then the DML estimator $\hat{\theta}_0$ concentrate in a $1/\sqrt{n}$ neighborhood of θ_0 and are approximately linear and centered Gaussian (Chernozhukov et al., 2018):*

$$\sqrt{n}\sigma^{-1}(\hat{\theta}_0 - \theta_0) = \frac{1}{\sqrt{n}} \sum_{i=1}^N \psi(D_i) + O_P(\rho_n) \sim N(0, I_d), \quad (8)$$

uniformly over $P \in P_n$, where the size of the remainder term obeys

$$\rho_n := n^{-1/2} + \gamma_n + r'_n + n^{1/2}\lambda_n + n^{1/2}\lambda'_n \leq \delta_n, \quad (9)$$

$\psi(\cdot) := \sigma^{-1}J_0^{-1}\psi(D; \theta_0, \eta_0)$ is the influence function, and the approximate variance is:

$$\sigma^2 := J_0^{-1}\mathbb{E}_P[\psi(D; \theta_0, \eta_0)\psi(D; \theta_0, \eta_0)^T](J_0^{-1})^T. \quad (10)$$

Equation (8) states that $\hat{\theta}_0$ is asymptotically normal with mean θ_0 and covariance σ^2/n . Equation (9) defines the remainder term, which captures the cumulative effect of small errors in the final asymptotic expansion. Intuitively, the terms γ_n , r'_n , λ_n , and λ'_n reflect the quality of nuisance function estimation and the degree to which orthogonality mitigates the influence of these errors on the target parameter. Equation (10) gives the asymptotic covariance matrix, where J_0 denotes the Jacobian of the score function, capturing its sensitivity to deviations of θ from θ_0 .

Taken together, the theorem establishes that the DML estimator for the scalar parameter θ_0 achieves \sqrt{n} -rate convergence and is approximately normally distributed. Both the convergence rate and the asymptotic distribution hold uniformly over a broad class of underlying data-generating processes.

When θ_0 is a function of $x \in \mathcal{X}$, such as the CME, we need an additional smoothing step to handle the infinite-dimensional target. The standard approach is to project $\theta(x)$ onto a finite but growing basis of dimension $K(n)$. For instance, with B-spline expansions, we write:

$$\theta_0(x) \approx p(x)^\top \beta_0,$$

where $p(x) \in \mathbb{R}^{K(n)}$. After constructing an orthogonal signal $\hat{\Lambda}_i$, we regress $\hat{\Lambda}_i$ on $p(X_i)$, obtaining $\hat{\beta}$. The final estimator of the function takes the form $\hat{\theta}_{K(n)}(x) = p(x)^\top \hat{\beta}$.

To ensure that $\hat{\theta}_{K(n)}(x)$ retains the \sqrt{n} -rate and satisfies both pointwise and uniform asymptotic normality, [Semenova and Chernozhukov \(2021\)](#) formally establish sufficient conditions on the estimation and approximation components. First, they require that the misspecification error from the sieve approximation, $\theta_0(x) - p(x)^\top \beta_0$, remains sufficiently small. In addition, they impose the following key conditions: (i) the complexity of the basis $p(x)$ must grow slowly with the sample size; (ii) the cross-fitted nuisance estimators $\hat{\eta}$ must converge to η_0 at a rate faster than $n^{-1/4}$; and (iii) the empirical process governing random fluctuations over the domain \mathcal{X} must be well-behaved, which is ensured by appropriate tail bounds and Lipschitz continuity conditions.

These assumptions jointly control three sources of error: approximation bias from the sieve representation, estimation error from the nuisance components, and uniform stochastic fluctuations of the orthogonal signal. Together, they allow the \sqrt{n} -consistency and asymptotic normality guarantees—typically established for finite-dimensional parameters—to be extended to the infinite-dimensional target $\theta(x)$.

4.2 Binary Treatment

In the case of binary treatment, [Semenova and Chernozhukov \(2021\)](#) show that the Neyman-orthogonal score for the CME can be constructed using the following expression:

$$\Lambda_i(\eta) = \mu(1, V_i) - \mu(0, V_i) + \frac{D_i(Y_i - \mu(1, V_i))}{\pi(V_i)} - \frac{(1 - D_i)(Y_i - \mu(0, V_i))}{1 - \pi(V_i)} \quad (11)$$

where $\mu_0(w, v) = \mathbb{E}[Y_i \mid D_i = d, V_i = v]$ is the outcome model and $\pi(v) = \Pr(D_i = 1 \mid V_i = v)$ is the propensity score.

Equation (11) share the same form of the AIPW signal in Equation (7), which is orthogonal with respect to the nuisance parameter $\eta_0(v)$, defined as $\eta_0(v) := \{\pi_0(v), \mu_0(1, v), \mu_0(0, v)\}$. This AIPW-style Neyman score is first-order insensitive to small estimation errors in $\hat{\mu}(\cdot)$ and $\hat{\pi}(\cdot)$, preserving the orthogonality property. It also provides the foundation for establishing both pointwise and uniform asymptotic theory for the resulting DML estimator for the CME $\theta(x)$. [Bonvini, Zeng, Yu, Kennedy and Keele \(2025\)](#) propose an alternative signal that allows the influence of X on Y to depend partially on other covariates in Z , aiming to isolate effect heterogeneity attributable solely to X . We do not pursue this approach, as our goal is not to interpret the CME as the causal moderation effect of X on Y .

Under the unconfoundedness assumption introduced in Chapter 1 (Assumption 3), the CME can be expressed as the conditional expectation of an observable signal. Specifically, Chapter 3 shows that, when $Y_i(d) \perp\!\!\!\perp D_i \mid V_i = v$,

$$\mathbb{E}[\Lambda_i(\eta) \mid X_i = x] = \theta(x).$$

if either the outcome models or the propensity score model is correctly specified. In the

DML framework, we do not require the functional forms to be exactly correct. Instead, we rely on machine learning models to consistently estimate the nuisance components as the sample size becomes sufficiently large.

With binary treatment, we make the following modeling assumption.

Assumption 10 (Interactive Regression Model, IRM)

$$\begin{aligned} Y_i &= g_0(D_i, V_i) + u_i, & \mathbb{E}[u_i \mid D_i, V_i] &= 0 \\ D_i &= m_0(V_i) + \epsilon_i, & \mathbb{E}[\epsilon_i \mid V_i] &= 0 \end{aligned}$$

where $D_i \in \{0, 1\}$ is a binary treatment; $V_i = (X_i, Z_i)$ is the full covariate vector; $g_0(\cdot)$ and $m_0(\cdot)$ are unknown functions describing how (D_i, V_i) influence Y_i and how V_i predicts D_i , respectively.

The IRM is restrictive in that it requires the error terms u_i and ϵ_i to enter the outcome and treatment equations additively and not interact with D_i or V_i . It is termed “interactive” because it allows $Y_i(1)$ and $Y_i(0)$ to follow arbitrarily different functional forms, specifically, $g_0(1, V_i)$ and $g_0(0, V_i)$. With the IRM, the CME is given by:

$$\theta(x) = \mathbb{E}[g_0(1, x, Z) - g_0(0, x, Z) \mid X = x]$$

The IRM is general, encompassing both the linear interaction model and the smooth varying coefficient model (SVCVM) in the kernel estimator as special cases. Specifically, the linear interaction model assumes

$$\mathbb{E}[Y_i \mid D_i, X_i, Z_i] = \beta_0 + \beta_1 D_i + \beta_2 X_i + \beta_3 (D_i \cdot X_i) + \beta_4 Z_i,$$

which constrains $g_0(\cdot)$ to be linear in $(D_i, X_i, D_i \cdot X_i, Z_i)$. Similarly, the SVCVM assumes

$$\mathbb{E}[Y_i \mid D_i, X_i, Z_i] = f(X_i) + q(X_i)D_i + Z_i\gamma(X_i),$$

which requires $g_0(D_i, X_i = x, Z_i) = f(x) + q(x)D_i + Z_i\gamma(x)$. Both models are silent on how D_i is related to V_i .

In the binary treatment case, we first estimate the nuisance functions using machine

learning methods with cross-fitting. We then construct the AIPW-style Neyman-orthogonal signal for each unit i . Since $\theta(x) = \mathbb{E}[\Lambda_i(\eta_0) \mid X_i = x]$, the CME can be recovered by taking sample analogs of $\{\hat{\Lambda}_i\}$ at each value of $X_i = x$ when X is discrete. To make this process concrete, we provide pseudo-code with cross-fitting below.

Algorithm 3 DML Estimation of CME (Binary D)

```

1: Inputs:
2:   Data:  $\{(X_i, Z_i, D_i, Y_i)\}$  for  $i = 1, \dots, n$ 
3:    $D_i \in \{0, 1\}$  is binary treatment
4:    $V_i := (X_i, Z_i)$  are controls ( $X_i$  is the moderator)
5:    $Y_i$  is the outcome
6:   Number of folds  $K$  (e.g.,  $K = 2, 5$ , or  $10$ )
7:   Choice of basis or smoothing method for the final projection step
8: Outputs:
9:   Estimated function  $\hat{\theta}(x) = \mathbb{E}[Y_i(1) - Y_i(0) \mid X_i = x]$ 
10: 1) Partition data into  $K$  folds
11:   Randomly split the indices  $\{1, \dots, n\}$  into  $K$  disjoint sets:  $I_1, I_2, \dots, I_K$ 
12:   Each  $I_k$  is the “holdout” set for fold  $k$ ,  $I_k^c = \{1, \dots, n\} \setminus I_k$  be the “training” set.
13: 2) Estimate nuisance functions (cross-fitting)
14: for  $k = 1$  to  $K$  do
15:   (a) On the training set  $I_k^c$ :
16:   * Fit outcome models:
17:      $\mu_1(v) \approx \mathbb{E}[Y \mid D = 1, V = v]$ ,  $\mu_0(v) \approx \mathbb{E}[Y_i \mid D_i = 0, V_i = v]$ 
18:   * Fit propensity model:
19:      $\pi(v) \approx \Pr(D_i = 1 \mid V_i = v)$ 
20:   (b) For each observation  $i$  in the holdout set  $I_k$ :
21:   * Predict  $\mu_1(v_i), \mu_0(v_i), \pi(v_i)$ :  $\hat{\mu}_1^{(-k)}(v_i), \hat{\mu}_0^{(-k)}(v_i), \hat{\pi}^{(-k)}(v_i)$ 
22: end for
23: 3) Compute AIPW-style Neyman-orthogonal signal
24: for each fold  $k$ , for each  $i$  in  $I_k$  do
25:    $\Lambda_i(\hat{\mu}_1^{(-k)}, \hat{\pi}^{(-k)}) =$ 
26:      $\hat{\mu}_1^{(-k)}(V_i) - \hat{\mu}_0^{(-k)}(V_i) + [D_i * (Y_i - \hat{\mu}_1^{(-k)}(V_i))] / \hat{\pi}^{(-k)}(V_i)$ 
27:      $- [(1 - D_i) * (Y_i - \hat{\mu}_0^{(-k)}(V_i))] / [1 - \hat{\pi}^{(-k)}(V_i)]$ 
28: end for
29: 4) Project signal onto  $X$  to obtain  $\hat{\theta}(x)$ 
30:   Regress  $\Lambda_i$  on  $[\tilde{D}_i \cdot g(X_i)]$ ,  $g(\cdot)$  are basis functions of  $X$ .
31:    $\hat{\theta}(x) = \arg \min_g \sum_{i=1}^n [\Lambda_i - g(X_i)]^2$ .
32: Return:
33:   The function  $\hat{\theta}(x) =$  estimated CME as a function of  $X$ .

```

We now demonstrate how to implement this procedure using the `interflex` package. Using data from **Example 6** based on [Noble \(2024\)](#), we compare the results from AIPW-Lasso to those from the DML estimators.

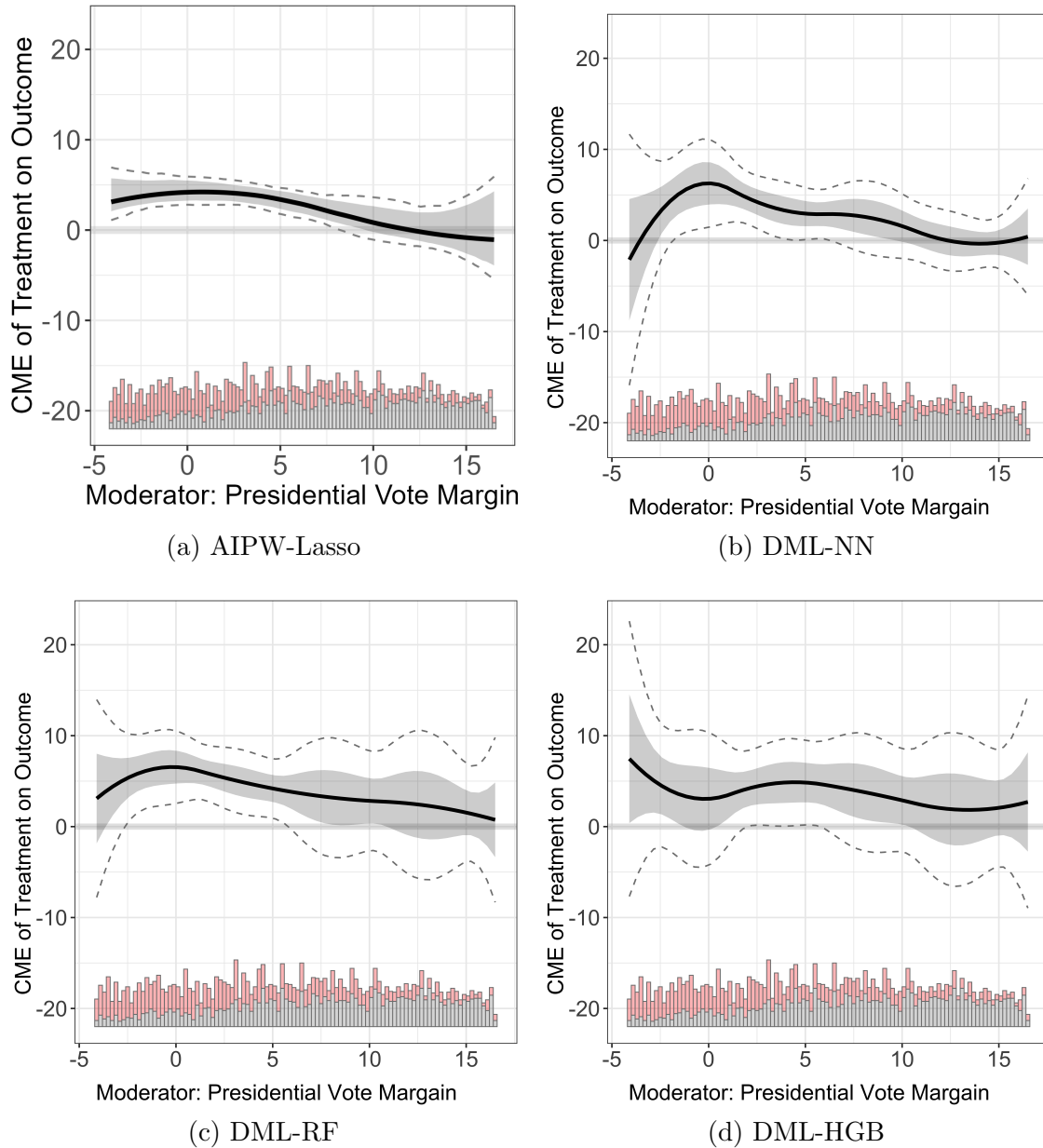
```
1 # R code excerpt
```

```

2
3 library(interflex)
4 D="opp" # Out-partisanship of Lawmakers
5 Y="pres_ref" # Frequency of Presidential References
6 X="pres_vote_margin" #Presidential Vote Margain
7 Z=c("prev_vote","majority","leadership","seniority","tot_speech")
8
9 ## For code to generate plot (a), see last chapter
10
11 ## DML estimator with neural network machine learning method
12 out.dml.nn<-interflex(estimator='DML',
13                       data = d, model.y="nn", model.t = "nn",
14                       Y=Y,D=D,X=X, Z = Z,
15                       treat.type = "discrete", na.rm = TRUE,
16                       vartype = "bootstrap", parallel = TRUE)
17 plot(out.dml.nn)
18
19 ## DML estimator with random forest machine learning method
20 out.dml.rf<-interflex(estimator='DML',
21                       data = d, model.y="rf", model.t = "rf",
22                       Y=Y,D=D,X=X, Z = Z,
23                       treat.type = "discrete", na.rm = TRUE,
24                       vartype = "bootstrap", parallel = TRUE)
25 plot(out.dml.rf)
26
27 ## DML estimator with histogram gradient boosting machine learning method
28 out.dml.hgb<-interflex(estimator='DML',
29                        data = d, model.y="hgb", model.t = "hgb",
30                        Y=Y,D=D,X=X, Z = Z,
31                        treat.type = "discrete", na.rm = TRUE,
32                        vartype = "bootstrap", parallel = TRUE)
33 plot(out.dml.hgb)

```

Figure 15: Replicating Noble (2024) Figure 2: AIPW-Lasso vs DML Estimators



Notes: The treatment D is out-partisanship of lawmakers, the outcome Y is frequency of presidential references in Congressional speeches. (a) CME estimates from AIPW-Lasso; (b)-(d) CME estimates from the DML estimator, with nuisance parameter estimated with NN, RF, and HGB, respectively. The gray ribbon show the 95% pointwise confidence intervals, respectively. The dashed lines represent 95% uniform confidence intervals.

Figure 15 compares CME estimates from the AIPW-Lasso estimator (a) and the DML estimators (b)–(d). As before, we trim the sample based on the moderator X , restricting it to the central 95% quantile range to improve overlap. AIPW-Lasso yields monotonically decreasing CME estimates in x , with fairly narrow confidence intervals. The DML estimators produce broadly similar patterns but with much wider confidence intervals. Substantively, both methods suggest that the presidential-reference treatment has a modestly positive effect on the outcome in areas of low constituency partisanship. AIPW-Lasso shows a statistically significant treatment effect for $X \in [-5, 10]$, while the DML estimators, despite greater uncertainty, indicate a significant effect for out-party legislators when $X \in [0, 5]$.

4.3 Continuous Treatment

With continuous treatment, the Neyman orthogonality condition designed in [Semenova and Chernozhukov \(2021\)](#) is robust to small errors in nuisance parameter $\eta_0 = \{\mu_0(d, v), e_0(d | v)\}$, with $\mu_0 = \mathbb{E}[Y | D = d, V = v]$, $e_0(D | V_i)$ is $f_{D|V}(d | v)$. The general Neyman-orthogonal score is:

$$\Lambda_i(\eta) = -\partial_d \log e(d | v) [Y - \mu(d, v)] + \partial_d \mu(d, v)$$

Again, we can show CME is the conditional expectation of an observable signal given unconfoundedness assumption.

$$\mathbb{E}[\Lambda_i(\eta) | X_i = x] = \mathbb{E} \left[\frac{\partial Y_i(d)}{\partial d} | X_i = x \right].$$

We provide the proof in the Appendix.

A fully nonparametric estimation of $f_{D|V}(d | v)$ is highly sample-intensive. Therefore, in practical applications, we adopt the canonical partially linear regression model (PLRM) from [Robinson \(1988\)](#) as the data-generating process, similar to the continuous treatment

settings discussed in Chapter 3.

$$\begin{aligned} Y_i &= \theta(X_i) \cdot D_i + \mu(V_i) + \epsilon_i, \\ D_i &= \pi(V_i) + \xi_i, \quad \mathbb{E}[\xi | V_i] = 0 \end{aligned}$$

where $\mathbb{E}[\epsilon | D_i, V_i] = 0$ is given by unconfoundedness.

The first equation states that Y_i depends on D_i through the CME at X_i , plus a baseline function $\mu(V_i)$. This is the main outcome equation, where function $\theta(\cdot)$ is the parameters of interest. The second equation characterizes how the confounding variables V_i influence the treatment variable D_i . Both $\mu(\cdot)$ and $\pi(\cdot)$ are high-dimensional nuisance functions. We collect these as $\eta_0 = \{\mu(\cdot), \pi(\cdot)\}$.

By imposing a partially linear structure on the treatment assignment mechanism, the PLRM simplifies the task of modeling $f(d | x)$. However, this comes at the cost of assuming a linear additive relationship. For example, if D depends on V in a more complex way—such as through interactions or heteroskedasticity—the assumption that $\mathbb{E}[\xi | V_i] = 0$ may be violated, leading to misspecification.

Similar to the binary treatment setting with the IRM, traditional parametric methods represent restricted forms of the partially linear model, where $\theta(\cdot)$ is assumed to be linear in X , i.e., $\theta(X) = \beta_1 + \beta_3 X$, and $\mu(\cdot)$ is linear in (X, Z) , so that $\mu(X, Z) = \beta_0 + \beta_2 X + \beta_4' Z$. The semiparametric smooth varying coefficient model (SVCMM) can also be embedded into the partially linear framework by letting $\theta(X) = g(X)$ and $\mu(X, Z) = f(X) + Z\gamma(X)$.

The PLRM allows for the construction of a Neyman orthogonal score via the “partialling out” approach. In the previous chapter, we introduced a continuous treatment extension of AIPW that partialled out covariates from both Y and D to identify the CME. The approach in Algorithm 2 is already orthogonal, ensuring that small misspecifications in $\hat{\mathbb{E}}[Y | V_i]$ and $\hat{\mathbb{E}}[D | V_i]$ do not spill over into the estimation of the CME.

The key difference here is that we explicitly adopt a DML procedure. While the PO-Lasso approach in the previous chapter trains and evaluates the nuisance models on the

same sample, DML partitions the data into folds. It trains the nuisance functions using flexible machine learning methods—converging at rate $o_P(n^{-1/4-\delta})$ —on a subset of folds, and evaluates them on the remaining holdout fold. We provide pseudo-code below to clarify the cross-fitting process.

Algorithm 4 DML Estimation of CME (Continuous D)

1: **Inputs:**
2: Data: $\{(X_i, Z_i, D_i, Y_i)\}$ for $i = 1, \dots, n$
3: $D_i \in \{0, 1\}$ is a continuous treatment
4: $V_i := (X_i, Z_i)$ are covariates, in which X_i is the moderator
5: Y_i is the outcome
6: Number of folds K (e.g., $K = 2, 5$, or 10)
7: Choice of machine learning algorithms and smoothing method
8: **Outputs:**
9: Estimated function $\hat{\theta}(x) = \mathbb{E}[\partial_d Y(d) \mid X_i = x]$
10: **1) Partition data into K folds**
11: Randomly split the indices $\{1, \dots, n\}$ into K disjoint sets: I_1, I_2, \dots, I_K
12: Each I_k is the “holdout” set for fold k , $I_k^c = \{1, \dots, n\} \setminus I_k$ be the “training” set.
13: **2) Estimate nuisance functions (cross-fitting)**
14: **for** $k = 1$ to K **do**
15: (a) On the training set I_k^c :
16: * Fit outcome models: $\mu(v) \approx \mathbb{E}[Y_i \mid V_i = v]$
17: * Fit propensity model: $\pi(v) \approx \Pr(D_i = 1 \mid V_i = v)$
18: (b) For each observation i in the holdout set I_k :
19: * Predict $\mu(v_i), \pi(v_i)$: $\hat{\mu}^{(-k)}(v_i), \hat{\pi}^{(-k)}(v_i)$
20: **end for**
21: **3) Form residuals for each i in I_k**
22: **for** each fold k , for each i in I_k **do**
23: $\tilde{Y}_i = Y_i - \hat{\mu}^{(-k)}(V_i), \tilde{D}_i = D_i - \hat{\pi}^{(-k)}(V_i)$.
24: **end for**
25: After all folds, We now have full set of out-of-fold residuals pairs:
26: $\{(X_i, \tilde{D}_i, \tilde{Y}_i)\}$ for i in I_k .
27: **4) Project signal onto X to obtain $\hat{\theta}(x)$**
28: Regress \tilde{Y}_i on $[\tilde{D}_i \cdot g(X_i)]$, $g(\cdot)$ are basis functions of X .
29: $\tilde{Y}_i = \theta(X_i) \cdot \tilde{D}_i + \epsilon_i$
30: **Return:**
31: The function $\hat{\theta}(x)$ = estimated CME as a function of X .

We provide an R code excerpt to implement the estimation using the `interflex` package. Using data from **Example 12**, we compare the results from the PO-Lasso estimator with those from the DML estimators.

```

1 # R code excerpt
2
3 library(interflex)

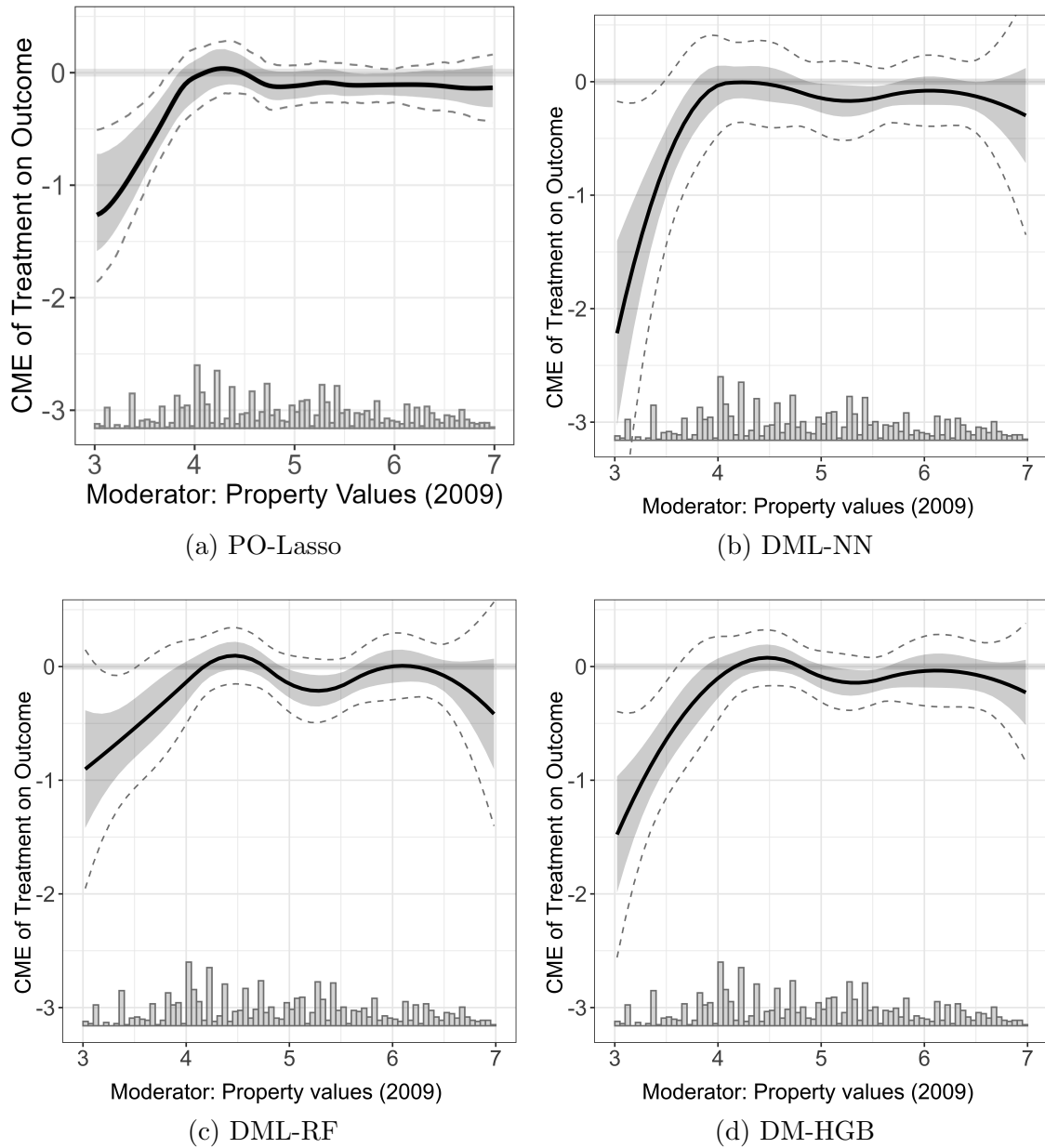
```

```

4
5 D="Dpop1000_asm_dr_3" #Change in Congestion
6 Y="Dakp_3" #Change in AKP vote share
7 X="lograyic09" #Property values (2009)
8 Z=c('Duniversity_3', 'Dodr_3', 'Dydr_3', 'Dpopulation_3', 'Dhospital_pri_3',
      ', 'Dhospital_pub_3')
9
10 ## For code to generate plot (a), see last chapter
11
12 ## DML estimator with neural network machine learning method
13 out.dml.nn<-interflex(estimator='DML',
14                       data = d, model.y="nn", model.t = "nn",
15                       Y=Y,D=D,X=X, Z = Z, treat.type = "continuous",
16                       na.rm = TRUE,
17                       vartype = "bootstrap",parallel = TRUE)
18 plot(out.dml.nn)
19
20 ## DML estimator with random forest machine learning method
21 out.dml.rf<-interflex(estimator='DML',
22                       data = d, model.y="rf", model.t = "rf",
23                       Y=Y,D=D,X=X, Z = Z, treat.type = "continuous",
24                       na.rm = TRUE,
25                       vartype = "bootstrap",parallel = TRUE)
26 plot(out.dml.rf)
27
28 ## DML estimator with histogram gradient boosting machine learning method
29 out.dml.hgb<-interflex(estimator='DML',
30                        data = d, model.y="hgb", model.t = "hgb",
31                        Y=Y,D=D,X=X, Z = Z, treat.type = "continuous",
32                        na.rm = TRUE,
33                        vartype = "bootstrap",parallel = TRUE)
34 plot(out.dml.hgb)

```

Figure 16: Replicating Adiguzel, Cansunar and Corekcioglu (2023): PO-Lasso vs DML Methods



Notes: The treatment D measures change in congestion level, the outcome Y measures change in the vote share for the incumbent AKP party. (a) CME estimates from PO-Lasso; (b)-(d) CME estimates from the DML estimator, with nuisance parameter estimated with NN, RF, and HGB, respectively. The gray ribbon show the 95% pointwise confidence intervals, respectively. The dashed lines represent 95% uniform confidence intervals.

Figure 16 displays CME estimates of the effect of changes in congestion on AKP vote share across communities with varying median property values. The estimation sample is trimmed to the range $3 \leq \log(\text{property value}) \leq 7$ due to sparse observations outside that interval. We have previously shown the CME estimates from PO-Lasso in the last chapter, now displayed in panel (a). Panels (b)-(d) show that the DML estimator produces similar patterns, with slightly bigger estimates when X is small. They also yield wider confidence intervals.

4.4 Discrete Outcome

Finally, we explore the application of the AIPW and DML estimators to models with discrete outcomes. Traditional parametric approaches for binary or count data typically rely on link functions—such as logit, probit, Poisson, or negative binomial—to capture nonlinearity between predictors and the outcome. However, this introduces two key challenges. First, it becomes difficult to disentangle the nonlinearity imposed by the link function from the intrinsic nonlinearity of the CME. Second, when the treatment D is continuous, the derivative $\frac{\partial Y}{\partial D}$ depends on both X and D , requiring an additional averaging over D to recover a coherent measure of the CME: $\mathbb{E} \left[\frac{\partial Y}{\partial D} \mid X = x \right]$.

When the treatment is binary, the link function can be naturally incorporated into the AIPW and DML estimators by modifying the learner to model the outcome appropriately. When the treatment is continuous, although the theoretical framework underlying the PO-Lasso and DML estimators is based on the partially linear regression model—which does not explicitly account for the link function—these methods can still serve as good approximations. This is done by treating the composite structure $g^{-1} \circ m$ as a single nuisance component while preserving Neyman orthogonality.

Link Functions in Discrete Outcome Models In parametric approaches for discrete outcomes, the composite structure

$$\mathbb{E}[Y \mid D, X] = g^{-1}(m(D, X))$$

is used to connect the conditional mean of the outcome $\mu = \mathbb{E}[Y \mid D, X]$ with a linear or nonlinear predictor $m(D, X)$ through the inverse link function $g^{-1}(\cdot)$. Common choices for the link function $g(\cdot)$ include:

- **Logit Link:**

$$g(\mu) = \log\left(\frac{\mu}{1-\mu}\right) \iff \mu = \frac{1}{1 + \exp\{-m(D, X)\}}.$$

- **Probit Link:**

$$g(\mu) = \Phi^{-1}(\mu) \iff \mu = \Phi(m(D, X)),$$

where $\Phi(\cdot)$ denotes the cumulative distribution function of the standard normal distribution.

- **Poisson Link:**

$$g(\mu) = \log(\mu) \iff \mu = \exp\{m(D, X)\}.$$

- **Negative Binomial Link:** Often the negative binomial model also employs a log link,

$$g(\mu) = \log(\mu) \iff \mu = \exp\{m(D, X)\},$$

but the model further accommodates over-dispersion via an additional dispersion parameter.

These link functions serve to map the latent index $m(D, X)$ into the appropriate support for μ . For binary outcomes, the inverse link ensures that μ remains within $[0, 1]$, while for count outcomes, the log link guarantees a positive mean. In classical specifications, the predictor $m(D, X)$ is often modeled as a linear combination of the treatment, covariates, and their

interactions. For example, one common formulation is

$$m(D, X) = \beta_0 + \beta_1 D + \beta_2 X + \beta_3(D \times X),$$

where the different coefficients capture the main effects and the interaction effect, thereby allowing for a nuanced representation of how D and X jointly influence the outcome.

Challenges in Estimating the CME with Parametric Methods In the discrete outcome setting, the target parameter varies with the nature of the treatment D . For a binary treatment, one seeks to estimate the average treatment effect, $\mathbb{E}[Y(1) - Y(0) \mid X]$. Under the composite structure

$$\mathbb{E}[Y \mid D, X] = g^{-1}(m(D, X)),$$

and a typical parametric specification such as

$$m(D, X) = \beta_0 + \beta_1 D + \beta_2 X + \beta_3(D \times X),$$

this difference can be written as

$$\mathbb{E}[Y(1) - Y(0) \mid X] = g^{-1}(\beta_0 + \beta_1 + \beta_2 X + \beta_3 X) - g^{-1}(\beta_0 + \beta_2 X).$$

In contrast, for a continuous treatment, the focus is on estimating the CME defined as $\mathbb{E} \left[\frac{\partial Y}{\partial D} \mid X = x \right]$. Applying the chain rule to the composite model yields

$$\mathbb{E} \left[\frac{\partial Y}{\partial D} \mid D, X \right] = g^{-\prime}(m(D, X)) \cdot \frac{\partial m(D, X)}{\partial D}.$$

With the same linear specification, one obtains $\frac{\partial m(D, X)}{\partial D} = \beta_1 + \beta_3 X$, so that

$$\mathbb{E} \left[\frac{\partial Y}{\partial D} \mid D, X \right] = g^{-\prime}(\beta_0 + \beta_1 D + \beta_2 X + \beta_3(D \times X)) \cdot (\beta_1 + \beta_3 X).$$

This expression illustrates the key role of the link function: the derivative of its inverse, $g^{-\prime}(\cdot)$, introduces additional nonlinearity that makes the marginal effect a function of both D and X . In the absence of a link function (i.e., when g^{-1} is the identity), $\frac{\partial Y}{\partial D}$ simplifies to $\beta_1 + \beta_3 X$, depending solely on X . Thus, the first challenge is disentangling the nonlinearity imposed by the link function from the inherent nonlinearity in the predictor $m(D, X)$. The

second challenge, particularly pertinent for continuous D , is that the derivative $\frac{\partial m(D, X)}{\partial D}$ depends on both D and X when a link function is present, necessitating an additional averaging over D to obtain the CME:

$$\text{CME}(X) = \mathbb{E}_D \left[\mathbb{E} \left[\frac{\partial Y}{\partial D} \mid D, X \right] \mid X \right].$$

This highlights the critical importance of properly incorporating the link function when estimating the CME in continuous treatment settings.

Incorporating Discrete Outcomes The DML estimator offer a unified framework for handling discrete outcomes by leveraging the composite structure

$$\mathbb{E}[Y \mid D, X] = g^{-1}(m(D, X)),$$

where $g(\cdot)$ is a link function and $m(D, X)$ is a predictor that can be specified as linear or nonlinear functions of X and D .

In the binary treatment case, the target parameter is $\mathbb{E}[Y(1) - Y(0) \mid X]$. Here, the DML and AIPW-Lasso approaches can be implemented as described in the algorithm above, and one may replace the regressor learner for the outcome model with a classifier (e.g., logistic or probit regression) that ensures the fitted values $\hat{Y}(1)$ and $\hat{Y}(0)$ remain in the interval $[0, 1]$.

In contrast, when the treatment D is continuous, the focus shifts to estimating $\mathbb{E} \left[\frac{\partial Y}{\partial D} \mid X = x \right]$. It is important to note that while replacing regression models with classification models in the outcome fitting may be feasible for binary treatments, such substitution is not recommended when D is continuous. As discussed in [Alves \(2022\)](#), the theory of orthogonalization and the PLRM—characterized by $Y = \theta(X) \cdot D + \mu(V) + \epsilon$ —requires regression-based estimation to ensure theoretical validity.

Although we cannot explicitly account for the link function when the treatment is continuous, the DML and PO-Lasso estimators, which are based on PLRM, can still serve as a good approximation. They treat the composite structure $g^{-1} \circ m$ as a single component, use machine learning to learn it, and yield $\mathbb{E} \left[\frac{\partial Y}{\partial D} \mid X = x \right]$ based on the PLRM.

4.5 Summary

This chapter introduces DML as a robust method to estimate the CME when dealing with high-dimensional or complex nuisance functions. The central concept underlying DML is Neyman orthogonality, a condition ensuring that small estimation errors in nuisance functions, such as outcome models or propensity scores, do not bias the CME estimate to first order. This property generalizes the double robustness of AIPW introduced in Chapter 3, allowing flexible machine learning methods like neural networks, random forests, and histogram gradient boosting to approximate intricate relationships within nuisance parameters. While orthogonalization constructs estimators insensitive to regularization biases, cross-fitting mitigates overfitting by independently estimating nuisance parameters and causal effects using different subsets of data. Together, these strategies enable valid inference with a convergence rate of \sqrt{n} , extending to infinite-dimensional parameters through smoothing techniques like kernel and B-spline regressions.

The chapter further discuss specific applications of DML in binary and continuous treatment scenarios. For binary treatments, DML constructs orthogonal signals using an AIPW-style formula and cross-fitting, which isolates moderators from additional covariates. For continuous treatments, it employs a partial linear regression framework, orthogonally residualizing treatment and outcome variables against confounding variables. We provide empirical examples of implementing DML through the `interflex` package, demonstrating its application in real-world political science contexts.

Chapter 5. Monte Carlo Evidence

In prior discussions, we examined various methods for estimating the CME, including the linear interaction model, the semiparametric kernel estimator, the AIPW-Lasso estimator—by which we mean AIPW with basis expansion and double-selection Lasso—and the more recently developed DML methods. This chapter uses Monte Carlo simulations to compare the performance of these methods in a binary treatment setting. Specifically, we aim to assess the relative advantages of the kernel estimator, AIPW-Lasso estimator, and DML estimators in terms of accuracy and associated computational cost under different scenarios.

Our simulation results highlight a key finding: for DML to perform well, a sufficiently large sample size is essential. Without enough observations, its advantages—such as handling high-dimensional data and capturing complex relationships—may not fully materialize, and it can underperform compared to the kernel estimator. In contrast, AIPW-Lasso, which relies on simpler learners, performs well even with small to medium-sized samples and matches the performance of DML methods with default or untuned hyperparameters.

Furthermore, while the kernel estimator can adeptly capture nonlinearities in the CME, AIPW-Lasso and DML offer additional strengths in addressing nonlinearities among the other covariates. Researchers are therefore encouraged to consider AIPW-Lasso and DML when working with large datasets and when nonlinear relationships extend beyond the moderator variable.

We also compare the performance of three DML learners—neural networks (NN), random forests (RF), and histogram gradient boosting (HGB)—using both default and fine-tuned hyperparameters through cross-validation and grid search. Although fine-tuning can improve model fit and CME estimation, it is time-consuming and may require prior knowledge to set up appropriate hyperparameter grids.

In the remainder of this chapter, we present three DGPs. First, we use a simple DGP to compare the kernel estimator, AIPW-Lasso, and various DML estimators in a setting where

covariates affect the outcome linearly. Second, we introduce nonlinear relationships between covariates and the outcome to assess how well these methods adapt. Finally, we consider a substantially more complex DGP to evaluate the performance of NN, RF, and HGB under both default and tuned hyperparameters.

5.1 Simulation Study 1: Linear Covariate Effects

In the first simulation study, the covariate affects the outcome linearly. In this setting, the kernel estimator (with an appropriately chosen bandwidth) can approximate the true marginal effect accurately. Our simulations show that, with sufficiently large sample sizes, DML methods perform comparably to the kernel estimator with cross-validated bandwidth. However, for smaller samples, DML methods can be more sensitive to noise, often resulting in underfitting of their machine learning models.

To properly evaluate these methods, we define the outcome Y_i as

$$Y_i = \theta(X_i)D_i + g(V_i) + \varepsilon,$$

where $\theta(X_i)$ is the CME of D_i on Y_i , $g(V_i) = \mathbb{E}[Y_i \mid D_i = 0, V]$ is the model for untreated counterfactual outcome, and $\varepsilon \sim N(0, 1)$ is the i.i.d. error term. The covariates $V_i = [X_i, Z_i]$ are i.i.d drawn from a uniform distribution: X_i, Z_i are i.i.d drawn from $\text{Unif}(-\sqrt{3}, \sqrt{3})$. The CME is quadratic in x : $\theta(x) = x^2$, and V_i enters the outcome model $g(V_i)$ linearly: $g(V_i) = 1 + X_i + 0.5Z_i$.

The propensity score $\Pr[D_i = 1 \mid V_i]$ follows a logistic model:

$$\pi(V_i) = \Pr[D_i = 1 \mid V_i] = \frac{\exp(0.5X_i + 0.5Z_i)}{1 + \exp(0.5X_i + 0.5Z_i)} = \text{logit}^{-1}(0.5X + 0.5Z),$$

and the treatment variable D_i is sampled from $D_i \sim \text{Bernoulli}(\pi(V_i))$.

Because the CME is nonlinear in X_i , the linear interaction model is biased. Recall that the kernel estimator is specified as follows:

$$Y_i = f(X_i) + h(X_i)D_i + Z\gamma(X_i) + \epsilon_i$$

With a properly selected bandwidth, it can approximate the DGP effectively with $f(X_i) = 1 + X_i$, $h(X_i) = X_i^2$, and $\gamma(X_i) = 0.5$. Bandwidth selection via cross-validation, which targets out-of-sample predictive accuracy, helps to reduce bias in the estimate of $\theta(X_i)$.

The AIPW-Lasso and DML estimators take a different approach. They model both the outcome and the propensity score as functions of V :

$$\eta = \left\{ \underbrace{\mathbb{E}(Y_i \mid D_i = 1, V)}_{\mu(1, V_i)}, \underbrace{\mathbb{E}(Y_i \mid D_i = 0, V)}_{\mu(0, V_i)}, \underbrace{\mathbb{E}(D_i \mid V_i)}_{\pi(V_i)} \right\},$$

and construct the orthogonal signal of the outcome as

$$\Lambda_i(\hat{\eta}) = \hat{\mu}(1, V_i) - \hat{\mu}(0, V_i) + \frac{D_i [Y_i - \hat{\mu}(1, V_i)]}{\hat{\pi}(V_i)} - \frac{(1 - D_i) [Y_i - \hat{\mu}(0, V_i)]}{1 - \hat{\pi}(V_i)}.$$

DML differs from AIPW-Lasso in that it requires cross-fitting. Specifically, DML partitions the data into five folds and uses four folds to train machine learning models for estimating $\mu(\cdot, V_i)$ and $\pi(V_i)$. These estimates are then applied to the hold-out fold to compute $\hat{\eta}$. Using these estimates, the DML algorithm computes the orthogonal signal of Y_i in the hold-out fold. This process is repeated across all five folds, and the resulting orthogonal signals $\Lambda_i(\hat{\eta})$ are stacked together.

In the final step, both AIPW-Lasso and DML reduce the signals $\Lambda_i(\hat{\eta})$ to the one-dimensional CME in X_i . We use the AIPW-Lasso estimator with kernel regression, as discussed in Chapter 3. For DML, as introduced in Chapter 4, we regress $\Lambda_i(\hat{\eta})$ on a set of basis functions of the moderator X_i , denoted $\phi(X_i)$, to estimate the CME as $\phi(X_i)' \beta$, where β is a vector of regression coefficients. We use a B-spline basis with 5 degrees of freedom and polynomial degree 2 for each spline segment.

With this DGP, the true nuisance functions are $\mu_i(1, V_i) = X_i^2 + 1 + X_i + 0.5Z_i$, $\mu(0, V_i) = 1 + X_i + 0.5Z_i$, $\pi(V_i) = \text{logit}^{-1}(0.5X_i + 0.5Z_i)$. Although these functions are not complex, small samples can still challenge machine learning model fittings, leading to underfitting or convergence issues. Moreover, the cross-fitting procedure—which reduces the training data in each fold—may further amplify these issues when data are limited.

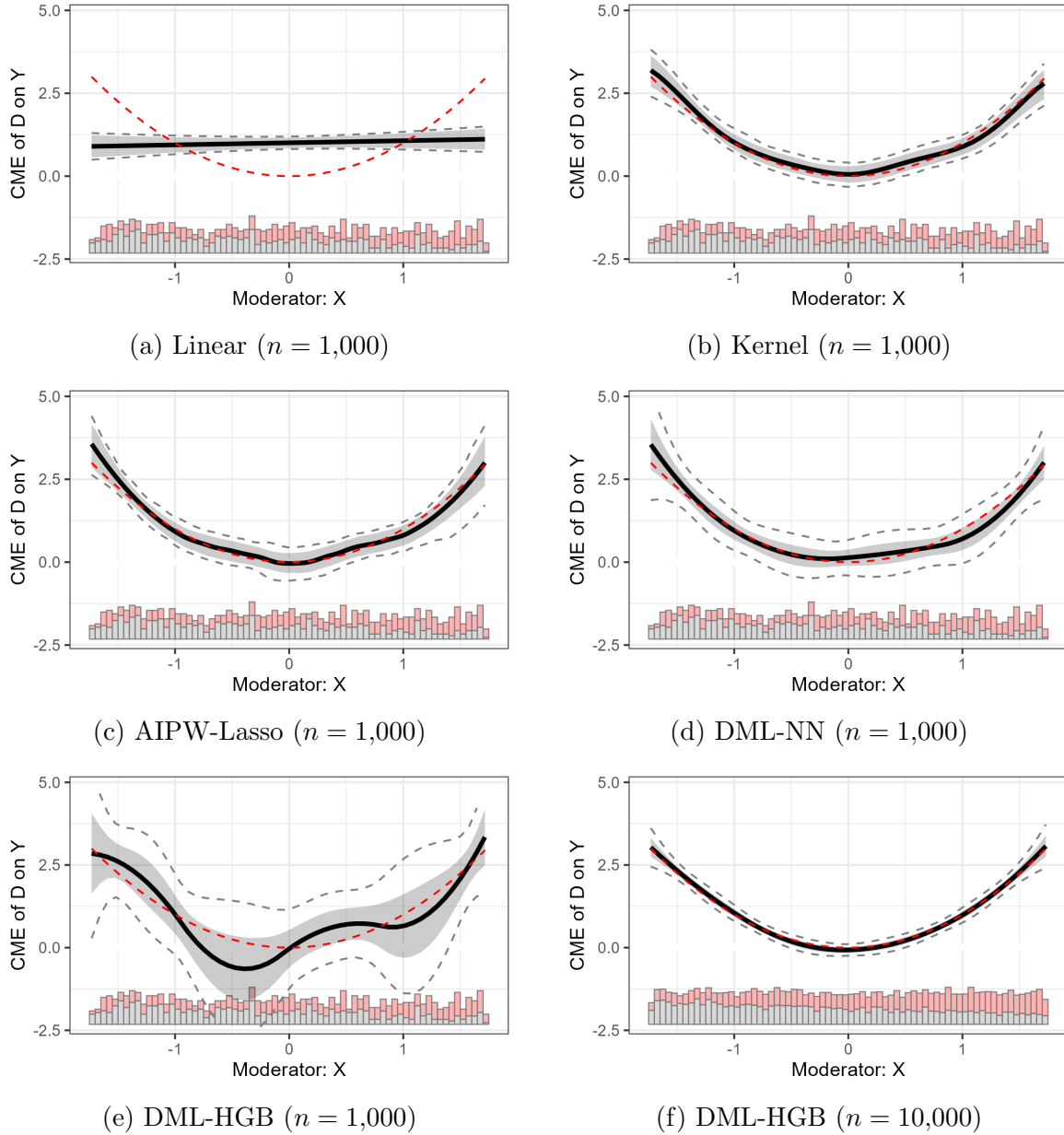
In Figure 17, we compare the estimated CME to the true CME for a single simulation from the DGP. The first row presents model-based approaches, including the linear estimator (based on the linear interaction model) and the kernel estimator (with bandwidth selected via cross-validation). The second row shows results from the IPW-Lasso and AIPW-Lasso estimators, both using basis expansion and post-selection Lasso for variable selection. The third row presents the DML method, with both the outcome and propensity score models fitted using NN. At the bottom of each panel, we display the distribution of treated units (in red) and control units (in gray) along the moderator X using histograms.

Figure 17 shows that the linear estimator exhibits substantial bias, while the kernel estimator closely approximates the true CME. AIPW-Lasso performs comparably to the kernel method, offering more stable estimates and narrower confidence intervals. DML-NN yields similar point estimates but with slightly wider confidence intervals. At $n = 1,000$, DML-HGB performs poorly, with uniform confidence intervals that nearly always cover zero. However, at $n = 10,000$, its performance improves markedly, and the estimated CME closely aligns with the truth. These results suggest that both kernel and AIPW-Lasso estimators are well suited for estimating nonlinear CMEs when covariates enter the outcome model linearly and the sample size is moderate.

To evaluate the performance of each method in terms of accuracy and computational efficiency as the sample size increases, we compare two metrics in Figure 18: the weighted mean squared error (WMSE) and execution time. WMSE measures the discrepancy between the true CME, $\theta(X_i)$, and its estimate, $\hat{\theta}(X_i)$, weighted by the probability density of X_i , $f_X(X_i)$. Since X_i is uniformly distributed in this simulation, the weights are constant over X . Execution time serves as a practical metric for computational efficiency.

Figure 18 presents results for the linear estimator, the kernel estimator, the AIPW-Lasso estimator, and DML methods using three different learners (NN, RF, and HGB). As expected, the linear estimator has the highest WMSE across all sample sizes due to substantial bias. The kernel estimator achieves relatively low WMSE but incurs higher

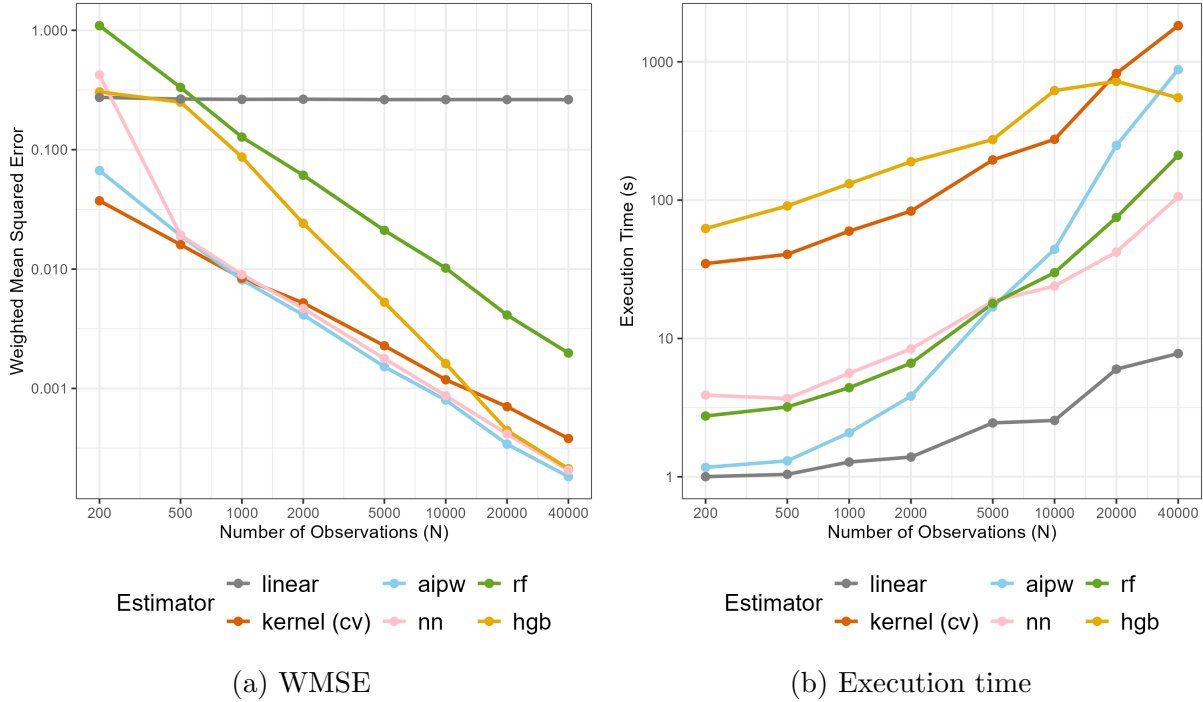
Figure 17: Comparison of Estimators with DGP1



Note: In each figure: the red dashed line represents the true CME; the black solid line represents the estimated CME; the shaded area represents the pointwise confidence intervals, while the dashed gray lines represent the uniform confidence intervals.

computational costs because of bandwidth selection via cross-validation. The AIPW-Lasso estimator performs slightly better in WMSE and is generally less computationally demanding than the kernel method in small samples, although its runtime increases rapidly as the sample size grows. Among the DML estimators, DML-NN performs comparably to AIPW-Lasso and

Figure 18: Performance of Different Methods: DGP1



Notes: The above figures shows how weighted mean squared error (left) and execution time (right) changes as the sample size increases. Both axes in each figure is in log scale.

becomes more efficient in runtime when $n > 5,000$. HGB achieves low WMSE once n exceeds 10,000, but its execution time grows substantially for larger n . Random forest performs worse than both the NN and HGB in this setting.

With this DGP, the only source of nonlinearity is in the CME, while the covariate Z_i enters the outcome model linearly. Under these conditions, the kernel, AIPW-Lasso, and DML estimators can effectively capture the quadratic CME when the sample size is sufficiently large. However, with smaller samples, DML methods may suffer from slow convergence and high variance, leading to worse performance. Therefore, when the sample size is small or moderate and computational efficiency is a key concern, AIPW-Lasso offers the best trade-off between accuracy and runtime. As the dataset grows, both AIPW-Lasso and DML methods become increasingly competitive in accuracy, albeit with greater computational cost.

5.2 Simulation Study 2: Nonlinear Covariates Effects

We use the second simulation study to illustrate the advantages of the AIPW-Lasso and DML methods when covariates enter the outcome model nonlinearly. Based on the first simulation study, we modify only the outcome model as follows:

$$g(V_i) = 1 + X_i + e^{2Z_i+2}.$$

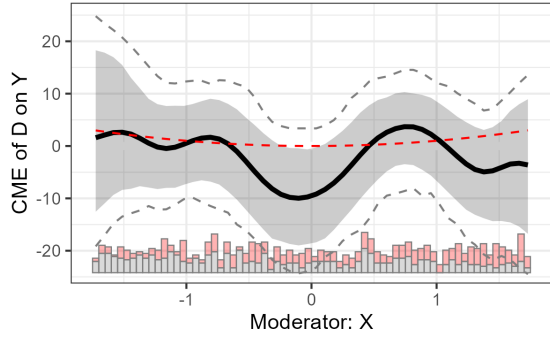
The CME, $\theta(X_i)$, the propensity score, $\pi(V_i)$, and the distributions of X and Z_i remain unchanged. While the kernel estimator can effectively capture nonlinearity in the moderator itself, it struggles to accommodate nonlinearities in other covariates. Specifically, the kernel estimator restricts Z_i to enter linearly via $\gamma(X_i)$, making it incapable of modeling terms such as e^{2Z_i+2} . By contrast, the AIPW-Lasso and DML methods can flexibly capture more complex effects of Z_i on Y_i through basis expansion or machine learning algorithms.

In Figure 19, we compare the estimated CME with the true CME in a single simulated sample based on this DGP. The first row presents the kernel estimator (with bandwidth selected via cross-validation) for $n = 1,000$ and $n = 10,000$. The second row shows results from the AIPW-Lasso estimator for $n = 1,000$ and $n = 10,000$, using basis expansion and post-selection Lasso for variable selection. The third row presents the DML method, with both the outcome and propensity score models fitted using NN.

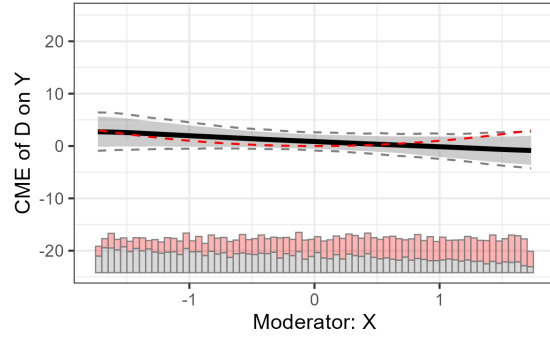
Unlike the first scenario, the kernel estimator fails to approximate the CME accurately at either sample size. For $n = 1,000$, cross-validation selects a small bandwidth, resulting in highly noisy estimates. At $n = 10,000$, the selected bandwidth is much larger, causing the kernel estimator to resemble the biased linear estimator and still fail to capture the nonlinearity introduced by e^{2Z+2} . In contrast, the AIPW-Lasso estimator performs remarkably well, even at $n = 1,000$, likely because the exponential term is well approximated by the B-spline expansion of Z_i . The DML method with the NN learner exhibits high variance at smaller n , but its accuracy becomes comparable to that of AIPW-Lasso as n increases.

Figure 20 summarizes the WMSE and execution time of each estimator based on 200

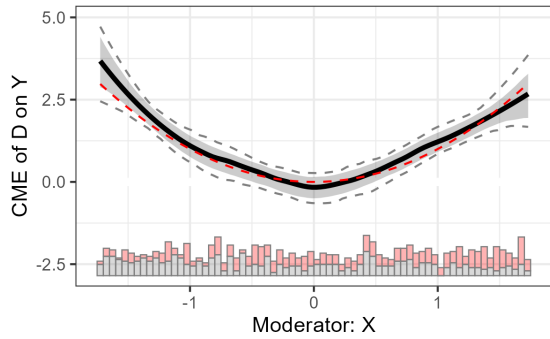
Figure 19: Comparison of Estimators with DGP2



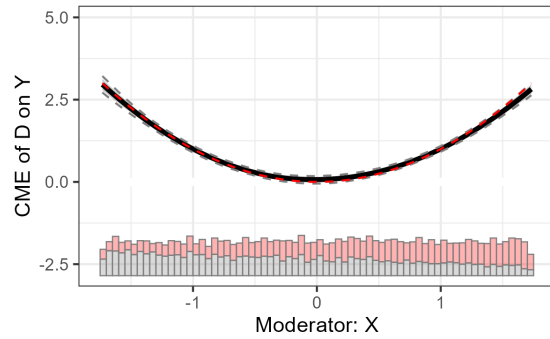
(a) Kernel ($n = 1,000$)



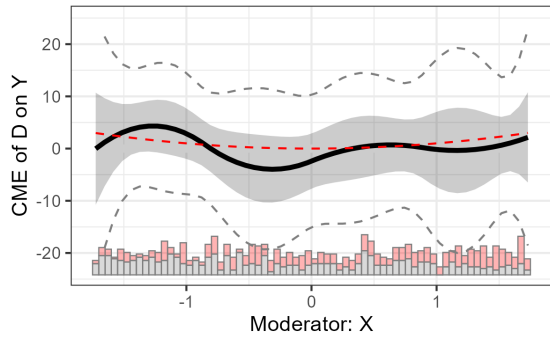
(b) Kernel ($n = 10,000$)



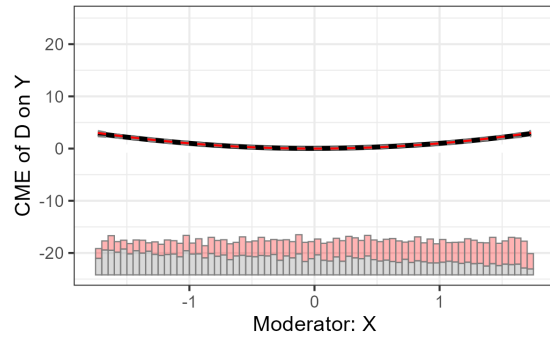
(c) AIPW-Lasso ($n = 1,000$)



(d) AIPW-Lasso ($n = 10,000$)



(e) DML-NN ($n = 1,000$)



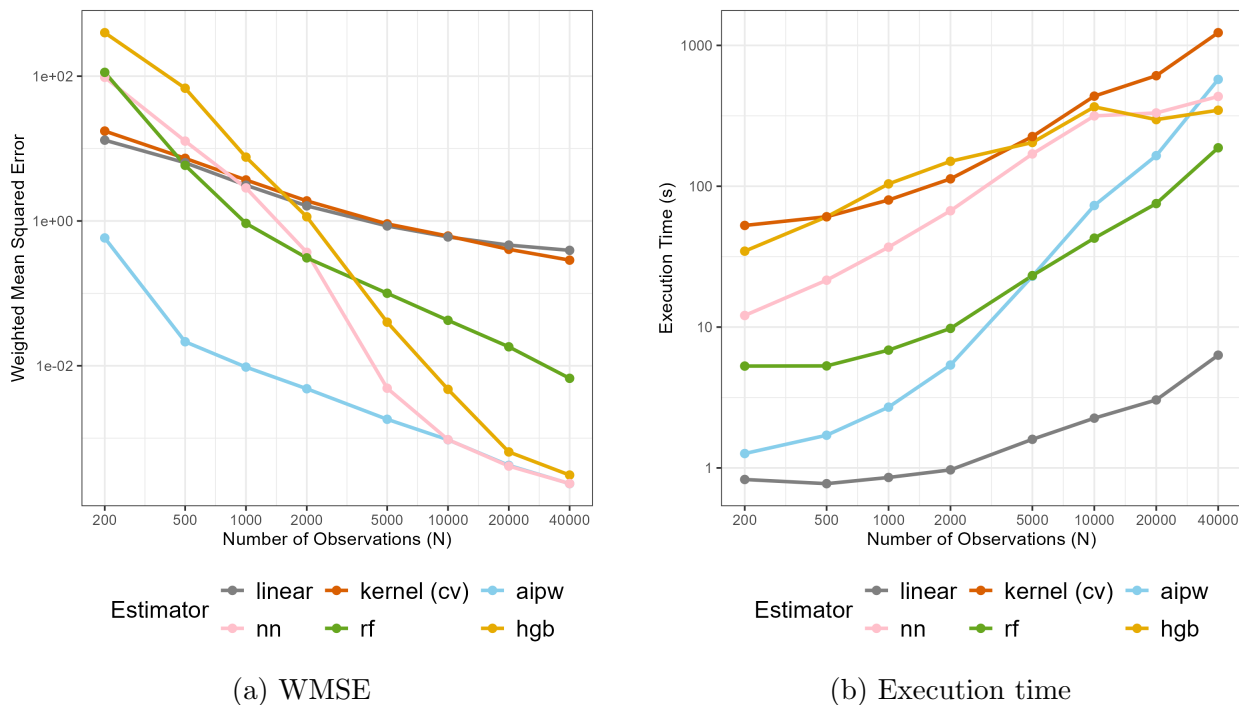
(f) DML-NN ($n = 10,000$)

Note: In each figure: the red dashed line represents the true CME; the black solid line represents the estimated CME; the shaded area represents the pointwise confidence intervals, while the dashed gray lines represent the uniform confidence intervals. At the bottom of each figure, we display histograms showing the distribution of treated units (in red) and control units (in gray) along the moderator X .

simulation runs. We evaluate the linear estimator, the kernel estimator with cross-validation, the AIPW-Lasso estimator with basis expansion and post-selection Lasso, and DML methods using NN, RF, or HGB. Under this DGP, both the linear and kernel estimators exhibit

substantial bias, even at large n . By contrast, DML estimators improve significantly after approximately 3,000 observations, with nn and hgb achieving particularly low WMSE, albeit with higher computational cost than rf. Notably, the AIPW-Lasso estimator consistently attains low WMSE (as seen in Figure 19) with moderate computational overhead when the sample size is not large, although its runtime increases rapidly as n grows.

Figure 20: Performance of Different Methods: DGP2



Notes: The above figures shows how weighted mean squared error (left) and execution time (right) changes as the sample size increases. Both axes in each figure is in log scale.

In short, compared with the first study, the introduction of nonlinearity in $g(V_i)$ through e^{2Z+2} renders the kernel estimator ineffective at capturing this structure, resulting in biased CME estimates. In contrast, AIPW-Lasso and DML methods can flexibly accommodate nonlinearities in additional covariates. Therefore, when nonlinearities extend beyond the moderator, kernel methods become less suitable, and AIPW-Lasso or DML are more likely to provide greater accuracy and, in some cases, more efficient computation. AIPW-Lasso offers advantages over DML estimators in both execution time for large samples and accuracy when the sample size is small.

5.3 Simulation Study 3: Fine-tuning DML

For many machine learning methods, model tuning is crucial to ensure strong performance. In this third simulation study, we compare how different ML learners—NN, RF, and HGB—perform under default hyperparameters versus hyperparameters fine-tuned via cross-validation, using a more complex DGP. Although default settings are convenient and sometimes adequate, they often fail to capture the underlying complexity of the data, resulting in underfitting or overfitting depending on the context. In DML, where both the outcome and propensity score models must be estimated, it is especially unlikely that a single set of hyperparameters will perform well for both. Cross-validation allows for more targeted tuning by optimizing out-of-sample predictive performance separately for each model component. By comparing default and cross-validated configurations side by side, we highlight the trade-off between computational cost—since cross-validation can be time-intensive—and the potential for improved accuracy through more careful tuning.

In this setting, we consider a nonlinear outcome model and a nonlinear propensity score model, each depending on a single moderator X and four additional covariates Z_{1i} , Z_{2i} , Z_{3i} , and Z_{4i} . Specifically, the outcome variable Y_i is then given by

$$Y_i = \theta(X_i) D_i + g(V_i) + \epsilon_i,$$

in which $D_i \sim \text{Bernoulli}(\pi(V_i))$ and $\epsilon_i \sim \mathcal{N}(0, 1)$ and

$$\begin{aligned} g(V_i) = & 1 + X_i + \exp(2X_i + 2) + 3 \sin(X_i + Z_{i1}) + 2X_i Z_{i2} \\ & + Z_{i3} \mathbf{1}\{Z_{i3} > 0\} - 4 \frac{\sin(Z_{i4})}{Z_{i4}} + 2 Z_{i3}^2 Z_{i4}. \end{aligned}$$

The propensity score model is given by:

$$\pi(V_i) = \text{logit}^{-1}\{0.25 + X_i - X_i^2 - Z_{1i}^2 + 2X_i Z_{1i} Z_{2i} - \text{logit}^{-1}(Z_{1i} + Z_{3i}) + 2Z_{2i}^2 \cos(Z_{4i})\}$$

This highly nonlinear specification poses a challenge for all estimation methods and underscores the importance of hyperparameter tuning in flexible learners.

Tuning NN. Our NN model begins with the default parameter settings in `scikit-learn`'s `MLPRegressor` and `MLPClassifier`, which include a single hidden layer of 100 neurons, ReLU activation, the Adam optimizer, an L2 regularization term (`alpha`) of 0.0001, and a maximum of 1,000 training iterations. To allow for greater flexibility, we focus our hyperparameter search on four key components: layer architecture, activation function, solver, and regularization strength. Specifically, we vary the hidden layer configurations among (50,), (100,), and (50, 50), allowing for both simpler single-layer networks and deeper architectures capable of capturing more complex relationships. We compare the `tanh` and `relu` activation functions to account for different gradient behaviors and consider both stochastic gradient descent (`sgd`) and Adam (`adam`) as solvers, given their distinct convergence properties. Finally, we tune the L2 penalty term `alpha` over $\{10^{-4}, 10^{-3}, 10^{-2}\}$, balancing the trade-off between bias and variance. Although a broader grid could yield further refinements, we limit the search space to ensure adequate coverage of key parameters while controlling the computational burden of cross-validation in repeated simulation runs.

The code snippet below demonstrates how to implement this hyperparameter tuning using the `interflex` package:

```
1 param_grid_nn <- list(  
2   hidden_layer_sizes = list(  
3     list(50L),  
4     list(100L),  
5     list(50L, 50L)  
6   ),  
7   activation = c("tanh", "relu"),  
8   solver = c("sgd", "adam"),  
9   alpha = c(1e-4, 1e-3, 1e-2)  
10 )  
11  
12 sol.nn.cv <- interflex(data = sim_data, Y="Y", D="D", X="X", Z=Z.list,  
   estimator="DML", CV = TRUE, model.t="nn", model.y="nn", param.grid.y =
```

```
param_grid_nn, param.grid.t = param_grid_nn)
```

Tuning RF. Our random forest model starts from the default parameter settings in `scikit-learn`'s `RandomForestRegressor` and `RandomForestClassifier`, which include 100 estimators (`n_estimators = 100`) and an unrestricted tree depth. In our grid search, we broaden the search space by allowing `n_estimators` to be 100 or 300, striking a balance between computational overhead and variance reduction through ensemble averaging. We also vary `max_depth` among `{NULL, 5, 10}` so that the model can adapt its complexity based on data size and noise levels. To control the formation of splits, we choose `min_samples_split` in `{2, 10}` and `min_samples_leaf` in `{1, 5}`, thereby mitigating the risk of overfitting by requiring more observations in node splits and leaves. Furthermore, we compare `max_features` set to 1.0 (all features considered) versus 0.8 (a subsample of features at each split) to foster diversity among the trees. Finally, we explore both `bootstrap = TRUE` (standard bootstrap sampling) and `FALSE` (sampling without replacement) to gauge their effect on variance reduction.

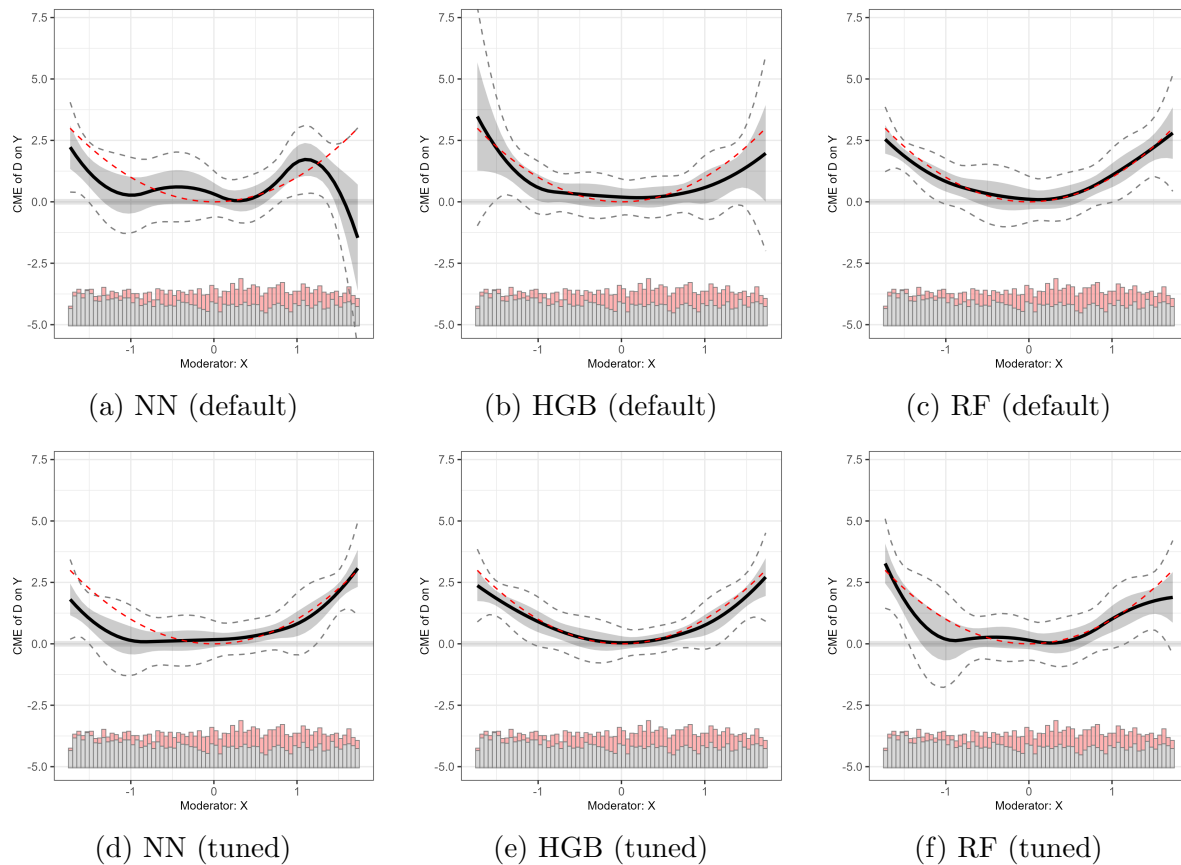
Tuning HGB. Our HGB model starts from the default parameter settings in `scikit-learn`'s `HistGradientBoostingRegressor` and `HistGradientBoostingClassifier`, which use a learning rate of 0.1 and a maximum of 100 boosting iterations. We tune several other key hyperparameters to enhance flexibility while avoiding overfitting. Specifically, we let `learning_rate` range over `{0.01, 0.1}`, spanning conservative to more aggressive updates, and allow up to either 100 or 200 boosting iterations (`max_iter`). We examine two distinct values for `max_leaf_nodes` (31 and 127) to regulate tree complexity, and vary `max_depth` among `{NULL, 3, 5}` to impose a bound on tree depth only when potentially beneficial. In addition, `min_samples_leaf` takes values `{5, 20}` to guard against overfitting by avoiding extremely small leaves, while `l2_regularization` in `{0.0, 1.0}` manages the trade-off between bias and variance. Finally, we tune `max_features` in `{1.0, 0.8}`, controlling the fraction of features available at each split.

In Figure 21, we compare the estimated CME to the true CME under two different hyperparameter settings (default vs. fine-tuned). The first row displays estimates obtained using each learner’s default hyperparameters, while the second row shows estimates based on cross-validated hyperparameters, all derived from a single simulation of the data with $N = 5000$.

Notably, the NN learner illustrates the importance of fine-tuning hyperparameters to the specific data-generating process. For the outcome model, the selected hyperparameters are `activation = tanh`, `alpha = 1e-4`, `hidden_layer_sizes = (50,50)`, and `solver = adam`; in contrast, the propensity score model performs best with `activation = tanh`, `alpha = 0.01`, `hidden_layer_sizes = (50,50)`, and `solver = sgd`. The divergence in optimal specifications across these two models underscores the importance of using cross-validation, as the complexities of the outcome and propensity score functions may differ and therefore require different levels of model flexibility. Moreover, comparing subfigure (a) (default hyperparameters) to subfigure (d) (cross-validated hyperparameters) shows that DML with NN learners consistently produces more accurate CME estimates when hyperparameters are properly tuned, rather than relying on default settings.

In contrast to the results from NN, the HGB learner shows only modest improvement when moving from default hyperparameters to those selected via cross-validation. For the outcome model, the chosen hyperparameters are `l2_regularization = 1`, `learning_rate = 0.1`, `max_depth = 5`, `max_features = 1`, `max_iter = 200`, `max_leaf_nodes = 31`, and `min_samples_leaf = 20`. The propensity score model retains the same values for the penalty term, learning rate, and minimum samples per leaf but uses `max_leaf_nodes = 127` and `max_iter = 100`. Although these configurations differ meaningfully—particularly in tree size—between the outcome and propensity models, the resulting CME estimates show only a slight numerical gain relative to the default settings, as illustrated in Figure 21 (b) and (e). This suggests that the default HGB parameters already perform reasonably well in captur-

Figure 21: Estimated CME based on a single simulation following the Third DGP



Note: In each subfigure, the black solid line represents the estimated CME, while the red dashed line denotes the true CME. The shaded gray areas illustrate the point-wise confidence intervals, and the gray dashed lines depict the uniform confidence intervals. At the bottom of each subplot, a histogram displays the distribution of treated and control units across varying values of the moderator X .

ing the underlying signal, with cross-validation offering incremental rather than substantial improvements.

Using a similar procedure for the random forest learner, cross-validation selects `bootstrap = TRUE`, `max_depth = 10`, `max_features = 0.8`, `min_samples_leaf = 1`, `min_samples_split = 2`, and `n_estimators = 300` for the outcome model, while the propensity score model adopts the same values except for `min_samples_leaf = 5`. These settings indicate slightly deeper trees, a broader feature subset, and an increased number of trees compared to the defaults, potentially improving variance reduction. However, comparing Figure 21,(c) and (f), we find that these adjustments do not lead to notice-

able improvement in the estimated CME, and the overall fit remains inferior to both the NN and HGB learners. This outcome may indicate that the random forest is not particularly well-suited for capturing the nonlinear structures present in this DGP, or it may suggest that further specialized tuning—or larger sample sizes—are required to achieve performance comparable to the other methods.

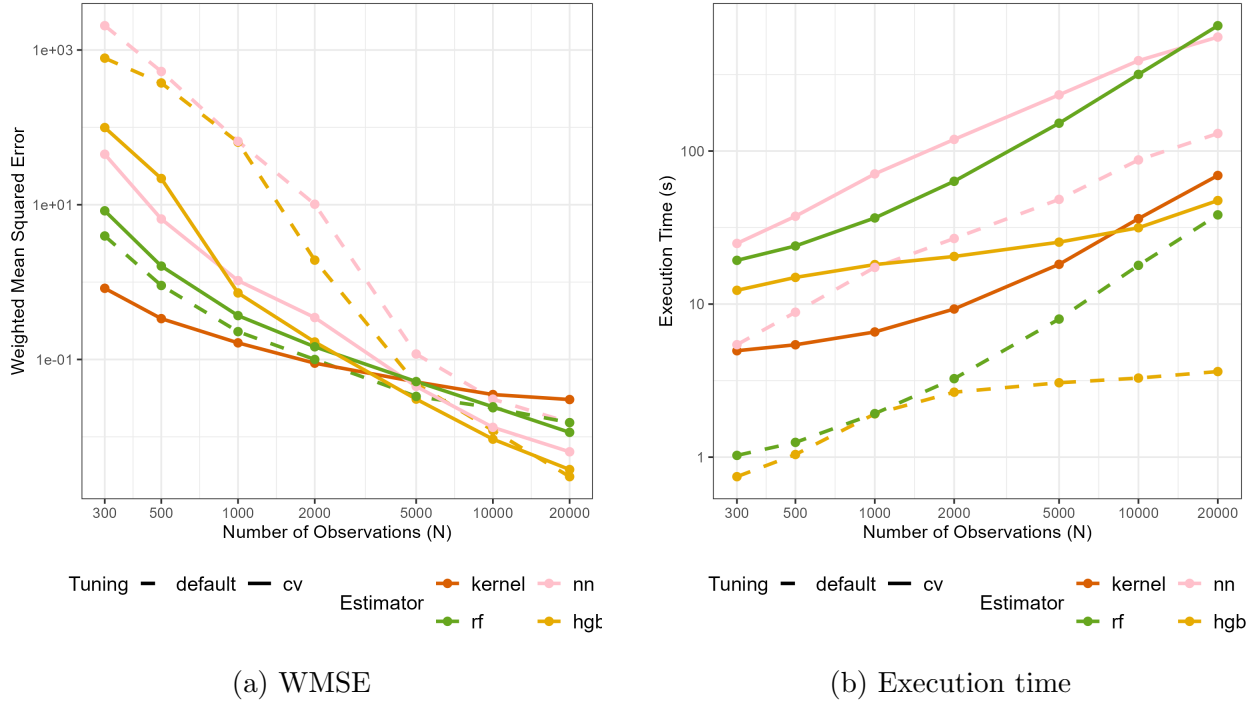
In Figure 22, we compare the WMSE and execution time of the kernel estimator and DML methods with different ML learners. These comparisons include both default parameters and parameters selected via cross-validation, based on 100 simulations of the previously described DGP.

First, we observe that all DML methods outperform the kernel estimator when the sample size n is sufficiently large. Second, focusing on NN and HGB, we find that cross-validating hyperparameters consistently yields lower WMSE, especially when the number of observations is not very large. This likely reflects the fact that fine-tuned parameters help mitigate overfitting when the sample size is moderate. By contrast, RF doesn't show noticeable improvements from cross-validation, suggesting that while hyperparameter tuning optimizes out-of-sample predictive performance, this does not always translate into immediate gains in CME estimation. Finally, we note that applying cross-validation substantially increases execution time, highlighting a trade-off between computational cost and improved model fit.

5.4 Summary

Several patterns have emerged across the three simulation studies. First, kernel-based methods, AIPW-Lasso, and DML approaches can all successfully capture nonlinearities in the CME itself, provided the sample size is sufficiently large. When the DGP is relatively simple—particularly when only the moderator enters the outcome model nonlinearly—the kernel estimator (with cross-validated bandwidth) and AIPW-Lasso (with basis expansion) perform effectively, with AIPW-Lasso also offering modest computational cost. In contrast, when additional covariates enter the outcome model nonlinearly, kernel-based methods tend

Figure 22: Performance of Different Methods: DGP3



Notes: The above figures shows how weighted mean squared error (left) and execution time (right) changes as the sample size increases. Both axes in each figure is in log scale.

to break down, whereas the flexibility of AIPW-Lasso and DML allows them to capture more complex dependencies. However, the effectiveness of DML remains strongly dependent on having enough observations to mitigate underfitting and fully exploit the capacity of advanced machine learning models.

Another key insight is that hyperparameter tuning matters, especially in high-complexity settings. While default parameters may sometimes suffice, targeted cross-validation often leads to more accurate CME estimates, as most clearly demonstrated by the NN learner in the third simulation study. Nonetheless, tuning can be time-consuming and does not always produce substantial improvements—for example, HG shows only marginal gains, and RF may even perform slightly worse after tuning. In practice, researchers must weigh the potential accuracy gains against the computational burden and consider how well each method’s assumptions align with their data.

Chapter 6. Conclusion

Understanding conditional treatment effects—how the effect of a treatment D on an outcome Y varies with a moderating variable X —is essential in social science research. Despite significant advances, current methods face notable challenges, including unclear estimands, misinterpretation of statistical results, lack of sufficient overlap in empirical data, rigid assumptions on functional forms, and difficulty with complex settings like discrete outcomes. This Element introduces a robust methodological framework that overcomes these limitations and ensures valid statistical inference for the key estimand, the conditional marginal effects (CME).

The linear interaction model is still the widely used in empirical research. Despite its popularity, this model often suffers from inadequate common support, misspecifications, and multiple testing issues. To mitigate these issues, we advocate for diagnostic tools such as inspecting raw data and the binning estimator. Moreover, the framework proposes methods like uniform confidence intervals via bootstrapping to address multiple comparisons and improve inferential validity. The semiparametric kernel estimator proposed by [Hainmueller, Mummolo and Xu \(2019\)](#) relaxes functional form assumptions. We further improve it robustness by incorporating adaptive kernels and fully moderated specifications.

This Element then advances beyond classical approaches by introducing augmented inverse propensity score weighting (AIPW). The AIPW estimator for the CME combines outcome modeling and propensity score weighting, providing double robustness—maintaining consistency if either the propensity score or outcome model is correctly specified. It takes three steps: (i) estimating the outcome and propensity score model, (ii) constructing the signals for treatment effects; (iii) smoothing over the moderator X . Compared with inverse propensity score weighting (IPW) alone, AIPW improves estimation stability and reduces variance. To accommodate high-dimensional covariates and relax functional form assumptions, we further introduce basis expansions and Lasso regularization techniques, which sig-

nificantly stabilize estimation and improve precision. Finally, we extend AIPW to continuous treatments through partialing-out Lasso (PO-Lasso).

Double Machine Learning (DML) is subsequently presented as a powerful extension suitable for high-dimensional and complex nuisance parameters. DML achieves robust estimation through Neyman orthogonality, which ensures that small estimation errors in nuisance functions do not bias CME estimates to first order. This framework extends the double robustness of AIPW-Lasso and PO-Lasso by leveraging flexible machine learning methods, such as neural networks, random forests, and gradient boosting, to model complex relationships between covariates and the outcome and treatment. The combination of orthogonalization, which insulates estimators from regularization bias, and cross-fitting, which prevents overfitting by splitting the data, ensures valid inference at a root- n convergence rate. We also show that DML can accommodate empirical applications with discrete outcomes. We illustrate DML for binary and continuous treatments with empirical examples from political science, including orthogonal signal construction, residualization strategies, and application of the `interflex` package.

Moreover, we provide Monte Carlo evidence comparing kernel-based methods, AIPW-Lasso, and DML estimators. Simulation studies indicate that while kernel estimators effectively handle simple nonlinearities, they falter with complex covariate dependencies. In contrast, AIPW-Lasso and DML successfully model intricate nonlinearities, particularly in higher-dimensional settings, though their performance crucially depends on sample size and effective hyperparameter tuning. Tuning, while computationally costly, often significantly improves accuracy of the DML estimators, especially with complex learners like neural networks. However, simpler learners such as random forests show only marginal gains or even slight declines after tuning.

Finally, we offer the following practical recommendations for empirical researchers interested in estimating and interpreting conditional relationships:

- Clearly define the quantity of interest, e.g., the CME, and state key assumptions—such

as unconfoundedness, overlap, and functional form—before proceeding with the analysis.

- Assess data quality by checking for missing values and outliers, and evaluate the overlap assumption. If overlap is violated, consider trimming the data to improve balance.
- If the linear interaction model must be used for estimating the CME—for transparency, ease of computation and interpretation, or other reasons—supplement it with diagnostic tests for the rigid functional form, such as the binning estimator.
- Use flexible modeling strategies to estimate the CME.
 - For experimental data, the kernel estimator is typically sufficient. Efficiency may be improved by incorporating basis expansions and post-Lasso selection.
 - For observational data with small to medium samples, we recommend Lasso-based methods: AIPW-Lasso for binary treatments and PO-Lasso for continuous treatments.
 - For observational data with large samples, DML estimators are more appropriate. When using complex machine learners such as neural networks, random forest, and histogram gradient boosting, apply cross-validation to tune hyperparameters and reduce overfitting.
- Visualize estimated CME to facilitate intuitive understanding of effect heterogeneity.
- Interpret results with care. Specifically, (i) avoid overusing causal language—CME captures the effect of D along levels of the moderator X , but it does not represent the causal effect of X itself. (ii) When making inferences about the sign or magnitude of the CME over an interval, use uniform confidence intervals to ensure proper coverage.

All the estimation strategies and diagnostic tools discussed in this Element can be implemented using the `interflex` package in R.

A. Appendix

A.1 Chapter 1 Proofs

Here, we prove that the stratified difference-in-means (SDIM) estimator and IPW estimator of CME are numerically equivalent when all covariates V_i are discrete: $\hat{\theta}(x)_{SDIM} = \hat{\theta}(x)_{IPW}$.

Proof:

For $\hat{\theta}(x)_{SDIM}$, within stratum $X_i = x$, let n_{1v} be the number of treated unit ($D_i = 1$) in stratum $V_i = v$, n_{0v} be the number of treated unit ($D_i = 0$) in stratum $V_i = v$. The with-in stratum treated mean and control mean is:

$$\hat{\mu}^1(v) = \frac{1}{n_{1v}} \sum_{i: D_i=1, V_i=v} Y_i, \quad \hat{\mu}^0(v) = \frac{1}{n_{0v}} \sum_{i: D_i=0, V_i=v} Y_i.$$

The SDIM estimator of $\theta(x)$:

$$\hat{\theta}(x)_{SDIM} = \sum_v \left(\hat{\mu}^1(v) - \hat{\mu}^0(v) \right) \cdot \frac{n_v}{N_x},$$

where $N_x = \sum_v n_v$ is total number of units with $X_i = x$.

The IPW estimator of $\theta(x)$ writes:

$$\hat{\theta}(x)_{IPW} = \frac{1}{N_x} \sum_{i: X_i=x} \left[\frac{D_i Y_i}{\hat{\pi}(V_i)} - \frac{(1 - D_i) Y_i}{1 - \hat{\pi}(V_i)} \right]$$

where $\hat{\pi}$ estimate $\pi(v) = \Pr(D_i=1 \mid V_i = v)$. When all covariates V_i are discrete, a natural estimate $\hat{\pi} = n_{1v}/n_v$. Hence each treated unit i in stratum v gets weight $1/\hat{\pi} = n_v/n_{1v}$, the control unit gets weight $1/[1 - \hat{\pi}(v)] = n_v/n_{0v}$.

Write the IPW sum by grouping observations in the same stratum:

$$\hat{\theta}(x)_{IPW} = \frac{1}{N_x} \sum_v \left[\sum_{i \in \{D_i=1, V_i=v\}} \frac{D_i Y_i}{\hat{\pi}(v)} - \sum_{i \in \{D_i=0, V_i=v\}} \frac{(1 - D_i) Y_i}{1 - \hat{\pi}(v)} \right].$$

For units in stratum v with $D_i = 1$, we have $\frac{D_i}{\hat{\pi}(v)} = \frac{1}{n_{1v}/n_v} = \frac{n_v}{n_{1v}}$, thus:

$$\sum_{i \in \{D_i=1, V_i=v\}} \frac{D_i Y_i}{\hat{\pi}(v)} = \frac{n_v}{n_{1v}} \sum_{i \in \{D_i=1, V_i=v\}} Y_i = n_v \hat{\mu}^1(v).$$

Similarly, for units in the control group within stratum v :

$$\frac{1 - D_i}{1 - \hat{\pi}(v)} = \frac{1}{n_{0v}/n_v} = \frac{n_v}{n_{0v}} \sum_{i \in \{D_i=0, V_i=v\}} \frac{(1 - D_i) Y_i}{1 - \hat{\pi}(v)} = n_v \hat{\mu}^0(v)$$

Summing over $V_i = v$ and dividing by N_x gives:

$$\hat{\theta}(x)_{IPW} = \frac{1}{N_x} \sum v n_v \left[\hat{\mu}^1(v) - \hat{\mu}^0(v) \right] = \sum_v \left[\hat{\mu}^1(v) - \hat{\mu}^0(v) \right] \cdot \frac{n_v}{N_x},$$

which is numerically equivalent to the $\hat{\theta}(x)_{SDIM}$.

A.2 Chapter 3 Proofs

Identification based on IPW

Remark 1 Consider a binary treatment $D_i \in \{0, 1\}$ and covariates $V_i = (X_i, Z_i)$. Under unconfoundedness ($Y_i(d) \perp D_i \mid V_i$ for $d \in \{0, 1\}$) and overlap ($0 < \pi(V_i) < 1$), we aim to show:

$$\mathbb{E}\left[\frac{D_i}{\pi(V_i)} Y_i \mid V_i = v\right] = \mathbb{E}[Y_i(1) \mid V_i = v], \quad \mathbb{E}\left[\frac{1-D_i}{1-\pi(V_i)} Y_i \mid V_i = v\right] = \mathbb{E}[Y_i(0) \mid V_i = v].$$

Proof:

1. For treated units ($D_i = 1$):

$$\mathbb{E}\left[\frac{D_i}{\pi(V_i)} Y_i \mid V_i = v\right] = \frac{1}{\pi(v)} \mathbb{E}[D_i Y_i \mid V_i = v].$$

Using the law of total expectation:

$$\begin{aligned} \mathbb{E}[D_i Y_i \mid V_i = v] &= \mathbb{E}[D_i Y_i \mid V_i = v, D_i = 1] P(D_i = 1 \mid V_i = v) \\ &\quad + \mathbb{E}[D_i Y_i \mid V_i = v, D_i = 0] P(D_i = 0 \mid V_i = v). \end{aligned}$$

Since D_i is binary,

$$\mathbb{E}[D_i Y_i \mid V_i = v, D_i = 0] = 0.$$

On the other hand, for $D_i = 1$,

$$\mathbb{E}[D_i Y_i \mid V_i = v, D_i = 1] = \mathbb{E}[Y_i(1) \mid V_i = v, D_i = 1] = \mathbb{E}[Y_i(1) \mid V_i = v],$$

where the second equality relies on unconfoundedness. Therefore,

$$\mathbb{E}[D_i Y_i \mid V_i = v] = \mathbb{E}[Y_i(1) \mid V_i = v] \times \pi(v).$$

Substituting back:

$$\mathbb{E}\left[\frac{D_i}{\pi(V_i)} Y_i \mid V_i = v\right] = \frac{1}{\pi(v)} \times \left[\mathbb{E}[Y_i(1) \mid V_i = v] \pi(v)\right] = \mathbb{E}[Y_i(1) \mid V_i = v].$$

2. For control units ($D_i = 0$).

$$\mathbb{E}\left[\frac{1-D_i}{1-\pi(V_i)} Y_i \mid V_i = v\right] = \frac{1}{1-\pi(v)} \mathbb{E}[(1-D_i) Y_i \mid V_i = v].$$

Expanding:

$$\begin{aligned} \mathbb{E}[(1-D_i)Y_i \mid V_i = v] &= \mathbb{E}[(1-D_i)Y_i \mid V_i = v, D_i = 1] P(D_i = 1 \mid V_i = v) \\ &\quad + \mathbb{E}[(1-D_i)Y_i \mid V_i = v, D_i = 0] P(D_i = 0 \mid V_i = v). \end{aligned}$$

When $D_i = 1$, $(1-D_i)Y_i = 0$. When $D_i = 0$,

$$\mathbb{E}[(1-D_i)Y_i \mid V_i = v, D_i = 0] = \mathbb{E}[Y_i(0) \mid V_i = v, D_i = 0] = \mathbb{E}[Y_i(0) \mid V_i = v].$$

Hence,

$$\mathbb{E}[(1-D_i)Y_i \mid V_i = v] = \mathbb{E}[Y_i(0) \mid V_i = v] [1 - \pi(v)].$$

Substituting:

$$\begin{aligned} \mathbb{E}\left[\frac{1-D_i}{1-\pi(V_i)} Y_i \mid V_i = v\right] &= \frac{1}{1-\pi(v)} \times \left[\mathbb{E}[Y_i(0) \mid V_i = v] (1 - \pi(v))\right] \\ &= \mathbb{E}[Y_i(0) \mid V_i = v]. \end{aligned}$$

Identification based on AIPW

Remark 2 Let us define the augmented inverse-propensity weighting (AIPW) quantity:

$$\Lambda(V_i) := \mu_1(V_i) + \frac{D_i}{\pi(V_i)}(Y_i - \mu_1(V_i)) - \mu_0(V_i) - \frac{1 - D_i}{1 - \pi(V_i)}(Y_i - \mu_0(V_i)),$$

The goal is to show that when either $\pi(V_i)$ or $\mu_{(d)}(V_i)$ is correctly specified, that is, if one of

$$\pi(V_i) = \Pr(D_i = 1 \mid V_i) \quad \text{and} \quad \mu_{(d)}(V_i) = \mathbb{E}[Y_i \mid D_i = (d), V_i].$$

holds, then

$$\mathbb{E}[\Lambda(V_i) \mid V_i = v] = \mathbb{E}[Y_i(1) - Y_i(0) \mid V_i = v],$$

This property is known as the double robustness of AIPW.

Proof

Case 1: The Outcome Model is Correct

Suppose the outcome model is correctly specified, i.e.,

$$\mu_{(d)}(V_i) = \mathbb{E}[Y_i \mid D_i = (d), V_i].$$

In this scenario, the *residuals* $Y_i - \mu_{(d)}(V_i)$ satisfy:

$$\mathbb{E}[Y_i - \mu_{(d)}(V_i) \mid V_i = v, D_i = (d)] = 0,$$

since $\mu_{(d)}(v)$ is the conditional mean of Y_i for each D .

We compute the conditional expectation of $\Lambda(V_i)$ given $V_i = v$:

$$\begin{aligned} \mathbb{E}[\Lambda(V_i) \mid V_i = v] &= \mathbb{E} \left[\mu_1(v) + \frac{D_i}{\pi(v)}(Y_i - \mu_1(v)) \right. \\ &\quad \left. - \mu_0(v) - \frac{1 - D_i}{1 - \pi(v)}(Y_i - \mu_0(v)) \mid V_i = v \right] \\ &= \underbrace{\mu_1(v) - \mu_0(v)}_{\text{deterministic terms}} \\ &\quad + \frac{1}{\pi(v)} \mathbb{E} \left[D_i(Y_i - \mu_1(v)) \mid V_i = v \right] \\ &\quad - \frac{1}{1 - \pi(v)} \mathbb{E} \left[(1 - D_i)(Y_i - \mu_0(v)) \mid V_i = v \right]. \end{aligned}$$

Since $\mu_{(d)}(v)$ is the true conditional mean, we have

$$\mathbb{E}[D_i(Y_i - \mu_1(v)) \mid V_i = v] = \pi(v) \mathbb{E}[Y_i - \mu_1(v) \mid V_i = v, D_i = 1] = \pi(v) \times 0 = 0,$$

and similarly,

$$\mathbb{E}[(1 - D_i)(Y_i - \mu_0(v)) \mid V_i = v] = (1 - \pi(v)) \times 0 = 0.$$

Hence,

$$\mathbb{E}[\Lambda(V_i) \mid V_i = v] = \mu_1(v) - \mu_0(v).$$

By definition of the potential outcomes, $\mu_1(v) = \mathbb{E}[Y_i(1) \mid V_i = v]$ and $\mu_0(v) = \mathbb{E}[Y_i(0) \mid V_i = v]$. Therefore,

$$\mathbb{E}[\Lambda(V_i) \mid V_i = v] = \mathbb{E}[Y_i(1) \mid V_i = v] - \mathbb{E}[Y_i(0) \mid V_i = v].$$

Case 2: The Propensity Score Model is Correct

Now assume the propensity score $\pi(V_i)$ is correctly specified, i.e.,

$$\pi(V_i) = \Pr(D_i = 1 \mid V_i).$$

We will show that the terms involving $\mu_1(V_i)$ and $\mu_0(V_i)$ cancel in expectation, leaving only the inverse-propensity weighted average of Y_i .

(a) Combining $\mu_1(V_i)$ Terms. Rewrite

$$\mu_1(v) - \frac{D_i}{\pi(v)} \mu_1(v) = \mu_1(v) \left(1 - \frac{D_i}{\pi(v)}\right).$$

Taking the conditional expectation:

$$\begin{aligned} \mathbb{E}\left[\mu_1(v) \left(1 - \frac{D_i}{\pi(v)}\right) \mid V_i = v\right] &= \mu_1(v) \left(1 - \frac{\mathbb{E}[D_i \mid V_i = v]}{\pi(v)}\right) \\ &= \mu_1(v) \left(1 - \frac{\pi(v)}{\pi(v)}\right) = 0. \end{aligned}$$

(b) Combining $\mu_0(V_i)$ Terms. Similarly,

$$-\mu_0(v) + \frac{1 - D_i}{1 - \pi(v)} \mu_0(v) = -\mu_0(v) \left(1 - \frac{1 - D_i}{1 - \pi(v)}\right).$$

Taking the conditional expectation:

$$\begin{aligned}\mathbb{E}\left[-\mu_0(v)\left(1 - \frac{1-D_i}{1-\pi(v)}\right) \mid V_i = v\right] &= -\mu_0(v)\left(1 - \frac{\mathbb{E}[1 - D_i \mid V_i = v]}{1 - \pi(v)}\right) \\ &= -\mu_0(v)\left(1 - \frac{1-\pi(v)}{1-\pi(v)}\right) = 0.\end{aligned}$$

(c) Remaining Inverse-Propensity Weighted Terms. All that remains is

$$\frac{D_i}{\pi(v)} Y_i - \frac{1 - D_i}{1 - \pi(v)} Y_i.$$

With a correctly specified propensity score, it follows from the IPW identity that

$$\mathbb{E}\left[\frac{D_i}{\pi(v)} Y_i - \frac{1-D_i}{1-\pi(v)} Y_i \mid V_i = v\right] = \mathbb{E}[Y_i(1) - Y_i(0) \mid V_i = v]$$

Hence, combining both cases shows that if *at least one* of the models (outcome or propensity score) is correct, then

$$\mathbb{E}[\Lambda(V_i) \mid V_i = v] = \mathbb{E}[Y_i(1) - Y_i(0) \mid V_i = v].$$

Thus, the AIPW estimator achieves consistency as long as at least one of the models—the outcome model or the propensity score model—is correctly specified. This dual safeguard significantly enhances the estimator’s robustness in practical applications where model misspecification is a concern.

A.3 Chapter 4 Proofs

Signals and CME To prove: $\mathbb{E}[\Lambda(\eta) \mid V = v] = \mathbb{E}[\partial_d Y(d) \mid V = v]$.

Proof

By tower rule, $\mathbb{E}[\Lambda(\eta) \mid X = x] = \mathbb{E}\left[\mathbb{E}[\Lambda(\eta) \mid V] \mid X = x\right]$, so it is suffice to show that $\mathbb{E}[\Lambda(\eta) \mid V = v] = \mathbb{E}[\partial_d Y(d) \mid V = v]$. We want to show:

$$\mathbb{E}[\Lambda(\eta) \mid V = v] = \partial_d \mu(d, v) = \mathbb{E}[\partial_d Y(d) \mid V = v].$$

Expanding on the Neyman orthogonal score:

$$\mathbb{E}[\Lambda(\eta) \mid V = v] = \mathbb{E}[\partial_d \mu(d, v) \mid V = v] - \mathbb{E}[\partial_d \log e(d, v) [Y - \mu(d, v)] \mid V = v]$$

Because $\partial_d \mu(d, v)$ do not depend on the randomness in Y :

$$\mathbb{E}[\Lambda(\eta) \mid V = v] = \partial_d \mu(d, v) - \mathbb{E}[\partial_d \log e(d, v) [Y - \mu(d, v)] \mid V = v]$$

Now we show the second part is zero in expectation. First, we recognize that taking expectation w.r.t. the distribution of (D, Y) given $V = v$ means integrating over $f_{D,Y|V}(d, y \mid v)$. Given unconfoundedness, we can write $f_{D,Y|V}(d, y \mid v) = f_{Y|D,V}(y \mid d, v) \times f_{D|V}(d \mid v)$, thus

$$\begin{aligned} \mathbb{E}[-\partial_d \log e(d, v) (Y - \mu(d, v)) \mid V = v] &= \\ \int_d \int_y \left(-\partial_d \log e(d, v) [y - \mu(d, v)] \right) f_{Y|D,V}(y \mid d, v) f_{D|V}(d \mid v) dy dd. \end{aligned}$$

Because $\int y f_{Y|D,V}(y \mid d, v) dy = \mu(d, v)$, it follows that $\int [y - \mu(d, v)] f_{Y|D,V}(y \mid d, v) dy = 0$.

Hence:

$$\mathbb{E}[-\partial_d \log e(d, v) (Y - \mu(d, v)) \mid V = v] = 0.$$

Therefore,

$$\mathbb{E}[\Lambda(\eta) \mid V = v] = \partial_d \mu(d, v) = \mathbb{E}[\partial_d Y(d) \mid V = v].$$

Score Definition To verify the Neyman orthogonality for the AIPW score, we show that the Gateaux derivative of the expected score with respect to the nuisance functions is zero at the true nuisance parameters.

For each unit i , define the AIPW score:

$$\Lambda_i(\eta) = \underbrace{\mu_1(V_i)}_{\text{depends on } \mu_1} - \underbrace{\mu_0(V_i)}_{\text{depends on } \mu_0} + \underbrace{\frac{D_i}{\pi(V_i)} [Y_i - \mu_1(V_i)]}_{\text{depends on both } e, \mu_1} - \underbrace{\frac{1 - D_i}{1 - \pi(V_i)} [Y_i - \mu_0(V_i)]}_{\text{depends on both } e, \mu_0}.$$

where η collectively denotes the nuisance functions $\eta = (\mu_1, \mu_0, e)$. At the true nuisance

parameters $\eta_0 = (\mu_1^0, \mu_0^0, \pi^0)$, this score identifies the pointwise CATE, and by extension can be used to form the CME after averaging out other covariates Z .

To show Neyman orthogonality, we must verify:

$$\left. \frac{\partial}{\partial \eta} \mathbb{E}[\Lambda_i(\eta)] \right|_{\eta=\eta_0} = 0.$$

We will look at the partial derivatives of $\mathbb{E}[\Lambda_i(\eta)]$ with respect to each nuisance function μ_1, μ_0 , *and*. In each case, we show the derivative is zero when evaluated at η_0 .

Derivative with Respect to μ_1 Consider a small directional perturbation $h_{\mu_1}(v)$ of μ_1 . The Gateaux derivative in that direction is:

$$\left. \frac{d}{dt} \right|_{t=0} \mathbb{E}[\Lambda_i(\mu_1 + t h_{\mu_1}, \mu_0, e)].$$

Within Λ_i , μ_1 appears in two places: $+\mu_1(V_i)$ and inside the term $\frac{D_i}{\pi(V_i)}[Y_i - \mu_1(V_i)]$. Taking the derivative yields:

$$\text{Partial w.r.t. } \mu_1 : h_{\mu_1}(V_i) - \frac{D_i}{\pi(V_i)} [h_{\mu_1}(V_i)] = h_{\mu_1}(V_i) \left(1 - \frac{D_i}{\pi(V_i)}\right).$$

Since $h_{\mu_1}(V_i)$ is a function of V_i :

$$\mathbb{E} \left[h_{\mu_1}(V_i) \left(1 - \frac{D_i}{\pi(V_i)}\right) \right] = \mathbb{E} \left[h_{\mu_1}(V_i) \mathbb{E} \left[1 - \frac{D_i}{\pi(V_i)} \mid V_i \right] \right].$$

At the true η_0 , $\pi^0(v) = \Pr(D_i = 1 \mid V_i = v)$. Therefore:

$$\mathbb{E} \left[1 - \frac{D_i}{\pi^0(V_i)} \mid V_i = v \right] = 1 - \frac{\mathbb{E}[D_i \mid V_i = v]}{\pi^0(v)} = 1 - \frac{\pi^0(v)}{\pi^0(v)} = 0.$$

By an identical argument, the derivative w.r.t. μ_0 also vanishes.

Derivative with Respect to π Now consider a small perturbation $h_e(v)$ of e . Within Λ_i , e appears in the denominators:

$$\frac{D_i}{\pi(V_i)} \quad \text{and} \quad \frac{1 - D_i}{1 - \pi(V_i)}.$$

Focusing on just the parts that depend on e , the derivative of $\frac{D_i}{\pi(V_i)} [Y_i - \mu_1(V_i)]$ and $-\frac{1-D_i}{1-\pi(V_i)} [Y_i - \mu_0(V_i)]$ sums to:

$$h_\pi(V_i) \left(-\frac{D_i}{\pi(V_i)^2} [Y_i - \mu_1(V_i)] + \frac{1-D_i}{[1-\pi(V_i)]^2} [Y_i - \mu_0(V_i)] \right).$$

Factor out $h_\pi(V_i)$ and condition on $V_i = v$:

$$\begin{aligned} & \mathbb{E} \left[h_\pi(V_i) \left(-\frac{D_i}{\pi(V_i)^2} (Y_i - \mu_1(V_i)) + \frac{1-D_i}{[1-\pi(V_i)]^2} (Y_i - \mu_0(V_i)) \right) \right] = \\ & \mathbb{E} \left[h_\pi(V_i) \mathbb{E} \left[-\frac{D_i}{\pi^0(v)^2} (Y_i - \mu_1^0(v)) + \frac{1-D_i}{[1-\pi^0(v)]^2} (Y_i - \mu_0^0(v)) \mid V_i = v \right] \right]. \end{aligned}$$

Define $\Gamma(v)$ as the sum of two expectations::

$$\Gamma(v) = \underbrace{\mathbb{E} \left[-\frac{D}{\pi^0(v)^2} (Y - \mu_1^0(v)) \mid V = v \right]}_{T_1(v)} + \underbrace{\mathbb{E} \left[\frac{1-W}{[1-\pi^0(v)]^2} (Y - \mu_0^0(v)) \mid V = v \right]}_{T_2(v)}.$$

We will show each of $T_1(v)$ and $T_2(v)$ is zero under the true nuisance parameters.

T₁(v) Vanishes

$$T_1(v) = -\frac{1}{\pi^0(v)^2} \mathbb{E} \left[D(Y - \mu_1^0(v)) \mid V = v \right].$$

Expand the inner expectation:

$$\mathbb{E}[D(Y - \mu_1^0(v)) \mid V = v] = \mathbb{E}[DY \mid V = v] - \mu_1^0(v) \mathbb{E}[W \mid V = v].$$

Evaluate at the true parameters:

$$\mathbb{E}[DY \mid V = v] = \Pr(D = 1 \mid V = v) \cdot \mathbb{E}[Y \mid D = 1, V = v] = \pi^0(v) \mu_1^0(v),$$

$$\mathbb{E}[W \mid V = v] = \pi^0(v).$$

Thus:

$$\mathbb{E}[DY \mid V = v] = \pi^0(v)\mu_1^0(v)$$

$$\mathbb{E}[D(Y - \mu_1^0(v)) \mid V = v] = \pi^0(v)\mu_1^0(v) - \mu_1^0(v)\pi^0(v) = 0.$$

Therefore $T_1(v) = -\frac{1}{\pi^0(v)^2} \cdot 0 = 0$.

T₂(v) Vanishes

$$T_2(v) = \frac{1}{[1 - \pi^0(v)]^2} \mathbb{E}\left[(1 - D)(Y - \mu_0^0(v)) \mid V = v\right].$$

Similarly, expand the inner expectation:

$$\mathbb{E}[(1 - D)(Y - \mu_0^0(v)) \mid V = v] = \mathbb{E}[(1 - D)Y \mid V = v] - \mu_0^0(v)\mathbb{E}[(1 - D) \mid V = v].$$

Evaluate at the true parameter:

$$\mathbb{E}[(1 - D)Y \mid V = v] = (1 - \pi^0(v))\mu_0^0(v)$$

$$\mathbb{E}[(1 - D) \mid V = v] = 1 - \pi^0(v).$$

Thus,

$$\mathbb{E}[(1 - D)(Y - \mu_0^0(v)) \mid V = v] = (1 - \pi^0(v))\mu_0^0(v) - \mu_0^0(v)(1 - \pi^0(v)) = 0.$$

Thus, $T_2(v) = \frac{1}{[1 - \pi^0(v)]^2} \cdot 0 = 0$.

Putting the two parts together: $\Gamma(v) = T_1(v) + T_2(v) = 0 + 0 = 0$ which means for every v :

$$\mathbb{E}\left[-\frac{D}{\pi^0(v)^2}(Y - \mu_1^0(v)) + \frac{1 - D}{[1 - \pi^0(v)]^2}(Y - \mu_0^0(v)) \mid V = v\right] = 0.$$

Consequently,

$$\mathbb{E}\left[h_\pi(V_i)\left(-\frac{D_i}{\pi^0(V_i)^2}(Y_i - \mu_1^0(V_i)) + \frac{1 - D_i}{[1 - \pi^0(V_i)]^2}(Y_i - \mu_0^0(V_i))\right)\right] = 0,$$

for any directional perturbation $h_e(\cdot)$. This completes the proof that the derivative of $\mathbb{E}[\Lambda_i(\eta)]$ w.r.t. e is zero at η_0 .

By combining this argument with the analogous derivatives w.r.t. μ_1 and μ_0 , we conclude

that

$$\frac{\partial}{\partial \eta} \mathbb{E}[\Lambda_i(\eta)] \Big|_{\eta=\eta_0} = 0$$

for all directions of perturbation. Hence, the AIPW score is Neyman-orthogonal to first-order errors in η , which underlies its double robustness property and the extension to DML settings.

References

- Adiguzel, Fatih Serkant, Asli Cansunar and Gozde Corekcioglu. 2023. “Out of sight, out of mind? Electoral responses to the proximity of health care.” *The Journal of Politics* 85(2):667–683.
- Alves, Matheus Facure. 2022. “Causal inference for the brave and true.” *São Paulo, Brazil*. Available at <https://matheusfacure.github.io/python-causality-handbook/01-Introduction-To-Causality.html>.
- Bansak, Kirk. 2020. “Estimating Causal Moderation Effects with Randomized Treatments and Non-Randomized Moderators.” *Journal of the Royal Statistical Society Series A: Statistics in Society* 184:65–86.
- Beiser-McGrath, Janina and Liam F Beiser-McGrath. 2020. “Problems with products? Control strategies for models with interaction and quadratic effects.” *Political Science Research and Methods* 8(4):707–730.
- Belloni, Alexandre, Daniel Chen, Victor Chernozhukov and Christian Hansen. 2012. “Sparse models and methods for optimal instruments with an application to eminent domain.” *Econometrica* 80(6):2369–2429.
- Belloni, Alexandre and Victor Chernozhukov. 2013. “Least squares after model selection in high-dimensional sparse models.” *Bernoulli* (2):521 – 547.
- Belloni, Alexandre, Victor Chernozhukov and Christian Hansen. 2014. “Inference on treatment effects after selection among high-dimensional controls.” *Review of Economic*

Studies 81(2):608–650.

- Benjamini, Yoav and Yosef Hochberg. 1995. “Controlling the false discovery rate: a practical and powerful approach to multiple testing.” *Journal of the Royal statistical society: series B (Methodological)* 57(1):289–300.
- Blackwell, Matthew and Michael P Olson. 2022. “Reducing model misspecification and bias in the estimation of interactions.” *Political Analysis* 30(4):495–514.
- Bonvini, Matteo, Zhenghao Zeng, Miaoqing Yu, Edward H Kennedy and Luke Keele. 2025. “Flexibly estimating and interpreting heterogeneous treatment effects of laparoscopic surgery for cholecystitis patients.” *arXiv preprint arXiv:2311.04359*.
- Brambor, Thomas, William Roberts Clark and Matt Golder. 2006. “Understanding interaction models: Improving empirical analyses.” *Political analysis* 14(1):63–82.
- Chapman, Terrence L. 2009. “Audience beliefs and international organization legitimacy.” *International Organization* 63(4):733–764.
- Chernozhukov, Victor, Christian Hansen and Martin Spindler. 2015. “Post-selection and post-regularization inference in linear models with many controls and instruments.” *American Economic Review* 105(5):486–490.
- Chernozhukov, Victor, Denis Chetverikov, Mert Demirer, Esther Duflo, Christian Hansen, Whitney Newey and James Robins. 2018. “Double/debiased machine learning for treatment and structural parameters.”
- Clark, William Roberts and Matt Golder. 2006. “Rehabilitating Duverger’s theory: Testing the mechanical and strategic modifying effects of electoral laws.” *Comparative Political Studies* 39(6):679–708.
- Crump, Richard K, V Joseph Hotz, Guido Imbens and Oscar Mitnik. 2006. “Moving the goalposts: Addressing limited overlap in the estimation of average treatment effects by changing the estimand.”
- Esarey, Justin and Jane Lawrence Sumner. 2018. “Marginal effects in interaction models: Determining and controlling the false positive rate.” *Comparative Political Studies*

51(9):1144–1176.

- Fan, Jianqing, Nancy E Heckman and Matt P Wand. 1995. “Local polynomial kernel regression for generalized linear models and quasi-likelihood functions.” *Journal of the American Statistical Association* 90(429):141–150.
- Franzese, Robert and Cindy Kam. 2009. *Modeling and interpreting interactive hypotheses in regression analysis*. University of Michigan Press.
- Hainmueller, Jens, Jonathan Mummolo and Yiqing Xu. 2019. “How much should we trust estimates from multiplicative interaction models? Simple tools to improve empirical practice.” *Political Analysis* 27(2):163–192.
- Hastie, Trevor J. 2017. Generalized additive models. In *Statistical models in S*. Routledge pp. 249–307.
- Heckman, James J, Robert J LaLonde and Jeffrey A Smith. 1999. The economics and econometrics of active labor market programs. In *Handbook of labor economics*. Vol. 3 Elsevier pp. 1865–2097.
- Hirano, K and GW Imbens. 2004. “The propensity score with continuous treatments. applied bayesian modeling and causal inference from incomplete-data perspectives.”.
- Holland, Paul W. 1986. “Statistics and causal inference.” *Journal of the American statistical Association* 81(396):945–960.
- Huddy, Leonie, Lilliana Mason and Lene Aarøe. 2015. “Expressive partisanship: Campaign involvement, political emotion, and partisan identity.” *American Political Science Review* 109(1):1–17.
- Imbens, Guido W and Donald B Rubin. 2015. *Causal Inference in Statistics, Social, and Biomedical Sciences*. Cambridge university press.
- Imbens, Guido and Yiqing Xu. 2024. “Lalonde (1986) after nearly four decades: Lessons learned.” *arXiv preprint arXiv:2406.00827* .
- Li, Fan, Laine E Thomas and Fan Li. 2019. “Addressing extreme propensity scores via the overlap weights.” *American journal of epidemiology* 188(1):250–257.

- Montiel Olea, José Luis and Mikkel Plagborg-Møller. 2017. “Simultaneous confidence bands: Theoretical comparisons and suggestions for practice.”
- Neyman, J. 1923. “On the Application of Probability Theory to Agricultural Experiments (with discussion).” *Statistical Science* 5:465–472.
- Neyman, Jerzy. 1959. “Optimal asymptotic tests of composite hypotheses.” *Probability and statistics* pp. 213–234.
- Neyman, Jerzy. 1979. “C (α) tests and their use.” *Sankhyā: The Indian Journal of Statistics, Series A* pp. 1–21.
- Noble, Benjamin S. 2024. “Presidential Cues and the Nationalization of Congressional Rhetoric, 1973–2016.” *American Journal of Political Science* 68(4):1386–1402.
- Robins, James M, Andrea Rotnitzky and Lue Ping Zhao. 1994. “Estimation of regression coefficients when some regressors are not always observed.” *Journal of the American statistical Association* 89(427):846–866.
- Robinson, Peter M. 1988. “Root-N-consistent semiparametric regression.” *Econometrica: Journal of the Econometric Society* pp. 931–954.
- Rubin, D. B. 1974. “Estimating causal effects of treatments in randomized and nonrandomized studies.” *Journal of Educational Psychology* 66:688–701.
- Rubin, Donald B. 1986. “Comment: Which Ifs Have Causal Answers.” *Journal of the American Statistical Association* 81(396):961–962.
- Semenova, Vira and Victor Chernozhukov. 2021. “Debiased machine learning of conditional average treatment effects and other causal functions.” *The Econometrics Journal* 24(2):264–289.
- VanderWeele, Tyler J. 2009. “On the Distinction Between Interaction and Effect Modification.” *Epidemiology* 20:863–871.